University of Iowa
Iowa Research Online

Spring 2017

The effects of movement speeds and magnetic disturbance on inertial measurement unit accuracy: the implications of sensor fusion algorithms in occupational ergonomics applications

Howard Chen
University of Iowa

Follow this and additional works at: https://ir.uiowa.edu/etd

Part of the Industrial Engineering Commons

Recommended Citation

Chen, Howard. "The effects of movement speeds and magnetic disturbance on inertial measurement unit accuracy: the implications of sensor fusion algorithms in occupational ergonomics applications." PhD (Doctor of Philosophy) thesis, University of Iowa, 2017.
https://doi.org/10.17077/etd.29a72vle

Follow this and additional works at: https://ir.uiowa.edu/etd

Part of the Industrial Engineering Commons

THE EFFECTS OF MOVEMENT SPEEDS AND MAGNETIC DISTURBANCE ON
INERTIAL MEASUREMENT UNIT ACCURACY: THE IMPLICATIONS OF
SENSOR FUSION ALGORITHMS IN OCCUPATIONAL ERGONOMICS
APPLICATIONS

by

Howard Chen

A thesis submitted in partial fulfillment
of the requirements for the Doctor of Philosophy
degree in Industrial Engineering in the
Graduate College of
The University of Iowa

May 2017

Thesis Supervisors: Associate Professor Nathan Fethke
Professor Geb Thomas

Graduate College
The University of Iowa
Iowa City, Iowa

CERTIFICATE OF APPROVAL

_____

PH.D. THESIS

_____

This is to certify that the Ph.D. thesis of

Howard Chen

has been approved by the Examining Committee for
the thesis requirement for the Doctor of Philosophy degree
in Industrial Engineering at the May 2017 graduation.

Thesis Committee: _____
                      Nathan Fethke, Thesis Supervisor

                      _____
                      Geb Thomas, Thesis Supervisor

                      _____
                      Fredric Gerr

                      _____
                      Thomas Schnell

                      _____
                      David Wilder

ACKNOWLEDGEMENTS

mind. He gave me the necessary resources to establish my own research interest and pushed me to my intellectual limits. Of course, this journey would be impossible if it wasn't for the unconditional support from my parents.

ABSTRACT

Accurate risk assessment tools and methods are necessary to understand the relationship between occupational exposure to physical risk factors and musculoskeletal disorders. Ergonomists typically consider direct measurement methods to be the most objective and accurate of the available tools. However, direct measurement methods are often not used due to cost, practicality, and worker/workplace disruption.

Inertial measurement units (IMUs), a relatively new direct measurement technology used to assess worker kinematics, are attractive to ergonomists due to their small size, low cost, and ability to reliably capture information across full working shifts. IMUs are often touted as a field-capable alternative to optical motion capture systems (OMCs). The error magnitudes of IMUs, however, can vary significantly (>15°) both within and across studies. The overall goals of this thesis were to (i) provide knowledge about the capabilities and limitations of IMUs in order to explain the inconsistencies observed in previous studies that assessed IMU accuracy, and (ii) provide guidance for the ergonomics community to leverage this technology. All three studies in this dissertation systematically evaluated IMUs using a repetitive material transfer task performed by thirteen participants with varying movement speeds (15, 30, 45 cycles/minute) and magnetic disturbance (absent, present). An OMC system was used as the reference device.

This first study systematically evaluated the effects of motion speed and magnetic disturbance on the spatial orientation accuracy of an inertial measurement unit (IMU) worn on the hand. Root-mean-square differences (RMSD) exceeded 20° when inclination measurements (pitch and roll) were calculated using the IMU's accelerometer. A linear Kalman filter and a proprietary, embedded Kalman filter reduced inclination RMSD to <3° across all movement speeds. The RMSD in the heading direction (i.e., about gravity) increased (from <5° to 17°) under magnetic disturbance. The linear Kalman filter and the embedded Kalman filter reduced heading RMSD to <12° and <7°, respectively. This study indicated that the use of IMUs and Kalman filters can improve inclinometer measurement accuracy. However, magnetic disturbances continue to limit the accuracy of three-dimensional IMU motion capture.

The goal of the second study was to understand the capability of IMU inclinometers to improve estimates of angular displacements and velocities of the upper arm. RMSD and peak displacement error

iv

exceeded 11° and 28° at the fastest transfer rate (45 cycles/min) when upper arm elevation was calculated using the IMU accelerometer. The implementation of a Kalman filter reduced RMS and peak errors to <1.5° and <2.3°, respectively. Similarly, the RMS and peak error for accelerometer-derived velocities exceeded 81°/s and 221.3°/s, respectively, at the fastest transfer rate. The Kalman filter reduced RMS and peak errors to <9.2°/s and < 25.1°/s, respectively.

The third study was conducted to evaluate the relationship between magnetic field strength variation and magnetic heading deviation. In this study, the presence of the metal plate increased magnetic heading deviations from <12° (90th-10th percentile) to approximately 30°. As expected, the magnetic field strength standard deviation increased from 1.0uT to 2.4uT. While this relationship may differ across other sources of magnetic disturbance, the results reinforce the notion that local magnetic field disturbances should be minimized when using IMUs for human motion capture.

Overall, the findings from this thesis contribute to the ergonomics community's understanding of the current capabilities and limitations of IMUs. These studies suggest that while the touted capabilities of the IMUs (full-body motion capture in workplace settings) may be unattainable based on current sensor technology, these sensors are still significantly more accurate than the accelerometer-based inclinometers commonly used by ergonomists to measure motions of the upper arms.

PUBLIC ABSTRACT

Musculoskeletal disorders of the upper extremity are among the most common and expensive of all occupational injuries and illnesses. Understanding and measuring the risk factors associated with these conditions is important for improving worker health and well-being. The measurement systems available for this purpose, however, are quite limited. Inertial measurement units (IMUs), a relatively new technology available for measuring important aspects of worker motion in the field, offer improved data collection prospects for ergonomists. However, the accuracy of IMUs can vary beyond clinically-acceptable levels. The overall goals of this thesis were to (i) provide knowledge about the capabilities and limitations of IMUs in order to explain the inconsistencies observed in previous studies that have assessed IMU accuracy, and (ii) provide guidance for the ergonomics community to leverage this technology within its current capabilities. The studies in this dissertation systematically examined factors known to adversely affect IMU accuracy. Results suggested that the advertised capabilities of IMUs (full-body motion capture in workplace settings) may not be achievable using current sensor technologies. However, these sensors are still substantially more accurate than the devices commonly used by ergonomists to measure upper extremity postures and movements in field settings.

TABLE OF CONTENTS

LIST OF TABLES

LIST OF FIGURES

CHAPTER 1

INTRODUCTION AND BACKGROUND

1.1 Work-Related Musculoskeletal Disorders

The term 'musculoskeletal disorders' refers to a wide range of health outcomes affecting the muscles, tendons, ligaments, and peripheral nerves (Punnett and Wegman 2004). These outcomes cause pain and functional impairment to various body segments and joints including the neck, shoulder, elbow, forearm, wrist and hand (Li and Buckle 1999). Specific conditions include rotator cuff tendonitis, epicondylitis in the elbow, wrist tendonitis, hand-arm vibration syndrome, and carpal tunnel syndrome (CTS) (Bernard 1997).

Work-related musculoskeletal disorders (WMSDs) are an important occupational health problem. In 2014, WMSDs accounted for 33 percent of all non-fatal workplace injuries and illnesses requiring days away from work in the United States (BLS 2015). Recovery times associated with WMSDs can also be prolonged, particularly for outcomes of the upper extremity. Shoulder-related MSDs, wrist-related MSDs, and CTS required a median of 24 days, 18 days, and 30 days before returning to work, respectively, in 2012 (BLS 2013). The financial burden associated with WMSDs is also substantial. The direct costs (e.g. worker's compensation, medical costs) associated with WMSDs have been estimated to range from $13 to $54 billion annually, while estimates of the indirect costs associated (e.g. loss of productivity, worker training) exceed $160 billion (National Research Council 2001; Bernard 1997; American Academy of Orthopaedic Surgeons 2008).

Epidemiologic studies have investigated associations between both non-occupational and occupational risk factors and WMSDs. In general, it is widely believed that WMSDs can be attributed to a combination of personal, psychosocial, and physical risk factors (Bongers et al. 2006; Malchaire, Cock, and Vergracht 2001). Personal risk factors include age, gender, height, weight, hobbies, and general health status (Malchaire, Cock, and Vergracht 2001) Occupational psychosocial stressors, such as job insecurity, elements of work organization (e.g., "safety culture/climate" and downsizing), and job-specific factors

(e.g., shiftwork) also contribute to musculoskeletal health status (Landsbergis, Grzywacz, and LaMontagne 2014). In particular, variables derived from the well-known "demand/control" model of occupational psychosocial stress (Karasek et al. 1998) have been observed as independent risk factors for WMSDs in several epidemiologic studies (e.g., Punnett and Wegman 2004; Fethke et al. 2015). Most relevant to this thesis, however, WMSDs are associated with a consistent set of physical risk factors used to describe the extent of biomechanical loading imposed by a given work situation. Physical risk factors include the forces exerted, the postures (and movements) required to perform the functions of a job or task, the extent to which the forces/postures are repeated (i.e., the risk factor "repetition"), and mechanical vibration (Bernard 1997; Malchaire, Cock, and Vergracht; Spielholz et al. 2001).

Exposure to physical risk factors for musculoskeletal disorders is typically assessed using methods classified as self-report, observation-based, or direct measurement (David 2005; Spielholz et al. 2001; Li and Buckle 1999). In general, self-report methods are the least expensive and require less training to conduct, but the exposure information obtained is crude and often unreliable (David 2005). Observation-based methods (e.g. Hand Activity Level (Latko et al. 1997), Strain Index (Moore and Garg 1995)) are considered to be the most practical since they minimize worker/workplace disruption and require minimal equipment costs. Observation-based methods, however, may be subjected to observer biases and the time required to complete analyses can be substantial (Dartt et al. 2009; David 2005). Direct measurement methods (e.g. electromyography, optical motion capture [OMC]) are considered the most accurate and objective form for exposure assessment. Direct measurement methods, however, are traditionally limited by equipment cost, practicality, and potential for worker/workplace disruption (Spielholz et al. 2001; Amasay et al. 2009).

Considerable progress has been made towards understanding relationships between occupational physical risk factors and WMSDs. The association between exposure to non-neutral shoulder postures and upper extremity MSDs (UEMSDs), specifically, has been reported in several epidemiologic studies (Gerr et al. 2013; Svendsen et al. 2004; Nordander et al. 2016; Miranda et al. 2008; Ohlsson et al. 1995; Silverstein et al. 2008; Punnett et al. 2000). Risk estimates in these studies (e.g., odds ratios [OR] and hazard ratios [HR]) were adjusted for personal and/or psychosocial factors; however, different methods were used to

capture and summarize information about exposure to non-neutral shoulder postures. Miranda et al., (2008) reported that self-reported exposure to awkward postures (no/yes) at work was associated with a subsequent chronic shoulder disorder (OR: 1.9; 95% confidence interval [CI]: 1.1-3.2) among the Finnish adult population. Gerr et al., (2013) observed an association between percent of task time spent with upper arm elevation >90° (as a continuous variable, based on expert video analysis) and risk of neck/shoulder disorders (HR: 1.07; 95% CI: 1.0-1.15) among appliance manufacturing workers during a three-year prospective study. Similarly, Punnett et al., (2000) observed increases in risk estimates of shoulder disorders among automobile assembly workers as percent time spent with the upper arms elevated >90° (based on video analysis) increased; e.g., OR = 2.0 for more than 0% but less than 10% time with the right shoulder elevated >90° and OR = 3.9 for ≥10% time with the right shoulder elevated >90° (referent exposure category was 0% time with the right shoulder elevated >90°). The percentage of time with the upper arm elevated >90° was also used at the exposure variable and associated with shoulder outcomes (OR: 1.16; 95% CI: 1.08-1.25 for shoulder pain with disability and OR: 1.08; 95% CI: 1.4-1.13 for shoulder pain without disability) among machinists, car mechanics, and house painters (Svendsen et al. 2004). Although 90° of upper arm elevation is a common exposure "cutoff," other definitions have been used. For example, Silverstein et al., (2008) reported working in upper arm flexion ≥45° for ≥15% of the time was associated with rotator cuff syndrome (OR: 2.16; 95% CI: 1.22-3.83) in a cross-sectional study among active workers encompassing different occupational groups.

In general, the magnitudes and precision of the reported risk estimates in epidemiologic studies vary substantially, which limits the usefulness of these estimates to inform the occupational safety and health decision-making processes. In addition to methodological differences in study samples, study designs, and the extent to which confounding was controlled in the analyses, the heterogeneity in risk estimates may be partially explained by the common use of potentially biased and idiosyncratic self-report and observation-based exposure assessment methods in epidemiological studies of WMSDs (Gerr et al. 2013; Fethke et al. 2012). Direct measures of worker postures and movements are used less commonly, but, in conjunction with standardized data processing methods and summary metrics, enable greater comparability between study results. Recently, for example, Nordander et al., (2016), described the results of pooled analyses of up to 33 occupational groups from 16 separate cross-sectional studies. For each group

(which varied in size from 32 to 206 participants), information was available about the prevalence of shoulder-related musculoskeletal outcomes and the distributions (means and standard deviations) of a variety of physical exposure summary metrics derived from directly measured data. Linear relationships were observed between the group mean 99th percentile upper arm elevation and the prevalence of tension neck syndrome, and between the group mean 50th percentile upper arm angular velocity both bicipital tendonitis and infraspinatus tendonitis.

These studies have indicated that accurate risk assessment tools and methods are pertinent to improve our understanding of the relationship between occupational exposure to physical risk factors and musculoskeletal disorders. Modern ergonomics exposure assessment guidelines generally accept that direct measurement of working posture using instrumentation systems is preferable to self-report or observation-based methods. The cost of purpose-built hardware (e.g., electrogoniometers) available to quantify occupational physical risk factors in workplace settings, however, requires tradeoffs to be made between increased sampling durations and increased participants.

In contrast to electrogoniometers, inertial measurement units (IMUs) are inexpensive (<$5), generic sensors employed in a variety of modern electronic devices (e.g., smart phones, virtual reality, drones, fitness trackers) to measure motion. IMU technology will likely improve into the distant future given its demand and market capacity. In addition, human motion tracking is increasingly common outside of biomechanics, leading to development of consumer-oriented devices (e.g., Microsoft Kinect, Intel Realsense) for motion tracking. Given its small size, long recording times, and decreasing hardware costs, IMUs are increasingly adopted by the ergonomics community to quantify human motion in workplace settings (Schall et al. 2015; Douphrate et al. 2012). Since the sensors can be attached to any body segment, IMUs offer more flexibility compared to the electrogoniometers and accelerometers commonly used to directly measure exposure to non-neutral posture in the workplace setting.

1.2 Background

Human motion can be measured using an OMC system, electromagnetic tracking devices, electrogoniometers, and accelerometers. The most precise measurements of human motion are typically

achieved in the laboratory environment with an OMC or electromagnetic tracking device. Human motion in the workplace setting is commonly measured using an electrogoniometer or accelerometer. Each instrumentation system is briefly explained in subsequent sections.

1.2.1 Optical Motion Capture

An OMC is considered the gold standard for human motion measurement analysis (Cuesta-Vargas, Galán-Mercant, and Williams 2010). A marker-based OMC system uses cameras to track the position of individual markers in three-dimensional space. Each marker contains a unique identifier that is used to facilitate calculations of joint kinematics. At least two cameras are required to measure the position of a marker in three-dimensional space. Spatial orientation measurements require the simultaneous tracking of at least three markers attached to the same body segment. Standardized marker placement guidelines (e.g. ISB convention (Wu et al. 2005)) facilitate comparisons across studies.

Marker occlusion and soft-tissue artifacts affect the overall accuracy of OMC-based motion measurements. Marker occlusion occurs when a marker is detected by fewer than two cameras due to line-of-sight obstructions, resulting in loss of the marker position in three-dimensional space. Soft-tissue artifacts occur when the skin movement is different than the underlying bone structure (Corazza et al. 2006). The system cost, setup time, level of obtrusiveness, and need for the instrumented human to remain within a limited volume (i.e., in view of fixed-position cameras) are among the factors that preclude the use of OMC systems in workplace settings (Amasay et al. 2009). Ergonomists have also used inexpensive, consumer-grade markerless motion capture systems (e.g. Microsoft Kinect) to measure body movements (Xu and McGorry 2015; Dutta 2012; Bonnechère et al. 2014). Although this technology has shown promise, such systems are still subjected to the constraints of occlusion and a limited capture volume.

1.2.2 Electromagnetic Tracking

An electromagnetic tracking device captures the position and orientation based on measurements of the local magnetic field vector at the sensor (Welch and Foxlin 2002). This device consists of a source

that emits an electromagnetic field, and magnetometers that measure the strength and direction of the generated magnetic field (Cuesta-Vargas, Galán-Mercant, and Williams 2010; Huiyu Zhou and Hu 2008). Unlike an OMC, electromagnetic tracking devices do not require a line-of-sight connection between the transmitter and sensor. This device is generally reliable and accurate, but can be adversely affected by the presence of metals (Cuesta-Vargas, Galán-Mercant, and Williams 2010). Similar to an OMC system, electromagnetic tracking devices are only operable in constrained environments, limiting their use to a laboratory-based settings.

1.2.3 Electrogoniometers

Electrogoniometers are frequently used in workplace settings to directly measure human motion, particularly the motions of the distal upper extremity (Fethke et al. 2012; Asundi, Johnson, and Dennerlein 2012; Balogh et al. 2009; Cook, Burgess-Limerick, and Papalia 2004). An electrogoniometer is a mechanical device that spans a human joint and measures its angular displacement (Buchholz and Wellman 1997). Single-axis, dual-axis, and tri-axial elecrogoniometers are available to accommodate measurement of angular displacement in multiple movement planes (e.g., dual-axis devices are used to measure flexion/extension and radial/ulnar deviation of the wrist). Electrogonimeters, however, may restrict the natural movement of a joint, causing measurement error and potential misinterpretation of the results (Buckle and Jason Devereux 2002; Buchholz and Wellman 1997; Jonsson and Johnson 2001)..

1.2.4 Accelerometers

Piezoresistive accelerometers are frequently used as inclinometers to measure the inclination angle of the trunk and/or upper arm with respect to gravity (Fethke, Gant, and Gerr 2011; Fethke et al. 2016). Inclination is calculated under the assumption that the total measured acceleration is constant at 9.81 m/s^2, the acceleration due to gravity (Sabatini 2006). In general, accelerometer-derived inclination measurements are accurate (<1°) under static conditions, but can deviate significantly (>80°) during periods of rapid, dynamic movement (Amasay et al. 2009). The errors increase with higher angular velocities and are compounded by distance between the accelerometer and the joint center of rotation due to increases in

6

tangential and centripetal accelerations (Amasay et al. 2009; Bernmark and Wiktorin 2002). Moreover, piezoresistive accelerometers are not sensitive to rotation about the gravity vector (heading), which is critical for capturing joint angles of the wrist and elbow or to separate the motion planes of the trunk and shoulder (Bernmark and Wiktorin 2002; Amasay et al. 2009; Korshøj et al. 2014). Inertial measurement units (IMUs) overcome these limitations, in theory, through the addition of gyroscopes and magnetometers.

1.2.5 Inertial Measurement Units

Inertial measurement units are marketed as a solution for capturing human motion in three-dimensional space but without environmental constraints imposed by laboratory-based OMC or electromagnetic motion capture systems. An IMU measures spatial orientation with respect to gravity and magnetic north using a combination of gyroscope, accelerometer, and magnetometer measurements. Joint angles can be estimated from IMUs attached to adjacent body segments (Cloete and Scheffer 2008; Martori et al. 2013) and then summarized using metrics to describe exposure to posture and movement characteristics indicative of WMSD risk (Kazmierczak et al. 2005).

1.2.5.1 IMU Operation

An IMU traditionally refers to an inertial navigation system (INS), which tracks the position and orientation of an object relative to a known position, velocity, and orientation using an accelerometer and gyroscope (Woodman 2007). In the context of an INS, the gyroscope is used to determine orientation of an object and to rotate the accelerometer to the reference orientation. The position information is subsequently obtained by double-integrating the rotated accelerometer measurements with respect to time. An INS, however, is not practical for the purpose of human motion capture given its size and cost. In the context of human motion capture, an IMU refers to an attitude heading reference system (AHRS). An AHRS is commonly used to measure the orientation of an airplane using a combination of gyroscope, accelerometer, and magnetometer measurements. Recent advances in semiconductor technology pertaining to micro-electromechanical systems (MEMS) have provided inertial sensors that are more suitable for human motion capture, given their small size, cost, and durability (Pasciuto et al. 2015; Chang et al. 2008).

Fundamentally, the spatial orientation of an IMU can be calculated using two distinct methods: (i) with respect to its initial orientation by integrating the angular velocity measured by the gyroscope, or (ii) with respect to gravity and magnetic north using an accelerometer and magnetometer (Yun, Bachmann, and McGhee 2008; Valenti, Dryanovski, and Xiao 2015; Bergamini et al. 2014; Schiefer et al. 2014).

A MEMS-based gyroscope measures angular velocity, which is integrated with respect to time to obtain spatial orientation measurements (Sabatini 2006). Gyroscope-derived orientation measurements are unaffected by linear acceleration and magnetic disturbance. Gyroscopes differ in their cost, size, and performance (Zhi 2016). The performance of a gyroscope is characterized by its bias stability, which is assumed to follow a normal statistical distribution (Xia, Yu, and Kong 2014). This error characteristic is known as random walk (Chang et al. 2008). A change in measurement bias will cause the resulting error to compound linearly with respect to time when calculating spatial orientation measurements. MEMS-based gyroscopes, despite their advantages, are not particularly accurate. Gyroscope-derived spatial orientation measurements can easily deviate more than $10°$ per minute relative to a known orientation (Bergamini et al. 2014; Luinge, Veltink, and Baten 2007).

Spatial orientation measurements derived using an accelerometer and magnetometer are broadly known as vector-based orientation measurements. Vector-based orientation measurements are considered to be time-invariant, in contrast to gyroscope-derived orientations. Spatial orientation can be determined given two or more vectors pointing to known directions. In this context, spatial orientation is derived from the gravity vector and the magnetic north vector.

The calculation of spatial orientation based on vector observations was originally developed to orient spacecraft using celestial bodies. Calculation of the optimal orientation estimate given multiple vector observations is classically known as Wahba's problem (Wahba 1965). Optimal solutions to Wahba's problem are obtained from redundant vector observations. The proposed solutions (Shuster and Oh 2012; Mortari 1997; Markley 1988) differ primarily by computation speed (Valenti, Dryanovski, and Xiao 2015). Deterministic solutions are obtained from two vectors that point to known directions (Valenti, Dryanovski, and Xiao 2015; Valenti, Dryanovski, and Xiao 2016; Yun, Bachmann, and McGhee 2008). The problem with deriving spatial orientation using the gravity and magnetic north vectors is the assumption that the

accelerometer is only measuring the direction of the gravity vector and the magnetometer is only measuring Earth's local magnetic field. In reality, the accelerometers cannot discern gravitational acceleration from accelerations due to motion. Similarly, the magnetometer measurements assume a homogenous magnetic field, which in reality is affected by ferromagnetic objects and electronic devices (Bachmann, Yun, and Peterson 2004). Depending on the formulation used to derive spatial orientation using vector observations, magnetic disturbance will either affect orientation around the gravity vector (heading) or across all motion planes (Yun, Bachmann, and McGhee 2008; Valenti, Dryanovski, and Xiao 2015; Valenti, Dryanovski, and Xiao 2016). Sensor fusion algorithms are used to combine gyroscope-derived orientation measurements with vector observations to improve measurement accuracy.

1.2.5.2 Sensor Fusion

The purpose of sensor fusion is to reduce the effects of random and systematic measurement errors by combining information from multiple sensors (Plamondon et al. 2007). Gyroscope, accelerometer, and magnetometer measurements can be combined using complementary filters (Bachmann et al. 2001; Madgwick, Harrison, and Vaidyanathan 2011; Valenti, Dryanovski, and Xiao 2015; Y. Tian, Wei, and Tan 2013), particle filters (Carmi and Oshman 2009; Yadav and Bleakley 2014), and Kalman filters (Foxlin 1996; Sabatini 2006; Valenti, Dryanovski, and Xiao 2016; Gabriele Ligorio and Sabatini 2016; Sun et al. 2013; Daniel Roetenberg et al. 2005; Sabatini 2011a; Brigante et al. 2011; Kraft; Makni, Fourati, and Kibangou 2014). A complementary filter combines the signal sources based on spectral frequency (Luinge and Veltink 2005), specifically the high-frequency components of gyroscope-derived orientation estimates with the low-frequency components of accelerometer and magnetometer-derived orientation estimates (Luinge and Veltink 2005). Complementary filters are relatively simple to implement in comparison to other algorithms and typically result in low computational overhead (Valenti, Dryanovski, and Xiao 2015). However, complementary filters fail to consider the stochastic error characteristics (e.g. white noise) associated with sensor measurements (Nowicki, Wietrzykowski, and Skrzypczyński 2015). In contrast, particle and Kalman filters combine measurements based on stochastic properties of sensor noise measurements (Sabatini 2011a). Particle filters use fewer underlying assumptions compared to Kalman

9

filters at the expense of high computation costs (Carmi and Oshman 2009). Kalman filters are widely used for motion tracking since they offer an appropriate balance between computational requirements and optimal estimation. (Sabatini 2011a).

1.2.5.2.1 Kalman Filters

When given multiple sources of data, Kalman filters are commonly used to smooth noisy data and to estimate the parameters of interest (Faragher 2012). The Kalman filter estimates the parameters of interest (state vector) based on the expected behavior of the system (process model) and the expected error behavior of individual sensors (measurement model) (Luinge and Veltink 2005). The process model predicts the next measurement and eliminates unreasonable estimates made by the sensor. The measurement model relates the process model to the noisy but stable sensor measurements. A Kalman filter will provide optimal estimates for linear systems with the assumption that the process and measurement noise are normally distributed (Bachmann 2000). Variations of the Kalman filter, including the Unscented Kalman Filter (UKF) and the Extended Kalman Filter (EKF), were developed to address non-linear systems. The UKF approximates the Gaussian probability distribution of the non-linear system using a set of sample points while the EKF linearizes the system using a Jacobian matrix (LaViola 2003). The UKF, in general, offers better performance and filter stability compared to the EKF at the expense of increased computational overhead (Sabatini 2011a).

Kalman-based sensor fusion algorithms for IMUs are prevalent in literature. With few exceptions, an aspect of the process model involves calculating spatial orientation using gyroscope measurements, which is non-linear. The majority of the proposed filters use an EKF-based approach since the computational overhead of the UKF provides only marginal benefits for this application (LaViola 2003; Sabatini 2011a). Most filters differ in the process model. The orientation information derived from an EKF can be described using Euler angles (Foxlin 1996), nine-element direction cosine matrices (Daniel Roetenberg et al. 2005), and, most commonly, as quaternions (Sabatini 2011a). In addition to the estimated orientation, the prediction model may account for gyroscope bias (Daniel Roetenberg et al. 2005; Ali and El-Sheimy 2013; Brigante et al. 2011), accelerometer bias (Sabatini 2006), magnetometer bias (Sabatini

10

2006; Sabatini 2011a), and linear acceleration (Lee, Park, and Robinovitch 2012; Gabriele Ligorio and Sabatini 2015; Daniel Roetenberg et al. 2005) to attenuate disturbances. Several proposed EKF formulations have pre-combined the accelerometer and magnetometer measurements into a quaternion vector to reduce computation costs, with differing approaches on the calculation of the quaternion-based measurement vector (Valenti, Dryanovski, and Xiao 2016; Ali and El-Sheimy 2013; Yun and Bachmann 2006). However, the measurement vector typically consists of accelerometer and magnetometer measurements to simplify the measurement noise structure (Sabatini 2011a).

The tradeoffs between gyroscope-derived and accelerometer/magnetometer-derived spatial orientation measurements are determined by the tuning parameters of the Kalman filter. The tuning parameters can be obtained from sensor specifications (Sun et al. 2013), calculation of sensor standard deviation under static conditions (Gabriele Ligorio et al. 2016), Allan variance (Chang et al. 2008), or empirically (Bergamini et al. 2014). Additional mechanisms can be implemented to ensure that the total acceleration and magnetic field strength are within the expected range of gravity and magnetic north, respectively. These mechanisms would increase accelerometer and magnetometer noise parameters if the total acceleration and magnetic field strength measurements were outside the expected range (Sun et al. 2013; Sabatini 2006; Daniel Roetenberg et al. 2005; Gabriele Ligorio and Sabatini 2016), therefore relying extensively on gyroscope-derived measurements with the expectation of time-dependent errors. Regardless of the filtering approach and its permutations, the assumptions of (i) homogenous measurements of gravity and magnetic field, and (ii) time-varying gyroscope errors remain valid. Consequently, magnetic disturbance can only be mitigated for short timeframes (Gabriele Ligorio and Sabatini 2016).

Researchers have also proposed alternative filtering and motion capture approaches. These include Kalman filter designs that take into account (i) a biomechanical model (El-Gohary and McNames 2012; El-Gohary and McNames 2015; Zhang, Wong, and Wu 2011; Miezal, Taetz, and Bleser 2016), (ii) motion dynamics, (El-Gohary and McNames 2012; El-Gohary and McNames 2015), and kinematic constraints (El-Gohary and McNames 2015; Miezal, Taetz, and Bleser 2016; Luinge and Veltink 2005; H. Zhou and Hu 2010). Filtering strategies such as zero-velocity updates (El-Gohary and McNames 2012; Schiefer et al. 2014; Meina, Rykaczewski, and Rutkowski 2016) and attaching multiple gyroscopes to the same circuit

11

board (Chang et al. 2008) aim to increase the measurement timeframe that IMUs can be used in magnetically-disturbed environments before the errors accumulate. IMU measurements have also been used in conjunction with other reference devices, such as a localized magnetic coil (D. Roetenberg, Slycke, and Veltink 2007; Tadayon et al. 2016), permanent magnets (Meina, Rykaczewski, and Rutkowski 2016), potentiometers (Plamondon et al. 2007; Taunyazov, Omarali, and Shintemirov 2016), e-textiles (Tognetti et al. 2015), GPS (Matthew Brodie, Walmsley, and Page 2008), ultra-wideband positioning systems (Zihajehzadeh et al. 2015; Kok, Hol, and Schön 2015; Yoon et al. 2017), body-mounted cameras (e.g. visual odometry) (Oskiper et al. 2007; Vignais et al. 2013; Shiratori et al. 2011), and OMCs (Bó, Hayashibe, and Poignet 2011; Yushuang Tian et al. 2015; Won, Melek, and Golnaraghi 2010). However, these approaches have not been readily adopted in practice.

1.2.5.3 Assessing IMU Accuracy

In general, the accuracy of an IMU is assessed by simultaneously measuring a motion pattern with the sensor and a reference device. An OMC is generally used as the reference device for this application (Cuesta-Vargas, Galán-Mercant, and Williams 2010). Mechanical gimbals (Lebel et al. 2013; Lebel et al. 2015), robotic arms (Martori et al. 2013; Mourcou et al. 2015; El-Gohary and McNames 2015), pendulums (Godwin, Agnew, and Stevenson 2009; M.a. Brodie, Walmsley, and Page 2008), and human motion (Bergamini et al. 2014; Gabriele Ligorio et al. 2016; Faber et al. 2013) have been used to provide a source of motion.

Several studies reported favorable results (<6° average error) (Plamondon et al. 2007; Faber et al. 2013; Kim and Nussbaum 2013; Martori et al. 2013; Bergamini et al. 2014), while others have reported inconsistent IMU error. For example, Schiefer et al., (2014) reported average root-mean-square (RMS) errors of 8.3° for the thorax and 8.6° for the left upper arm, but 14.5° for the right forearm and 16.8° for the head. Cloete et al., (2008) reported average RMS errors of 6.5° for right hip rotation, but 18.8° for right ankle rotation. Godwin et al., (2009) reported >20° RMS error (i) between different body segments within the same task and (ii) within the same body segment between different tasks. Robert-Lachaine et., (2016) reported errors less than 5° and greater than 40°, depending on the body segment.

In general, IMU accuracy has been evaluated in the context of both biomechanics (i.e. joint kinematics) (Martori et al. 2013; Schall et al. 2015; Schall Jr. et al. 2015; Plamondon et al. 2007; Kim and Nussbaum 2013; El-Gohary and McNames 2012), and spatial orientation (Lebel et al. 2013; Lebel et al. 2015; Bergamini et al. 2014; Gabriele Ligorio et al. 2016). Biomechanical-based assessments are relevant to those interested in alternatives to traditional optical and magnetic-based systems. These studies, however, may be unable to discern error magnitudes due to methodological differences from actual sensor error (Robert-Lachaine et al. 2016). A source of methodological difference between OMCs and IMCs is the differences in protocol used to define body segment orientation. When human motion is assessed using an OMC or magnetic tracking device, for example, the body segments are defined based on the position of bony landmarks (Wu et al. 2005; Kontaxis et al. 2009; Hsu et al. 2009). However, these landmarks are unavailable for IMCs due to the absence of positional information (de Vries et al. 2010). Alternative protocols used to define body segment orientation have been proposed and evaluated, with differences ranging from 15° to 40° across studies (de Vries et al. 2010; Ricci et al. 2014; Cutti et al. 2007; Robert-Lachaine et al. 2016) relative to established clinical protocols.

The errors associated with IMU spatial orientation measurements (i.e., heading, pitch and roll angles rather than kinematic variables) are relevant for understanding IMU error characteristics and the theoretical accuracy of biomechanical-based measurements using current sensor technologies. Errors in spatial orientation measurements are often presented when (i) developing and comparing sensor fusion algorithms and (ii) assessing factors that can negatively affect IMU accuracy (Lebel et al. 2013; Gabriele Ligorio et al. 2016; Bergamini et al. 2014; Sessa et al. 2012; Lebel et al. 2015). In general, IMU accuracy is affected by measurement timeframe (Lebel et al. 2015), sensor hardware (Lebel et al. 2013), sensor fusion algorithms (Gabriele Ligorio and Sabatini 2015), error calculation method (Faber et al. 2013), and alignment between the IMU and OMC (Mecheri et al. 2016; Chardonnens, Favre, and Aminian 2012). On a fundamental level, the accuracy of IMU-derived spatial orientation measurements are affected by measurement timeframe (Lebel et al. 2015), motion (Lebel et al. 2013; Kim and Nussbaum 2013), and magnetic disturbance (de Vries et al. 2009; Bachmann, Yun, and Peterson 2004), which is consistent with the expected error characteristics of the gyroscope, accelerometer, and magnetometer, respectively.

1.2.5.4 Gaps in Current Literature

Despite the development of more advanced IMUs, knowledge about the current capabilities and limitations of IMUs is lacking within the occupational ergonomics community. This may be in part due to the evaluation of commercial hardware that employ proprietary algorithms for converting raw IMU data to kinematic constructs, which limits the generalizability of these studies' results beyond potentially idiosyncratic commercial solutions. In addition, researchers often evaluate IMUs under nominal conditions with precautionary measures to control for magnetic disturbance (i.e. maintaining set distance between the system and known sources of disturbances) (Robert-Lachaine et al. 2016; Kim and Nussbaum 2013; Lebel et al. 2013; Lebel et al. 2015; Schiefer et al. 2014), which limits study generalizability to the laboratory environment (Schiefer et al. 2014). The results may also be confounded by unforeseen sources of magnetic disturbance (e.g. metal below the floor) (de Vries et al. 2009). Despite being a known issue, few studies have assessed the effects of local magnetic fluctuations on IMU error (de Vries et al. 2009; Bachmann, Yun, and Peterson 2004; Gabriele Ligorio et al. 2016).

As ergonomists continue to use accelerometers in field studies to describe the inclination of the trunk and upper arms with respect to the gravity vector (i.e., pitch angle) and the horizon (i.e., roll angle). Several researchers have proposed using sensor fusion algorithms to attenuate motion-related artifacts in an effort to improve inclinometer accuracy (Lee, Park, and Robinovitch 2012; Gabriele Ligorio and Sabatini 2015; Schall Jr. et al. 2015; Schall et al. 2015). However, none of these studies reported (i) the accuracy of accelerometer-derived angular displacement measurements, (ii) the accuracy of angular velocity measurements, or (iii) differences in motion assessment metrics used for health-based decision making in the context of occupational ergonomics. The relationship between inclinometer accuracy and motion assessment metrics and the ability of IMU-based inclinometers to improve measurement accuracy remains unknown. Previous work by Schall et al. provided direct comparisons of accelerometer and IMU-based inclinometers to an electrogoniometer used to measure trunk motion (Schall Jr. et al. 2015) and to a biomechanical-based optical motion capture system (Schall et al. 2015). The results showed (i) greater errors in the IMU measurements relative to the reference device (5-9° depending on motion plane and body segment) compared to previous studies and (ii) marginal differences between accelerometer-based and IMU-based inclination measurements. However, error sources not reflective of sensor accuracy (e.g.

14

measurement system misalignment (Mecheri et al. 2016), biomechanical modeling differences (Robert-Lachaine et al. 2016), soft-tissue artifacts (Cutti, Cappello, and Davalli 2006)) were not fully managed in Schall et al.'s work. The necessity of sensor fusion algorithms given the dynamics of human motion, the capability of sensor fusion algorithms to improve measurement accuracy, and the accuracy of motion-related risk assessment metrics due to sensor error, therefore, requires further investigation.

Another limitation of current studies is that the relationship between magnetic field strength variation and directional changes in the magnetic field has not been quantified. Despite this, magnetic field strength measurements are used to indicate periods of magnetic disturbance (Gabriele Ligorio et al. 2016; G. Ligorio and Sabatini 2015; Daniel Roetenberg et al. 2005) in recorded IMU data streams. Sensor fusion algorithms may also disregard magnetometer measurements when the magnetic field strength is outside a pre-determined threshold (Gabriele Ligorio and Sabatini 2016; Daniel Roetenberg et al. 2005; Sabatini 2006; Sun et al. 2013; Y. Tian, Wei, and Tan 2013). Recently, magnetic strength measurements were used in a machine learning algorithm to automate identification of valid IMU data segments (Lebel et al. 2016).

1.3 Summary and Specific Aims

Accurate exposure assessment methods are necessary to understand the relationship between physical risk factors and musculoskeletal disorders. Inertial measurement units (IMUs), a relatively new motion capture technology, are attractive to ergonomists due to their small size, relatively low cost, and ability to reliably capture information about worker movements across full working shifts. The current generation of gyroscopes used in these devices, however, are accurate for only short time periods. Time-dependent gyroscope errors are typically mitigated by using a sensor fusion algorithm that combines gyroscope measurements with accelerometer and magnetometer measurements. The accuracy of IMUs, therefore, is negatively affected by both increased motion speeds and localized magnetic disturbances. Consequently, whole-body motion capture in unconstrained environments over full working shifts may be unattainable based on current sensor technology.

The overall goal of this thesis was to (i) provide knowledge about the capabilities and limitations of IMUs to explain the inconsistencies observed in previous studies that assessed IMU accuracy and (ii)

provide guidance for the ergonomics community to leverage the potential benefits of IMUs for the purpose of exposure assessment given the current state of IMU technology.

The goal of the first study (**Specific Aim 1**) was to explain the inconsistencies observed in previous studies that assessed IMU accuracy. A limitation of current literature is the inconsistent error magnitudes reported, which can vary significantly (>15°) within studies (e.g. different task or sensor location) and across studies. We hypothesized IMU sensor accuracy is affected by increased motion speeds and magnetic disturbance. The objective of this study was to examine the effects of increased movement speeds and magnetic disturbance (and their interaction) on IMU spatial orientation accuracy.

The goal of the second study (**Specific Aim 2**) was to improve inclinometer accuracy. Ergonomists commonly use accelerometer-based inclinometers to quantify worker postures and movement velocities in field settings and for prolonged sampling durations (e.g., complete work shifts). IMU-based inclinometers that combine accelerometer and gyroscope measurements may significantly improve measurement accuracy compared accelerometer-based inclinometers, in particular with increased motion speeds. The primary objective of this study was to evaluate the effects of motion speed and sensor fusion algorithm on the accuracy of accelerometer- and IMU-derived upper arm elevation measurements. In addition, the impact on sensor fusion algorithm on metrics of upper arm elevation and velocity used in ergonomics exposure assessment was also explored.

The goal of the third study (**Specific Aim 3**) was to indirectly quantify the presence of magnetic disturbance. IMUs operate under the assumption of a homogenous local magnetic field. We hypothesize that when IMUs are used to quantify exposure to non-neutral postures over full working shifts in unconstrained environments, there will be data segments that will be adversely affected by magnetic disturbance. However, the homogeneity of the local magnetic field cannot be directly assessed without a reference device (e.g. OMC). Changes in magnetic field strength have been used to indicate periods of magnetic disturbance. However, the relationship between magnetic field strength and directional changes in the local magnetic field has never been quantified. We believe that variation in magnetic field strength could be used to indirectly assess the homogeneity of the magnetic field. This metric can be subsequently used to indirectly assess the accuracy of IMU-derived orientation measurements captured in unconstrained

www.manaraa.com

environments and used to identify data segments that are unaffected by magnetic disturbance. The specific objectives of this study were to (i) characterize the relationship between magnetic field strength variation and magnetic heading deviation and (ii) evaluate the effects of local magnetic disturbance and motion speed on the spatial orientation accuracy of IMUs in the context of repetitive distal upper extremity (upper arm, forearm, and hand) motion.

The subsequent chapters of this dissertation is structured as follows. Chapter 2 will provide a mathematical background pertaining IMU operation, including spatial orientation, sensor measurements, and device evaluation. Chapter 3 will examine the relationship between motion speed, magnetic disturbance, and IMU error. Chapter 4 will examine the error of upper arm elevation measurements calculated using various methods and its implication on exposure assessment metrics. Chapter 5 will examine the relationship between magnetic field strength variation and magnetic heading Chapter 6 will provide an overall conclusion.

CHAPTER 2

THEORETICAL BACKGROUND

The chapter will briefly discuss the equations used to describe spatial orientation, the operation of IMU sensors, sensor fusion algorithms, and methods to assess IMU accuracy. This chapter is largely based on several previously published works (Sabatini 2011a; Trawny and Roumeliotis 2005; Woodman 2007; Welch and Bishop 2006).

2.1 Spatial Orientation

The position and orientation of a rigid body is described using a series of translations and rotations with respect to a known position and orientation. The rigid body and the origin are both defined by establishing a coordinate frame, which consists of three mutually-orthogonal unit vectors. The orientation between the two coordinate frames is described using a rotation matrix.

2.1.1 Direction Cosine Matrix

Consider Frame A (2.1) with mutually orthogonal unit vectors $\vec{x}^A$, $\vec{y}^A$, $\vec{z}^A$. Each vector of Frame A consists of vector components x^A, y^A, z^A. Similarly, Frame B (2.2) consists of mutually-orthogonal unit vectors $\vec{x}^B$, $\vec{y}^B$, $\vec{z}^B$ with vector components x^B, y^B, z^B. The relationship between A and B is described by R_B^A in (2.3). R_B^A can also be calculated using the dot product (2.4). The dot product of two unit vectors is equivalent to the cosine of the angle between the two unit vectors, known as its direction cosine (2.5). Consequently, this matrix is known as the direction cosine matrix (DCM).

$$A = [\vec{x}^A \quad \vec{y}^A \quad \vec{z}^A] = \begin{bmatrix} x_1^A & x_2^A & x_3^A \\ y_1^A & y_2^A & y_3^A \\ z_1^A & z_2^A & z_3^A \end{bmatrix} \tag{2.1}$$

$$B = [\vec{x}^B \quad \vec{y}^B \quad \vec{z}^B] = \begin{bmatrix} x_1^B & x_2^B & x_3^B \\ y_1^B & y_2^B & y_3^B \\ z_1^B & z_2^B & z_3^B \end{bmatrix} \tag{2.2}$$

18

$$A = R_B^A B \tag{2.3}$$

$$R_B^A = AB^{-1} = \begin{bmatrix} \vec{x}^A \cdot \vec{x}^B & \vec{y}^A \cdot \vec{x}^B & \vec{z}^A \cdot \vec{x}^B \\ \vec{x}^A \cdot \vec{y}^B & \vec{y}^A \cdot \vec{y}^B & \vec{z}^A \cdot \vec{y}^B \\ \vec{x}^A \cdot \vec{z}^B & \vec{y}^A \cdot \vec{z}^B & \vec{z}^A \cdot \vec{z}^B \end{bmatrix} \tag{2.4}$$

$$\begin{bmatrix} \vec{x}^A \cdot \vec{x}^B & \vec{y}^A \cdot \vec{x}^B & \vec{z}^A \cdot \vec{x}^B \\ \vec{x}^A \cdot \vec{y}^B & \vec{y}^A \cdot \vec{y}^B & \vec{z}^A \cdot \vec{y}^B \\ \vec{x}^A \cdot \vec{z}^B & \vec{y}^A \cdot \vec{z}^B & \vec{z}^A \cdot \vec{z}^B \end{bmatrix} = \begin{bmatrix} cos\theta_{\vec{x}^A,\vec{x}^B} & cos\theta_{\vec{y}^A,\vec{x}^B} & cos\theta_{\vec{z}^A,\vec{x}^B} \\ cos\theta_{\vec{x}^A,\vec{y}^B} & cos\theta_{\vec{y}^A,y^B} & cos\theta_{\vec{z}^A,\vec{y}^B} \\ cos\theta_{\vec{x}^A,\vec{z}^B} & cos\theta_{\vec{y}^A,\vec{z}^B} & cos\theta_{\vec{z}^A,\vec{z}^B} \end{bmatrix} \tag{2.5}$$

The DCM possesses the following properties:

$$R^T R = I \tag{2.6}$$

$$det(R) = 1 \tag{2.7}$$

$$R^{-1} = R^T \tag{2.8}$$

where R^T is the transposition of R, and I is the identity matrix, and det is the matrix determinant.

The rotation matrix R_B^A, specifically, expresses the orientation of Frame A with respect to Frame B (Valenti, Dryanovski, and Xiao 2015). Similarly, R_A^B, defines the orientation of Frame B with respect to Frame A and is calculated using (2.9). The relationship between Frame A and B is defined in (2.10) and (2.11) for a vector with components $[x^B \quad y^B \quad z^B]^T$ in Frame B, and $[x^A \quad y^A \quad z^A]^T$ in Frame A.

$$R_A^B = (R_B^A)^T \tag{2.9}$$

$$[x^B \quad y^B \quad z^B]^T = R_A^B [x^A \quad y^A \quad z^A]^T \tag{2.10}$$

$$[x^A \quad y^A \quad z^A]^T = R_B^A [x^B \quad y^B \quad z^B]^T \tag{2.11}$$

The DCM is the foundation of spatial orientation. This representation, however, is non-intuitive and contains redundant parameters. The DCM is commonly converted to other representations of spatial orientations.

2.1.2 Euler Rotation

A more intuitive method to describe spatial orientation is with a series of three sequential elemental rotations. Specifically, the relationship between two coordinate frames is formed by establishing intermediary coordinate frames. These coordinate frames are created by rotating the previous coordinate frame a certain angle about its x-axis, y-axis, or z-axis. The DCM for a counter-clockwise (right-handed) elemental rotation around the x-axis (ϕ), y-axis (θ), and z-axis (ψ) of a coordinate frame is as follows:

$$R_x(\phi) = \begin{bmatrix} 1 & 0 & 0 \\ 0 & \cos\phi & -\sin\phi \\ 0 & \sin\phi & \cos\phi \end{bmatrix} \tag{2.12}$$

$$R_y(\theta) = \begin{bmatrix} \cos\theta & 0 & \sin\theta \\ 0 & 1 & 0 \\ -\sin\theta & 0 & \cos\theta \end{bmatrix} \tag{2.13}$$

$$R_z(\psi) = \begin{bmatrix} \cos\psi & -\sin\psi & 0 \\ \sin\psi & \cos\psi & 0 \\ 0 & 0 & 1 \end{bmatrix} \tag{2.14}$$

There are multiple rotation sequences since the Euler rotation is non-communicative. The DCM corresponding to a given Euler rotation sequence is obtained by applying (2.12), (2.13), and (2.14) in the desired order. A common rotation sequence is the aerospace rotation sequence, consisting of a rotation of ψ around the z-axis, followed by a rotation of θ around the y-axis, and a rotation of ϕ around the x-axis. The DCM for the aerospace rotation sequence and its transposition is shown in (2.15) and (2.16) respectively. The angle for this rotation sequence can be extracted from the DCM using (2.17).

$$R_B^A = R_z(\psi)R_y(\theta)R_x(\phi) = \begin{bmatrix} \cos\psi\cos\theta & \cos\psi\sin\theta\sin\phi - \cos\phi\sin\psi & \sin\psi\sin\phi + \cos\psi\cos\phi\sin\theta \\ \cos\theta\sin\psi & \cos\phi\cos\psi + \sin\theta\sin\phi\sin\psi & \cos\phi\sin\theta\sin\psi - \cos\psi\sin\phi \\ -\sin\theta & \cos\theta\sin\phi & \cos\theta\cos\phi \end{bmatrix} \tag{2.15}$$

$$R_A^B = (R_B^A)^T = R_x(-\phi)R_y(-\theta)R_z(-\psi) \tag{2.16}$$

$$\psi = \tan^{-1}(R_{21}/R_{11})$$

$$\theta = -\sin^{-1}(R_{31}) \tag{2.17}$$

$$\phi = \tan^{-1}(R_{32}/R_{33})$$

$$\text{where } R = \begin{bmatrix} R_{11} & R_{12} & R_{13} \\ R_{21} & R_{22} & R_{23} \\ R_{31} & R_{32} & R_{33} \end{bmatrix}$$

The Euler rotation is an intuitive method used to describe spatial orientation. However, (i) the Euler rotation requires specific definitions to be established with regards to the order of rotation and (ii) the use of Euler angles will cause gimbal lock, resulting in non-unique solutions. Specifically, gimbal lock occurs when the axis of the first rotation is parallel to the axis of the third rotation. In the aerospace rotation sequence, the z-axis and x-axis axis are parallel when the y-axis is rotated to $\pm 90°$. The result of gimbal lock is that a degree of freedom is lost. The sum of the angle of rotation around the z-axis and the angle of rotation around the x-axis is still relevant, but the individual angles are not, given that infinite solutions are possible.

2.1.3 Axis-angle representation

The relationship between two coordinate frames can also be described based on the direction and angle of rotation around a unit vector. The direction of rotation for unit vector $\vec{u}$ is given by the x- (u_x), y- (u_y), and z-components (u_z) of $\vec{u}$. The angle of rotation is specified by α, which is defined as a counter-clockwise rotation around $\vec{u}$. Given R_B^A, α and $\vec{u}$ can be calculated using (2.18) and (2.19), respectively, where $tr(R)$ is the trace function. Given α and $\vec{u}$, R_B^A can be calculated with (2.20), where $expm$ is the matrix exponential function. The main disadvantage of this representation is the non-trivial relationship between successive rotations.

$$\alpha = \cos^{-1}\left(\frac{tr(R) - 1}{2}\right) \tag{2.18}$$

$$\vec{u} = \frac{1}{2\sin(\alpha)}\begin{bmatrix} R_{32} - R_{23} \\ R_{13} - R_{31} \\ R_{21} - R_{12} \end{bmatrix} \tag{2.19}$$

$$R_B^A = expm(\alpha[\vec{u}\times]) \tag{2.20}$$

21

$$[\vec{u}\times] = \begin{bmatrix} 0 & -u_z & u_y \\ u_z & 0 & -u_x \\ -u_y & u_x & 0 \end{bmatrix}$$

(2.21)

2.1.4 Quaternions

The axis-angle representation is often parameterized with (2.22), which is known as a quaternion rotation vector. The quaternion vector contains a scalar component q_0 and vector component $\vec{\boldsymbol{q}}$. The scalar component is commonly defined as the first element of $\vec{q}$. However, it is also typical for the scalar component to be defined as the last element of $\vec{q}$ which will result in a different set of equations than those provided in this chapter.

$$\vec{q} = \begin{bmatrix} q_0 \\ \vec{\boldsymbol{q}} \end{bmatrix} = \begin{bmatrix} q_0 \\ q_1 \\ q_2 \\ q_3 \end{bmatrix} = \begin{bmatrix} \cos(\alpha/2) \\ \vec{u}\sin(\alpha/2) \end{bmatrix} = \begin{bmatrix} \cos(\alpha/2) \\ u_x\sin(\alpha/2) \\ u_y\sin(\alpha/2) \\ u_z\sin(\alpha/2) \end{bmatrix}$$

(2.22)

The quaternion equivalent of R_B^A is $\vec{q}_B^A$, which also describes the orientation of Frame A with respect to Frame B. The relationship between p_B (a 3-dimensional vector in Frame B) and p_A (a 3-dimensional vector in Frame A) in quaternions is defined as follows:

$$p_A = \vec{q}_B^A \otimes p_B \otimes \vec{q}_B^{A'}$$

(2.23)

$$p_B = \vec{q}_B^{A'} \otimes p_A \otimes \vec{q}_B^A$$

(2.24)

$$p_A = \begin{bmatrix} 0 & x^A & y^A & z^A \end{bmatrix}^T$$

(2.25)

$$p_B = \begin{bmatrix} 0 & x^B & y^B & z^B \end{bmatrix}^T$$

(2.26)

$$\vec{a} \otimes \vec{b} = \begin{bmatrix} a_0 \\ a_1 \\ a_2 \\ a_3 \end{bmatrix} \otimes \begin{bmatrix} b_0 \\ b_1 \\ b_2 \\ b_3 \end{bmatrix} = \begin{bmatrix} a_0b_0 - a_1b_1 - a_2b_2 - a_3b_3 \\ a_0b_1 + a_1b_0 + a_2b_3 - a_3b_2 \\ a_0b_2 - a_1b_3 + a_2b_0 + a_3b_1 \\ a_0b_3 + a_1b_2 - a_2b_1 + a_3b_0 \end{bmatrix}$$

(2.27)

$$\vec{q}' = \begin{bmatrix} q_0 \\ -\vec{\boldsymbol{q}} \end{bmatrix} = \begin{bmatrix} \cos\alpha & -u_x\sin\alpha & -u_y\sin\alpha & -u_z\sin\alpha \end{bmatrix}^T$$

(2.28)

22

where $\otimes$ is the quaternion product and q' is the quaternion conjugate of q (2.29). The quaternion conjugate is equivalent to the matrix transposition of a rotation matrix.

$$\vec{q}_A^B = \vec{q}_B^{A'} = \begin{bmatrix} q_0 \\ -\vec{q} \end{bmatrix}$$

(2.29)

The quaternion product can be written in expanded and condensed matrix form as follows:

$$\vec{a} \otimes \vec{b} = \begin{bmatrix} b_0 & -b_1 & -b_2 & -b_3 \\ b_1 & b_0 & b_3 & -b_2 \\ b_2 & -b_3 & b_0 & b_1 \\ b_3 & b_2 & -b_1 & b_0 \end{bmatrix} \begin{bmatrix} a_0 \\ a_1 \\ a_2 \\ a_3 \end{bmatrix} = \begin{bmatrix} a_0 & -a_1 & -a_2 & -a_3 \\ a_1 & a_0 & -a_3 & a_2 \\ a_2 & a_3 & a_0 & -a_1 \\ a_3 & -a_2 & a_1 & a_0 \end{bmatrix} \begin{bmatrix} b_0 \\ b_1 \\ b_2 \\ b_3 \end{bmatrix}$$

(2.30)

$$\vec{a} \otimes \vec{b} = \begin{bmatrix} a_0 \\ \vec{a} \end{bmatrix} \otimes \begin{bmatrix} b_0 \\ \vec{b} \end{bmatrix} = \begin{bmatrix} b_0 & -\vec{b}^T \\ \vec{b} & b_0 I_{3x3} - [\vec{b}\times] \end{bmatrix} \begin{bmatrix} a_0 \\ \vec{a} \end{bmatrix} = \begin{bmatrix} a_0 & -a^T \\ \vec{a} & a_0 I_{3x3} + [\vec{a}\times] \end{bmatrix} \begin{bmatrix} b_0 \\ \vec{b} \end{bmatrix}$$

(2.31)

where I_{3x3} is a 3x3 identity matrix. Equation (2.23) can be factored into (2.32), which implies the conversion from quaternion to DCM that is explicitly shown in (2.33).

$$\begin{bmatrix} x^A \\ y^A \\ z^A \end{bmatrix} = \begin{bmatrix} q_0^2 + q_1^2 - q_2^2 - q_3^2 & 2(q_1 q_2 - q_0 q_3) & 2(q_0 q_2 + q_1 q_3) \\ 2(q_0 q_3 + q_1 q_2) & q_0^2 - q_1^2 + q_2^2 - q_3^2 & 2(q_2 q_3 - 2q_0 q_1) \\ 2(q_1 q_3 - q_0 q_2) & 2(q_0 q_1 + q_2 q_3) & q_0^2 - q_1^2 - q_2^2 + q_3^2 \end{bmatrix} \begin{bmatrix} x^B \\ y^B \\ z^B \end{bmatrix}$$

(2.32)

$$R_B^A = \begin{bmatrix} q_0^2 + q_1^2 - q_2^2 - q_3^2 & 2(q_1 q_2 - q_0 q_3) & 2(q_0 q_2 + q_1 q_3) \\ 2(q_0 q_3 + q_1 q_2) & q_0^2 - q_1^2 + q_2^2 - q_3^2 & 2(q_2 q_3 - 2q_0 q_1) \\ 2(q_1 q_3 - q_0 q_2) & 2(q_0 q_1 + q_2 q_3) & q_0^2 - q_1^2 - q_2^2 + q_3^2 \end{bmatrix}$$

(2.33)

DCM can be converted into a quaternion using any of the following equations:

$$\begin{bmatrix} q_0 \\ q_1 \\ q_2 \\ q_3 \end{bmatrix} = \begin{bmatrix} 0.5\sqrt{1 + R_{11} + R_{22} + R_{33}} \\ (R_{32} - R_{23})/4q_0 \\ (R_{13} - R_{31})/4q_0 \\ (R_{21} - R_{12})/4q_0 \end{bmatrix}$$

(2.34)

$$\begin{bmatrix} q_0 \\ q_1 \\ q_2 \\ q_3 \end{bmatrix} = \begin{bmatrix} (R_{32} - R_{23})/4q_1 \\ 0.5\sqrt{1 + R_{11} - R_{22} - R_{33}} \\ (R_{12} + R_{21})/4q_1 \\ (R_{13} + R_{31})/4q_1 \end{bmatrix}$$

(2.35)

$$\begin{bmatrix} q_0 \\ q_1 \\ q_2 \\ q_3 \end{bmatrix} = \begin{bmatrix} (R_{13} - R_{31})/4q_2 \\ (R_{12} + R_{21})/4q_2 \\ 0.5\sqrt{1 - R_{11} + R_{22} - R_{33}} \\ (R_{23} + R_{32})/4q_2 \end{bmatrix} \tag{2.36}$$

$$\begin{bmatrix} q_0 \\ q_1 \\ q_2 \\ q_3 \end{bmatrix} = \begin{bmatrix} (R_{21} - R_{12})/4q_3 \\ (R_{13} + R_{31})/4q_3 \\ (R_{23} + R_{32})/4q_3 \\ 0.5\sqrt{1 - R_{11} - R_{22} + R_{33}} \end{bmatrix} \tag{2.37}$$

In each of the formulations, a quaternion component is calculated from the diagonal elements of the DCM, corresponding to q_0, q_1, q_2, and q_3 in (2.34), (2.35), (2.36), and (2.37), respectively, which is subsequently used to normalize the other quaternion components. The equation with the largest normalization factor is often used to alleviate the numerical instabilities when dividing by a small number.

The quaternion equivalent of (2.12), (2.13), and (2.14) is as follows:

$$\vec{q}_x(\phi) = [\cos(\phi/2) \quad \sin(\phi/2) \quad 0 \quad 0]^T \tag{2.38}$$

$$\vec{q}_y(\theta) = [\cos(\theta/2) \quad 0 \quad \sin(\theta/2) \quad 0]^T \tag{2.39}$$

$$\vec{q}_z(\psi) = [\cos(\psi/2) \quad 0 \quad 0 \quad \sin(\phi/2)]^T \tag{2.40}$$

Following the aerospace rotation sequence, the conversion from Euler angles to quaternions and from quaternions to Euler angles is obtained from (2.41) and (2.42), respectively.

$$\vec{q}_B^A = \vec{q}_z(\psi) \otimes \vec{q}_y(\theta) \otimes \vec{q}_x(\phi) = \begin{bmatrix} \cos(\psi/2)\cos(\theta/2)\cos(\phi/2) + \sin(\psi/2)\sin(\theta/2)\sin(\phi/2) \\ \cos(\psi/2)\cos(\theta/2)\sin(\phi/2) - \sin(\psi/2)\sin(\theta/2)\cos(\phi/2) \\ \cos(\psi/2)\sin(\theta/2)\cos(\phi/2) + \sin(\psi/2)\cos(\theta/2)\sin(\phi/2) \\ \sin(\psi/2)\cos(\theta/2)\cos(\phi/2) - \sin(\psi/2)\sin(\theta/2)\cos(\phi/2) \end{bmatrix} \tag{2.41}$$

$$\begin{bmatrix} \psi \\ \theta \\ \phi \end{bmatrix} = \begin{bmatrix} \tan^{-1}(2(q_0q_3 + q_1q_2)/(q_0^2 + q_1^2 - q_2^2 - q_3^2)) \\ \sin^{-1}(2(q_0q_2 - q_1q_3)) \\ \tan^{-1}(2(q_0q_1 + q_2q_3)/(q_0^2 - q_1^2 - q_2^2 + q_3^2)) \end{bmatrix} \tag{2.42}$$

2.1.5 Relative Orientation

In the context of IMUs, the orientation of the IMU is referenced to magnetic north and gravity. Given IMU measurements from two IMU units attached to adjacent body segments, the relative orientation

between the IMUs (R_C^B) can be calculated using (2.44) based on the relationship defined in (2.43), where R_B^A and R_C^A are the orientation provided by the IMU attached to the proximal and distal body segments, respectively. The quaternion equivalent is shown in (2.45) and (2.46), respectively..

$$R_C^A = R_B^A R_C^B$$

(2.43)

$$R_C^B = (R_B^A)^T R_C^A$$

(2.44)

$$\vec{q}_C^A = \vec{q}_B^A \otimes \vec{q}_C^B$$

(2.45)

$$\vec{q}_C^B = \vec{q}_B^{A'} \otimes \vec{q}_C^A$$

(2.46)

Spatial orientation can be described using various methods that are interchangeable. Euler rotation sequences are the most intuitive, but are order dependent and susceptible to singularities and gimbal lock. DCM describes spatial orientation on a fundamental level, but is non-intuitive and contains redundant parameters. Quaternion-based rotations can concisely represent spatial orientations without singularities with four parameters instead of 9. Consequently, spatial orientation is frequently represented using quaternions for IMUs.

2.2 Calculating Spatial Orientation

Spatial orientation (R_B^A) can be computed from vector measurements, or by integrating rotational velocities with respect to time. Vector-based calculations encompass spatial orientation calculated using an optical motion capture system (OMC) and using the combination of an accelerometer and magnetometer. Spatial orientation can be calculated deterministically given two vectors or through optimization-based approaches when provided with more than two vectors. The relationship defined in (2.1) is considered when calculating spatial orientation deterministically. This is expanded as follows:

$$[\vec{x}^A \quad \vec{y}^A \quad \vec{z}^A] = R_B^A[\vec{x}^B \quad \vec{y}^B \quad \vec{z}^B]$$

(2.47)

2.2.1 Optical Motion Capture Systems

A deterministic solution to OMC measurements is to define the local coordinate frame (Frame B) by attaching three markers (m_1, m_2, m_3) onto a rigid object or body segment. The first unit vector of the local coordinate frame ($\vec{x}^B$) is established as follows:

$$\vec{x}^B = (m_2 - m_1)/\|(m_2 - m_1\| \tag{2.48}$$

where $\|\cdot\|$ is the Euclidean norm operator. The construction of the second unit vector ($\vec{y}^B$) requires an intermediary unit vector and the cross product ($\times$) to establish a vector that is perpendicular to $\vec{x}^B$.

$$\vec{y}^B = \vec{x}^B \times (m_3 - m_1))/\|\vec{x}^B \times (m_3 - m_1))\| \tag{2.49}$$

The third vector of the coordinate frame ($\vec{z}^B$) is simply the cross product of $\vec{x}^B$ and $\vec{y}^B$.

$$\vec{z}^B = \vec{x}^B \times \vec{y}^B \tag{2.50}$$

The local frame is defined subsequently defined as

$$B = [\vec{x}^B \quad \vec{y}^B \quad \vec{z}^B] \tag{2.51}$$

The vectors are defined in the global frame (Frame A) is as follows:

$$\vec{x}^A = [1 \quad 0 \quad 0]^T \tag{2.52}$$

$$\vec{y}^A = [0 \quad 1 \quad 0]^T \tag{2.53}$$

$$\vec{z}^A = [0 \quad 0 \quad 1]^T \tag{2.54}$$

Given that $[\vec{x}^A \quad \vec{y}^A \quad \vec{z}^A]$ is an identity matrix, R_B^A becomes the following:

$$R_B^A = [\vec{x}^B \quad \vec{y}^B \quad \vec{z}^B]^T \tag{2.55}$$

This approach can also be extended to deriving spatial orientation using a combination of accelerometer and magnetometer measurements.

2.2.2.1 Accelerometers and Magnetometers

Similarly, the vectors in the body frame $(\vec{x}^B, \vec{y}^B, \vec{z}^B)$ can be defined using accelerometer measurements $\vec{a}^B = (a_x, a_y, a_z)$ and magnetometer measurements $\vec{m}^B = (m_x, m_y, m_z)$ as follows:

$$\vec{x}^B = \vec{a}^B / \|\vec{a}^B\| \tag{2.56}$$

$$\vec{y}^B = (\vec{x}^B \times \vec{m}^B) / \|\vec{x}^B \times \vec{m}^B\| \tag{2.57}$$

$$\vec{z}^B = (\vec{x}^B \times \vec{y}^B) \tag{2.58}$$

The vectors are defined in the global frame (Frame A) as follows:

$$\vec{x}^A = [0 \quad 0 \quad 1]^T \tag{2.59}$$

$$\vec{y}^A = [0 \quad 1 \quad 0]^T \tag{2.60}$$

$$\vec{z}^A = [-1 \quad 0 \quad 0]^T \tag{2.61}$$

The spatial orientation is calculated using the relationship defined in (2.1).

$$R_B^A = [\vec{x}^A \quad \vec{y}^A \quad \vec{z}^A][\vec{x}^B \quad \vec{y}^B \quad \vec{z}^B]^T \tag{2.62}$$

Alternatively, the relationship established in (2.10) can be extended to accelerometer measurements (2.63) since the sensing element of an accelerometer will register gravitational acceleration (g) in the z-direction in the global frame under static conditions.

$$[0 \quad 0 \quad g]^T = R_B^A [a_x \quad a_y \quad a_z]^T \tag{2.63}$$

R_B^A is solved by converting it to an Euler rotation sequence using (2.64) to account for the matrix dimension mismatch.

$$[0 \quad 0 \quad g]^T = R_z(\psi)R_y(\theta)R_x(\phi)[a_x \quad a_y \quad a_z]^T \tag{2.64}$$

27

Equation (2.75) can be expanded by applying (2.15) as following:

$$\begin{bmatrix} 0 \\ 0 \\ g \end{bmatrix} = \begin{bmatrix} \cos\psi\cos\phi & \cos\psi\sin\theta\sin\phi - \cos\phi\sin\psi & \sin\psi\sin\phi + \cos\psi\cos\phi\sin\theta \\ \cos\theta\sin\psi & \cos\phi\cos\psi + \sin\theta\sin\phi\sin\psi & \cos\phi\sin\theta\sin\psi - \cos\psi\sin\phi \\ -\sin\theta & \cos\theta\sin\phi & \cos\theta\cos\phi \end{bmatrix} \begin{bmatrix} a_x \\ a_y \\ a_z \end{bmatrix} \tag{2.65}$$

Equation (2.76) can be reordered using the relationship defined in (2.9) and (2.11), which results in (2.66) and can be further simplified into (2.67).

$$\begin{bmatrix} a_x \\ a_y \\ a_z \end{bmatrix} = \begin{bmatrix} \cos\psi\cos\phi & \cos\theta\sin\psi & -\sin\theta \\ \cos\psi\sin\theta\sin\phi - \cos\phi\sin\psi & \cos\phi\cos\psi + \sin\theta\sin\phi\sin\psi & \cos\theta\sin\phi \\ \sin\psi\sin\phi + \cos\psi\cos\phi\sin\theta & \cos\phi\sin\theta\sin\psi - \cos\psi\sin\phi & \cos\theta\cos\phi \end{bmatrix} \begin{bmatrix} 0 \\ 0 \\ g \end{bmatrix} \tag{2.66}$$

$$\begin{bmatrix} a_x \\ a_y \\ a_z \end{bmatrix} = \begin{bmatrix} -g\sin\theta \\ g\cos\theta\sin\phi \\ g\cos\theta\cos\phi \end{bmatrix} \tag{2.67}$$

Gravity is defined as the vector magnitude of the accelerometer measurements to ensure values are within the domain of the trigonometric functions. Pitch and roll measurements are calculated by solving (2.67), resulting in (2.68) and (2.69), respectively.

$$\theta_{accel} = \sin^{-1}\left(a_x / \sqrt{a_x^2 + a_y^2 + a_z^2} \right) = \tan^{-1}\left(-a_x / \sqrt{a_y^2 + a_z^2} \right) \tag{2.68}$$

$$\phi_{accel} = \tan^{-1}\left(a_y / a_z \right) \tag{2.69}$$

It can be inferred from (2.68) that rotation around the gravity axis is unavailable. Consequently, a second observation vector is required, which is offered by a magnetometer. Heading from the magnetometer is generally calculated after rotating the magnetometer measurements (m_x, m_y, m_z) to align with gravity using accelerometer measurement (2.70) to ensure magnetometer measurements do not affect inclination angles. Heading is subsequently calculated using (2.71), which can be simplified into (2.72). The measurements can be converted into a rotation matrix using (2.73) or into a quaternion vector with (2.41). Additional methods to combine accelerometer and magnetometers are discussed elsewhere (Valenti, Dryanovski, and Xiao 2015; Yun, Bachmann, and McGhee 2008). A limitation of the presented methods is that both increased motion speeds and magnetic disturbance will affect heading measurements.

$$[M_x \quad M_y \quad M_z]^T = R_y(\theta)R_x(\phi)[m_x \quad m_y \quad m_z]^T \tag{2.70}$$

$$\psi = \tan^{-1}\left(-M_y/M_x\right) \tag{2.71}$$

$$\psi = \tan^{-1}\left(\frac{m_z \sin\phi - m_y \cos\phi}{m_x \cos\theta + m_y \sin\theta \sin\phi + m_z \sin\theta \cos\phi}\right) \tag{2.72}$$

$$R_B^A = R_z(\psi)R_y(\theta)R_x(\phi) \tag{2.73}$$

<u>2.2.2.2 Gyroscopes</u>

A MEMS-based gyroscope is considered an angular rate sensor. Given angular rotation rates ω_x, ω_y, ω_z from a tri-axial gyroscope and a sampling time period of Δt, spatial orientation can be calculated as follows:

$$\vec{q}_{OLF,i}^{OGF} = \vec{q}_{OLF,i-1}^{OGF} \otimes \vec{q}\Delta t \tag{2.74}$$

where

$$\vec{q}\Delta t = [\cos(\Delta\alpha/2) \quad u_x \sin(\Delta\alpha/2) \quad u_y \sin(\Delta\alpha/2) \quad u_z \sin(\Delta\alpha/2)]^T \tag{2.75}$$

$$\Delta\alpha = \sqrt{\omega_x^2 + \omega_y^2 + \omega_z^2}/\Delta t \tag{2.76}$$

$$\vec{u} = \begin{bmatrix} u_x \\ u_y \\ u_z \end{bmatrix} = \left[\omega_x\Big/\sqrt{\omega_x^2 + \omega_y^2 + \omega_z^2} \quad \omega_y\Big/\sqrt{\omega_x^2 + \omega_y^2 + \omega_z^2} \quad \omega_z\Big/\sqrt{\omega_x^2 + \omega_y^2 + \omega_z^2}\right]^T \tag{2.77}$$

Typically, the quaternion rate of rotation is calculated using a first order approximation (2.78), which can be condensed into (2.79). The derivation of (2.78) is shown elsewhere (Gośliński, Nowicki, and Skrzypczyński 2015). This measurement is subsequently integrated with respect to time to obtain spatial orientation measurements.

$$\dot{q} = \frac{1}{2}q\otimes\omega = \begin{bmatrix} \dot{q}_0 \\ \dot{q}_1 \\ \dot{q}_2 \\ \dot{q}_3 \end{bmatrix} = \frac{1}{2}\begin{bmatrix} q_0 \\ q_1 \\ q_2 \\ q_3 \end{bmatrix} \otimes \begin{bmatrix} 0 \\ \omega_x \\ \omega_y \\ \omega_z \end{bmatrix} = \frac{1}{2}\begin{bmatrix} 0 & -\omega_x & -\omega_y & -\omega_z \\ \omega_x & 0 & \omega_z & -\omega_y \\ \omega_y & -\omega_z & 0 & \omega_x \\ \omega_z & \omega_y & -\omega_x & 0 \end{bmatrix}\begin{bmatrix} q_0 \\ q_1 \\ q_2 \\ q_3 \end{bmatrix} \tag{2.78}$$

$$\dot{q} = \Omega q$$

$$\Omega = \frac{1}{2}\begin{bmatrix} 0 & -\vec{\omega}^T \\ \vec{\omega} & -[\omega \times] \end{bmatrix} \tag{2.79}$$

Given discrete measurements in equally spaced time intervals, spatial orientation is calculated using (2.80) under the assumption that the angular velocity is constant between each sampling interval (zeroth-order integrator) or with (2.81) under the assumption that the change in angular velocity between each sampling interval is linear (first-order integrator). Equation (2.82) is obtained by substituting (2.78) into (2.81), which can be condensed into (2.83).

$$q_{k+1} = expm(\Omega_k \Delta t) q_k \tag{2.80}$$

$$q_{k+1} = \dot{q} \Delta t + q_k \tag{2.81}$$

$$q_{k+1} = \begin{bmatrix} 1 & -0.5\omega_x\Delta t & -0.5\omega_y\Delta t & -0.5\omega_z\Delta t \\ 0.5\omega_x\Delta t & 1 & 0.5\omega_z\Delta t & -0.5\omega_y\Delta t \\ 0.5\omega_y\Delta t & -0.5\omega_z\Delta t & 1 & 0.5\omega_x\Delta t \\ 0.5\omega_z\Delta t & 0.5\omega_y\Delta t & -0.5\omega_x\Delta t & 1 \end{bmatrix} \begin{bmatrix} q_{0,k} \\ q_{1,k} \\ q_{2,k} \\ q_{3,k} \end{bmatrix} \tag{2.82}$$

$$q_{k+1} = \left(0.5 \begin{bmatrix} 0 & -\vec{\omega}^T \\ \vec{\omega} & -[\omega \times] \end{bmatrix} \Delta t + I_{4x4} \right) q_k \tag{2.83}$$

A MEMS gyroscope contains the following error model (Chang et al. 2008; Xue et al. 2012):

$$\omega_{measured} = \omega_{true} + b_\omega + v_\omega \tag{2.84}$$

$$b_{\omega,k+1} = b_{\omega,k} + \dot{b}_\omega \Delta t \tag{2.85}$$

where the gyroscope noise v_ω and bias b_ω are both stochastic. The change in gyroscope bias rate $\dot{b}_\omega$ and white gyroscope noise v_ω are assumed to follow a normal distribution with a mean of zero and variances of σ_ω^2 and $\sigma_{\dot{b}}^2$, respectively.

$$v_\omega \sim N(0, \sigma_\omega^2) \tag{2.86}$$

$$\dot{b}_\omega \sim N(0, \sigma_{\dot{b}}^2) \tag{2.87}$$

2.2.3 Kalman Filter

The Kalman filter estimates its parameters based on the stochastic properties of the system. The filter contains a process model (2.88) and measurement model (2.89). The Kalman filter will provide optimal estimates to the parameters of interest for a linear system when the process noise (w_{k-1}) and measurement noise (v_k) follow a normal distribution with a mean of zero and variances of Q and R, respectively (Bachmann 2000).

$$x_k = Ax_{k-1} + Bu_{k-1} + w_{k-1} \tag{2.88}$$

$$z_k = Hx_k + v_k \tag{2.89}$$

$$p(w) \sim N(0, Q) \tag{2.90}$$

$$p(v) \sim N(0, R) \tag{2.91}$$

The process model (2.88) predicts x_k, a column vector containing the parameters of interest based on prior estimate x_{k-1} and control variable u_{k-1}. Matrices A and B relate x_{k-1} and u_{k-1} to x_k, respectively. The measurement model (2.89) compares x_k to sensor measurements z_k, where H is a matrix that relates x_k to z_k.

The implementation of the Kalman filter is a series of five recursive equations:

$$x_k^- = Ax_{k-1} + Bu_{k-1} \tag{2.92}$$

$$P_k^- = AP_{k-1}A^T + Q \tag{2.93}$$

$$K_k = P_k^- H^T (HP_k^- H^T + R)^{-1} \tag{2.94}$$

$$x_k = x_k^- + K_k(z_k - Hx_k^-) \tag{2.95}$$

$$P_k = (I - K_k H) P_k^- \tag{2.96}$$

Where I is the identity matrix, x_k^- is the predicted value of x_k, P_k^- is the predicted estimation error covariance, P_k is the updated estimation error covariance, and K_k is the Kalman gain calculated from Q and R.

Given the non-linear process and measurement equations:

$$x_k = f(x_{k-1}, u_{k-1}, w_{k-1}) \tag{2.97}$$

$$z_k = g(x_k, v_k) \tag{2.98}$$

The EKF can be applied as follows:

$$x_k^- = f(x_{k-1}, u_{k-1}, 0) \tag{2.99}$$

$$P_k^- = AP_{k-1}A^T + W_k Q_{k-1} W_k^T \tag{2.100}$$

$$K_k = P_k^- H^T (HP_k^- H^T + V_k Q_k V_k^T)^{-1} \tag{2.101}$$

$$x_k = x_k^- + K_k(z_k - g(x_k^-, 0)) \tag{2.102}$$

$$P_k = (I - K_k H) P_k^- \tag{2.103}$$

where A, W, H, and V are all Jacobin matrices. Matrix A contains the partial derivatives of f with respect x, W contains the partial derivatives of f with respect to w, H contains the partial derivatives of h with respect to x, and V contains the partial derivatives of h with respect to v.

The Kalman filter is often implemented by considering (2.97) and (2.98) as follows:

$$x_k = Fx_{k-1} + W_{k-1} w_{k-1} \tag{2.104}$$

$$z_k = Gx_{k-1} + V_k v_k \tag{2.105}$$

Consequently, (2.99) and (2.102) are modified to (2.106) and (2.107), respectively. Specific Kalman Filter designs will be presented in subsequent sections.

$$x_k^- = Fx_{k-1} \tag{2.106}$$

$$x_k = x_k^- + K_k(z_k - Gx_k^-) \tag{2.107}$$

32

A complementary filter combines measurements based on spectral characteristics. In this application, the complementary filter combines the low-frequency component of the vector measurements with the high frequency component of gyroscope measurements. In a simple case, the transfer function (s) for an angle derived using the complementary filter (ϑ_{comp}) is as follows (Zhi 2016):

$$\vartheta_{comp} = \frac{1}{1 + Ts}\vartheta_{accel} + \frac{Ts}{1 + Ts}\frac{1}{s}\dot{\vartheta} = \frac{\vartheta_{accel} + T\dot{\vartheta}}{1 + Ts} \tag{2.108}$$

where T determines the filter cutoff frequency, ϑ_{accel} is the accelerometer-derived measurement angle, and ω is the corresponding angular velocity measured by the gyroscope. Taking the backward difference results in the final equation.

$$\vartheta_{comp,k} = (1 - \alpha)\left(\vartheta_{comp,k-1} + \dot{\vartheta}_{k-1}\Delta t\right) + \alpha\vartheta_{accel,k} \tag{2.109}$$

Alternatively, the linear Kalman process (2.88) and measurement (2.89) equations can be formulated as follows:

$$\vartheta_k = \vartheta_{k-1} + \dot{\vartheta}_{k-1}\Delta t + w_{k-1} \tag{2.110}$$

$$\vartheta_{accel} = \vartheta_k + v_k \tag{2.111}$$

When implementing the Kalman filter, (2.92) and (2.95) reduces to

$$\vartheta_k = (1 - K_k)\left(\vartheta_{k-1} + \dot{\vartheta}_{k-1}\Delta t\right) + K_k\vartheta_{accel,k} \tag{2.112}$$

which has the same characteristic equation as the Complementary filter.

2.3 Assessing IMU error

Misalignment between OMC and IMU-derived orientation measurements must be managed since it can lead to over-estimation of IMU error. In theory, if q_{IGF}^{OGF}, the offset between the IMU global frame (IGF) and OMC global frame (OGF) is known, and if q_{OLF}^{ILF}, the offset between the IMU local frame (ILF) and OMC local frame (OLF) is known, the OMC-derived orientation measurements ($q_{OGF}^{OLF}(t)$) will be equal to the IMU-derived orientation measurements ($q_{IGF}^{ILF}(t)$).

$$q_{OLF}^{OGF}(t) = q_{IGF}^{OGF} \otimes q_{ILF}^{IGF}(t) \otimes q_{OLF}^{ILF}$$

(2.113)

One method to obtain these offsets is to solve q_{IGF}^{OGF} and q_{OLF}^{ILF} separately. The local offset (q_{OLF}^{ILF}) can be solved using angular rate measurements (Chardonnens, Favre, and Aminian 2012; de Vries et al. 2009). Given spatial orientation measurements, angular rate measurements from the OMC can be solved algebraically through (2.75), (2.76), and (2.77) by rearranging (2.74) as follows:

$$\vec{q}\Delta t = (\vec{q}_{OLF,i-1}^{OGF})' \otimes \vec{q}_{OLF,i}^{OGF}$$

(2.114)

The relationship in (2.115) was considered once OMC-derived angular rate measurements ($\omega_{OMC,x}$, $\omega_{OMC,y}$, $\omega_{OMC,z}$) were obtained. R_{OLF}^{ILF} was solved using (2.116) where -p is the pseudoinverse function.

$$\begin{bmatrix} \omega_{OMC,x,i} & & \omega_{OMC,x,n} \\ \omega_{OMC,y,i} & \cdots & \omega_{OMC,y,n} \\ \omega_{OMC,z,i} & & \omega_{OMC,z,n} \end{bmatrix} = R_{OLF}^{ILF} \begin{bmatrix} \omega_{x,i} & & \omega_{x,n} \\ \omega_{y,i} & \cdots & \omega_{y,n} \\ \omega_{z,i} & & \omega_{z,n} \end{bmatrix} \quad i = 1\ldots n$$

(2.115)

$$R_{OLF}^{ILF} = \begin{bmatrix} \omega_{OMC,x,i} & & \omega_{OMC,x,n} \\ \omega_{OMC,y,i} & \cdots & \omega_{OMC,y,n} \\ \omega_{OMC,z,i} & & \omega_{OMC,z,n} \end{bmatrix} \begin{bmatrix} \omega_{x,i} & & \omega_{x,n} \\ \omega_{y,i} & \cdots & \omega_{y,n} \\ \omega_{z,i} & & \omega_{z,n} \end{bmatrix}^{-p} \quad i = 1\ldots n$$

(2.116)

q_{IGF}^{OGF} was obtained from (2.117) using q_{ILF}^{IGF} derived from accelerometer measurements and magnetometer measurements (2.73) under static conditions at sample j, its corresponding OMC measurements at sample j, and the relationship established in (2.113).

$$R_{IGF}^{OGF} = R_{OLF}^{OGF}(j)(R_{ILF}^{IGF}(j)R_{OLF}^{ILF})^{-1}$$

(2.117)

The difference between IMU and OMC measurements at each sample is often quantified as the linear difference between the OMC-derived Euler angle ($\vartheta_{OMC,i}$) and IMU-derived Euler angle ($\vartheta_{IMU,i}$) (Schall Jr. et al. 2015; Schall et al. 2015).

$$d_i = \vartheta_{OMC,i} - \vartheta_{IMU,i}$$

(2.118)

A limitation of using the linear difference when quantifying IMU accuracy is to the occurrence of singularities. Consequently, more recent research has used the rotational difference between IMU and OMC spatial orientation measurements, which is consistent with joint angle calculations (Faber et al. 2013;

34

Gabriele Ligorio et al. 2016). Specifically, the sample-to-sample rotational difference $q_{d_i}(t)$ is defined as the offset between the global coordinates of the OMC and IMU after sensor alignment.

$$q_{d_i}(t) = q_{OLF}^{OGF}(t) \otimes q_{ILF}^{IGF}(t)' \tag{2.119}$$

q_{d_i} can subsequently be decomposed to Euler angles to provide a more relevant measurement.

The sample-to-sample difference can be averaged by calculating the root-mean-square error.

$$RMSE = \sqrt{\frac{1}{n}\sum_{i}^{n} d_i^2} \tag{2.120}$$

Bland and Altman limits of agreement (LoA) are also commonly used to quantify errors within each trial, which consist of the average and spread of the sample-to-sample differences (Schall Jr. et al. 2015; Robert-Lachaine et al. 2016). Other metrics to quantify IMU accuracy include the correlation of multiple correlation (CMC), and waveform distortion (WD) (Robert-Lachaine et al. 2016).

CHAPTER 3

EFFECTS OF MOTION SPEED AND MAGNETIC DISTURBANCE ON THE ACCURACY OF INERTIAL MEASUREMENT UNITS

3.1 Introduction

Accelerometers have for years been used in ergonomics field studies to describe the inclination of the trunk and upper arms with respect to the gravity vector (i.e., pitch angle) and the horizon (i.e., roll angle) (Åkesson et al. 1997; Fahrenberg et al. 1997). However, accelerometers are (i) most accurate when the motion to be assessed are static or quasi-static, and (ii) unable to capture information regarding motions about the gravity vector (i.e., heading angle) (Amasay et al. 2009; Bernmark and Wiktorin 2002). Without heading angles, accelerometers are not useful for measuring postures and movements of joints when a reference to gravity and the horizon cannot be reasonably assumed (e.g., flexion/extension of the wrist can occur with the wrist in any orientation with respect to gravity and the horizon). Inertial measurement units (IMUs), which package accelerometers with gyroscopes and magnetometers, are theoretically able to overcome the limitations of accelerometer-based measurement through the use of sensor fusion algorithms such as Kalman filters.

For field-based occupational ergonomics applications, IMUs are attractive due to their small size, relatively low cost, and ability to reliably capture information about worker posture and movement across full working shifts (Schall et al. 2015). These attributes are important, for example, when designing exposure assessment campaigns to estimate exposure to physical risk factors associated with musculoskeletal outcomes in epidemiological studies, or to facilitate quantitative evaluations of interventions. Commercial IMU-based motion capture systems are increasingly available and marketed to ergonomists. However, commercial systems typically use proprietary sensor fusion algorithms not well-understood by many ergonomics practitioners. Moreover, the accuracy of IMU-based motion capture remains an important issue.

Several studies have compared metrics of joint kinematics obtained using IMUs to those obtained using optical motion capture (Cloete and Scheffer 2008; Kim and Nussbaum 2013; Robert-Lachaine et al. 2016; Cuesta-Vargas, Galán-Mercant, and Williams 2010; Godwin, Agnew, and Stevenson 2009). For example, Cloete and Scheffer (2008) observed errors <6° for hip flexion/extension, but >15° for ankle rotation. Similarly, Godwin et al., (2009) reported errors >20° (i) between different body segments within the same task and (ii) within the same body segment between different tasks. While these studies are immediately applicable to practitioners, error magnitudes are influenced by the biomechanical models used. Robert-Lachaine et al., (2016) observed that differences in protocol between the IMU and OMC can account for differences >40°, while the actual sensor error was <5°. In addition, the use of commercial hardware with proprietary algorithms for converting raw IMU data to kinematic constructs limits the generalizability of these studies' results beyond potentially idiosyncratic commercial solutions.

The spatial orientation of IMUs (i.e., heading, pitch and roll angles rather than kinematic variables) is often presented when (i) developing and comparing sensor fusion algorithms and (ii) assessing factors that can negatively affect IMU accuracy. Such studies have generally reported greater accuracy (<6° average error) (Bergamini et al. 2014; Faber et al. 2013; Lebel et al. 2013; Gabriele Ligorio et al. 2016; Ricci, Taffoni, and Formica 2016) than those reporting kinematic variables. Spatial orientation is theoretically obtainable with a gyroscope. However, gyroscopes built using micro-electromechanical systems and packaged with IMUs are inaccurate, leading to time-dependent error known as gyroscopic drift. Deviations >10° per minute have been observed (Bergamini et al. 2014; Luinge, Veltink, and Baten 2007). Alternatively, IMU spatial orientation can be derived with respect to gravity and magnetic north assuming the measured acceleration is due solely to gravity and a homogenous local magnetic field (Yun, Bachmann, and McGhee 2008; Valenti, Dryanovski, and Xiao 2015). These measurements are considered time-invariant, but can be adversely affected by highly dynamic motion and fluctuations within the local magnetic field (Amasay et al. 2009; Bernmark and Wiktorin 2002; de Vries et al. 2009; Lebel et al. 2013) leading to deviations up to 180° (Bachmann, Yun, and Peterson 2004). Sensor fusion algorithms are used to address the limitations of these two methods. Regardless of the fusion algorithm, the primary source of information is generally the gyroscope, while accelerometer and magnetometer measurements are used to remove gyroscopic drift (Yun and Bachmann 2006). Dynamic and magnetic disturbances are often

37

attenuated through increased reliance on gyroscope measurements with the expectation of time-dependent errors during periods of disturbance (Gabriele Ligorio and Sabatini 2016; Daniel Roetenberg et al. 2005; Sabatini 2006; Sessa et al. 2012).

The primary objective of this pilot study was to examine the effects of movement speed and magnetic disturbance (and their interaction) on IMU spatial orientation accuracy during a repetitive upper extremity task. In order to extend generalizability, IMU spatial orientation was calculated using both non-proprietary and proprietary Kalman filter approaches. The potential benefit of estimating inclination using an IMU with sensor fusion compared to an accelerometer-only approach was also explored.

3.2 Methods

3.2.1 Participants

Thirteen participants (11 male; mean age= 27.2 ± 6.6 years; right-hand dominant) were recruited from the local community. Participants self-reported no history of orthopedic surgery in the upper extremity (shoulder, elbow, wrist, and hand), no physician-diagnosed musculoskeletal disorders disorder in the past six months, and no musculoskeletal pain in the two weeks prior to enrollment. The University of Iowa Institutional Review Board approved all study procedures, and informed consent was obtained from all participants.

3.2.2 Experimental Task

The experimental task (Figure 3.1) involved transferring wooden dowels (2 cm diameter x 8 cm length) for one minute from a waist-level container located directly in front of the participant to a shoulder-level container placed 45° diagonally with respect to the sagittal and frontal planes. Three levels of movement speed were assigned: 'slow' (15 cycles/min), 'medium' (30 cycles/min), and 'fast' (45 cycles/min). Pacing was controlled using a metronome. A metal plate (30.5 cm x 10 cm x 0.6 cm) was placed within the shoulder-level container to create a local magnetic field disturbance. Each participant

www.manaraa.com

performed six trials of the task, once at each of the three movement speeds both with and without the metal plate. Experimental conditions were randomized to control for potential order effects. Participants were given time to acclimate to the motion speeds before each trial began. Each one-minute trial was followed by a rest period of five minutes.
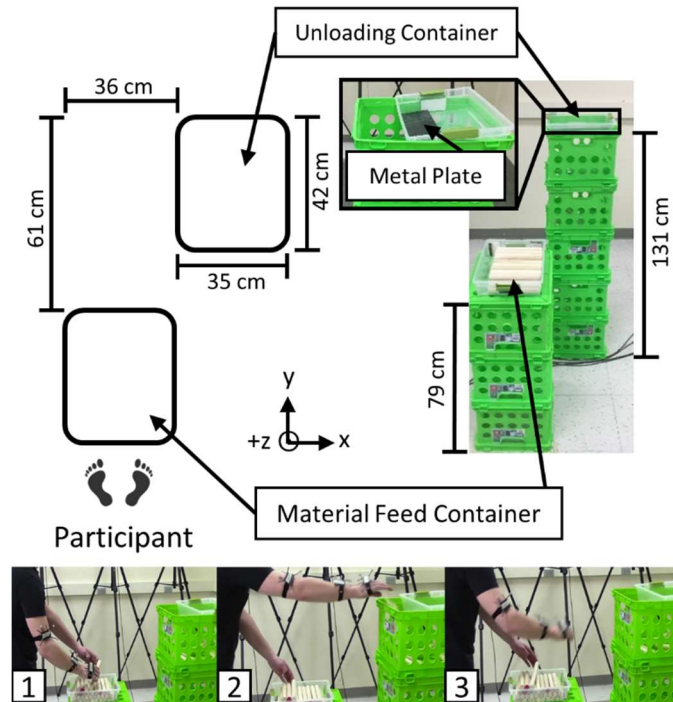
Figure 3.1. Experimental setup. Each transfer cycle consisted of (1) grasping a wooden dowel, (2) transferring the dowel to the unloading container, and (3) returning the hand back to the material feed container to grasp the next dowel.

3.2.3 Instrumentation and Data Processing

The spatial orientation of the hand was simultaneously measured using an IMU (SXT, Nexgen Ergonomics, Inc., Pointe Claire, Quebec, CA) and a six-camera OMC system (Optitrack Flex 13, NaturalPoint, Inc., Corvallis, OR, USA) that tracked a rigid marker cluster attached to the IMU surface (Figure 3.2). The IMU and OMC data were recorded at 128 Hz and 120 Hz, respectively (the maximum sampling rates for each system). Raw IMU data at each sample included acceleration, angular velocity, and magnetic field strength (all tri-axial), as well as a quaternion rotation vector a consisting of a real component (q_0) and imaginary components (q_1, q_2, q_3) output by a proprietary, embedded Kalman filter. Raw OMC data at each sample (i.e., spatial position of the marker cluster) were converted to a quaternion

39

rotation vector using the manufacturer's software (Motive, NaturalPoint, Inc., Corvallis, OR, USA). The fundamental objective of all post-processing was to calculate the spatial orientation of the IMU and of the OMC marker cluster using the Euler rotation convention of heading (ψ), pitch (θ), and roll (ϕ) angles. The IMU spatial orientation was estimated with three approaches: (i) using the raw IMU data streams (i.e., acceleration, angular velocity, and magnetic field strength) without sensor fusion, (ii) using modifications of a published, non-proprietary sensor fusion algorithm, and (iii) using the quaternion output from the IMU's embedded and proprietary Kalman filter. The spatial orientation derived from the OMC marker cluster was calculated using the quaternion output of the OMC system software. All other post-processing was accomplished using MATLAB (2016a, Mathworks, Natick, MA). The raw IMU data were down-sampled to 120 Hz to match the OMC sampling rate.

Figure 3.2. IMU and its associated marker
cluster attached to the hand of a participant

3.2.3.1 IMU spatial orientation: no sensor fusion.

IMU pitch (θ) and roll (ϕ) angles are calculated from the accelerometer output (a_x, a_y, a_z) using Equations (3.1) and (3.2).

$$\theta = \tan^{-1}\left(-a_x / \sqrt{a_y^2 + a_z^2}\right) \tag{3.1}$$

$$\phi = \tan^{-1}\left(a_y / a_z\right) \tag{3.2}$$

Heading angle (ψ, i.e., rotation around gravity) was calculated using the pitch and roll measurements combined with the magnetometer output (m_x, m_y, m_z) according to (3.3).

$$\psi = \tan^{-1}\left(\frac{m_z \sin\phi - m_y \cos\phi}{m_x \cos\theta + m_y \sin\theta \sin\phi + m_z \sin\theta \cos\phi}\right) \qquad (3.3)$$

The raw accelerometer data stream was low-pass filtered (2nd order Butterworth, 3 Hz corner frequency) prior to the Euler rotation angle calculations. Pitch and roll angles calculated without sensor fusion are described hereafter using the designation "Accel". Heading angles calculated using raw magnetometer measurements (m_x, m_y, m_z) are described hereafter using the designation "Mag." Heading measurements calculated using Mag contained pitch and roll measurements obtained from the non-proprietary sensor fusion algorithm to mitigate the effects of increased movement speeds on heading error.

3.2.3.2 IMU spatial orientation: non-proprietary sensor fusion

A Kalman filter that separated the gravity vector from linear acceleration (given gyroscope and accelerometer measurements) was used to compute the acceleration magnitudes as inputs into (3.1) and (3.2). Pitch and roll angles calculated in this manner are described hereafter using the designation "Accel-KF." Similarly, a Kalman filter that separated the magnetic north vector from transient magnetic field strength fluctuation (given gyroscope and magnetometer measurements) was used to compute the magnetic field strength magnitudes as inputs into (3.4). Heading angles calculated in this manner are described hereafter using the designation "Mag-KF." These Kalman filters were direct implementations of the "Linear Kalman Filter" that was previously proposed (Gabriele Ligorio and Sabatini 2015) and recently extended to account for magnetic disturbance (Gabriele Ligorio and Sabatini 2016). The Accel-KF and Mag-KF implemented, specifically, contain an identical Kalman Filter design but with different filter parameters. This filter was chosen based on simplicity in filter design and implementation.

Generally, the Kalman Filter contains a process model (3.4) and measurement model (3.5). The process model estimates x_k, a column vector containing the parameters of interest, from prior estimate x_{k-1} with a random variation of w_{k-1}. A and W are matrices that relate x_{k-1} and w_{k-1} to x_k, respectively. The measurement model compares x_k to sensor measurements z_k, where H is a matrix that relates x_k to z_k, and v_k is the random variation within the measurement model. The random process parameters w_{k-1} and v_k are assumed to follow normal distributions of $N(0, Q)$ and $N(0, R)$, respectively.

41

$$x_k = Ax_{k-1} + W_{k-1}w_{k-1} \tag{3.4}$$

$$z_k = Hx_k + v_k \tag{3.5}$$

The implementation of the Kalman filter is a series of five recursive equations:

$$x_k^- = Ax_{k-1} \tag{3.6}$$

$$P_k^- = AP_{k-1}A^T + W_kQW_k^T \tag{3.7}$$

$$K_k = P_k^-H^T(HP_k^-H^T + R)^{-1} \tag{3.8}$$

$$x_k = x_k^- + K_k(z_k - Hx_k^-) \tag{3.9}$$

$$P_k = (I - K_kH)\,P_k^- \tag{3.10}$$

where I is the identity matrix, P_k is the estimation error covariance, and K_k is the Kalman gain calculated from Q and R. The process equation (3.4) and measurement equation (3.5) for this implementation becomes the following:

$$\begin{bmatrix} g_i^b \\ a_i^b \end{bmatrix} = \begin{bmatrix} expm(-[\omega_{i-1}^b\times]\Delta t) & 0_{3x3} \\ 0_{3x3} & c_aI_{3x3}a_{i-1}^b \end{bmatrix}\begin{bmatrix} g_{i-1}^b \\ a_{i-1}^b \end{bmatrix} + \begin{bmatrix} -\Delta t[g_{i-1}^b\times] & 0_{3x3} \\ 0_{3x3} & c_bI_{3x3} \end{bmatrix}\begin{bmatrix} w_{i-1}^\omega \\ w_{i-1}^{gm} \end{bmatrix} \tag{3.11}$$

$$\begin{bmatrix} a_x \\ a_y \\ a_z \end{bmatrix} = \begin{bmatrix} I_{3x3} & I_{3x3} \end{bmatrix}\begin{bmatrix} g_i^b \\ a_i^b \end{bmatrix} + v_i^a \tag{3.12}$$

where g^b is direction of gravity vector and a^b is the acceleration separated by the filter when given gyroscope measurements $(\omega_x, \omega_y, \omega_z)$ and accelerometer measurements (a_x, a_y, a_z). Gauss Markov parameters c_a and c_b determine the separation of gravity from linear acceleration. The process covariance matrix (Q) and the measurement covariance matrix (R) is defined as follows:

$$Q = \begin{bmatrix} I_{3x3}\sigma_\omega^2 & 0_{3x3} \\ 0_{3x3} & I_{3x3} \end{bmatrix} \tag{3.13}$$

$$R = I_{3x3}\sigma_a^2 \tag{3.14}$$

where σ_ω^2 and σ_a^2 is the white gyroscope and accelerometer noise variance, respectively. Both are assumed to follow a normal statistical distribution with a mean of zero. The filter tuning parameters (Table 3.1) were obtained experimentally.

Table 3.1. Kalman filter parameters.

	Process Noise	**Measurement Noise**	**c_a**	**c_b**
Accel-KF	0.005 rad/s	0.008 m/s^2	0.3	0.08
Mag-KF	0.005 rad/s	0.3 μT	0.1	0.5

3.2.3.3 IMU Spatial Orientation: Embedded Kalman Filter

Equation (3.15) was used to convert the quaternion rotation vector output from the IMU's embedded Kalman filter to heading, pitch, and roll angles. The angles calculated in this manner are described hereafter with the designation "Em-KF."

$$\begin{bmatrix} \psi \\ \theta \\ \phi \end{bmatrix} = \begin{bmatrix} \tan^{-1}(2(q_0 q_3 + q_1 q_2)/(q_0^2 + q_1^2 - q_2^2 - q_3^2)) \\ \sin^{-1}(2(q_0 q_2 - q_1 q_3)) \\ \tan^{-1}(2(q_0 q_1 + q_2 q_3)/(q_0^2 - q_1^2 - q_2^2 + q_3^2)) \end{bmatrix} \tag{3.15}$$

The raw OMC orientation measurements were first low-pass filtered (2nd order Butterworth, 6 Hz corner frequency). Then, the quaternion rotation vector output from the OMC system software was converted to heading, pitch, and roll angles using (3.15).

3.2.3.4 Error Calculation

The offset between the local coordinate frames of the OMC and the IMU was calculated using angular rate measurements according to de Vries et al., (2010). After applying the local offset, the offset between the global coordinate frames of the OMC and the IMU was determined under static conditions using IMU-derived orientation using the Mag approach. For each trial, the root-mean-square difference (RMSD) between the IMU- and OMC-derived heading, pitch, and roll angles was calculated as:

$$RMSD_\vartheta = \sqrt{\frac{1}{n}\sum_{i=1}^{n}\left(\vartheta_{OMC,i} - \vartheta_{IMU,i}\right)^2} \tag{3.16}$$

43

where i is the sample number, n is the number of samples, and ϑ_{OMC} and ϑ_{IMU} are the Euler rotation angles measured by the OMC and IMU, respectively.

3.2.4 Statistical Analysis

Two-factor repeated measures analyses of variance were used to estimate the effects of movement speed, magnetic disturbance, and their interaction on estimates of RMSD in the heading, pitch, and roll directions. The Greenhouse-Geisser correction was used to adjust for violations of sphericity. All statistical analyses were performed using SPSS Statistics 23 (IBM, SPSS, Chicago, Illinois, USA).

3.3 Results

3.3.1 RMSD in the Pitch and Roll Directions

The motion trajectory of the IMU for a single trial is shown in Figure 3.3. Regardless of the IMU spatial orientation estimation approach, neither the main effect of magnetic disturbance nor the interaction between movement speed and magnetic disturbance on RMSD was significant in the pitch and roll directions. The main effect of movement speed on RMSD in pitch and roll, however, was significant for the Accel and Accel-KF approaches but not for the Em-KF approach (Table 3.2). In general, mean RMSD increased with increasing movement speed; large increases (4° during the 'slow' condition to 24° during the 'fast' condition) were observed when using the Accel approach and small increases (1.1° to 1.9°) when using the Accel-KF approach. For the 'medium' and 'fast' movement speeds, using a Kalman filter (i.e., either the Accel-KF or Em-KF approach) to estimate pitch and roll reduced RMSD by an order of magnitude compared to using only the accelerometer (i.e, the Accel approach). Sample-to-sample differences between OMC and IMU pitch measurements were not time-dependent (Figure 3.4).
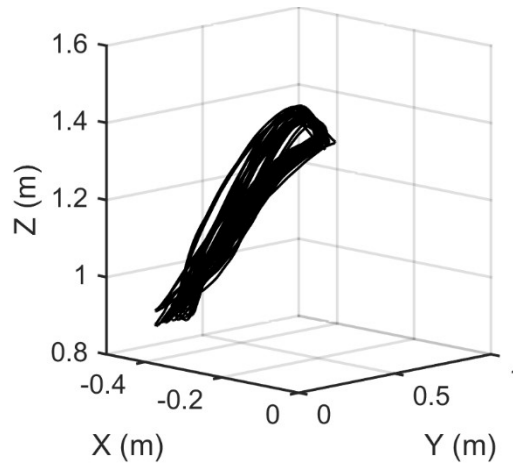
Figure 3.3. The motion trajectory of a single participant performing the task at 'medium' work speed without the presence of the metal plate. Measurements are calculated from the OMC marker cluster attached to the IMU located on the hand.

Table 3.2. Mean (SD) root-mean-square differences in pitch and roll (°) calculated using an accelerometer (Accel), a linear Kalman filter (Accel-KF) and an embedded proprietary Kalman Filter (Em-KF).

	Slow	Med	Fast	*p*-value
Pitch				
Accel	4.0(0.7)	11.3(1.7)	24.0(2.5)	<0.01
Accel-KF	1.1(0.5)	1.5(0.5)	1.9(0.4)	<0.01
Em-KF	1.5(0.8)	1.8(1.2)	1.7(0.9)	
Roll				
Accel	3.1(0.8)	6.4(1.7)	12.6(3.8)	<0.01
Accel-KF	1.0(0.5)	1.4(0.5)	1.5(0.5)	<0.01
Em-KF	2.2(1.4)	2.6(2.1)	2.1(1.4)	
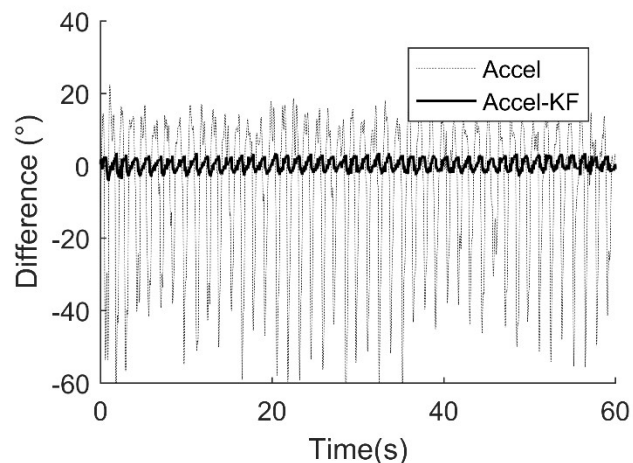
Figure 3.4. Sample-to-sample difference between OMC and IMU-derived pitch measurements during the 'fast' movement speed condition; IMU pitch angle estimated using the accelerometer data only (Accel) and a linear Kalman filter (Accel-KF)

45

For one participant, the heading RMSD from two trials processed using the Em-KF approach was more than four standard deviations greater than the mean heading angle RMSD across all subjects and testing conditions. These measurements were considered outliers and discarded from the analysis. Regardless of the IMU spatial orientation estimation approach, neither the main effect of movement speed nor the interaction between movement speed and magnetic disturbance on RMSD was significant in the heading direction. The main effect of magnetic disturbance on RMSD in the heading direction was significant for Mag, confirming that the metal plate altered the local magnetic field. The metal plate also adversely affected heading angle RMSD for both sensor fusion algorithms (Mag-KF, and Em-KF) (Table 3.3) although the proprietary Em-KF performed somewhat better than the non-proprietary Mag-KF. Sample-to-sample differences between OMC and IMU heading measurements were time-dependent when using sensor fusion, particularly the Em-KF (Figure 3.5).

Table 3.3. Mean (SD) root-mean-square difference in heading (°) calculated using a magnetometer (Mag), a linear Kalman filter (Mag-KF) and an embedded proprietary Kalman Filter (Em-KF).

	w/o Metal	w/Metal	*p*-value
Mag	3.3(1.0)	17.0(4.5)	<0.01
Mag-KF	4.1(1.9)	11.6(4.0)	<0.01
Em-KF	4.3(2.1)	7.0(4.1)	<0.05
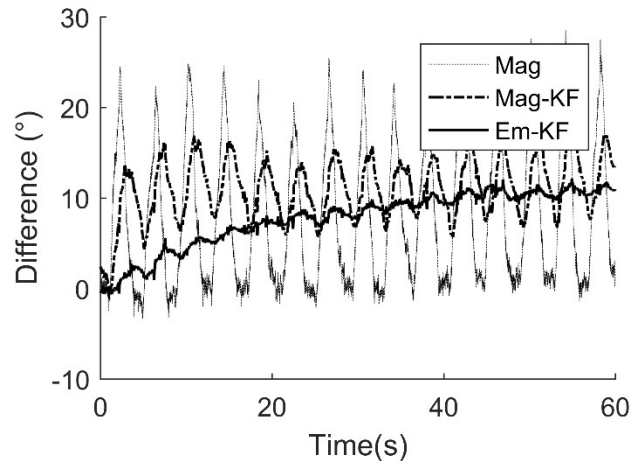
Figure 3.5. Sample-to-sample difference between OMC and IMU-derived heading measurements during the 'slow' movement speed; IMU heading angle was estimated using the magnetometer only (Mag), a linear Kalman filter (Mag-KF) and a proprietary embedded Kalman filter (Em-KF).

46

Consistent with other studies, pitch and roll angles estimated using only an accelerometer were less accurate as movement speed increased (Korshøj et al. 2014). This is primarily a function of increased tangential and centripetal acceleration magnitudes (Bernmark and Wiktorin 2002). While the accuracy of pitch and roll using the Accel-KF approach was influenced by movement speed, the magnitude of mean RMSD between the 'slow' and 'fast' movement speed was negligible ($<1°$). Both sensor fusion algorithms reduced RMSD in the pitch and roll directions to $<3°$across all movement speed conditions, which is consistent with previous studies (Gabriele Ligorio and Sabatini 2016; Bergamini et al. 2014; Gabriele Ligorio and Sabatini 2015). This finding suggests that IMU-derived inclination measurements improved measurement accuracy compared to accelerometer-derived inclination measurements commonly used to quantify non-neutral postures in the workplace within the context of occupational ergonomics.

The mean RMSD in the heading direction in testing conditions without the metal plate ($<5°$ RMSD) was consistent with previous studies ($<6°$) (Faber et al. 2013; Lebel et al. 2013; Bergamini et al. 2014; Gabriele Ligorio et al. 2016). As anticipated, the presence of the metal plate degraded the heading angle accuracy, though to a lesser extent when sensor fusion was used. We suspect that the addition of magnetic disturbance compensation strategies (e.g., vector selection) would improve measurement accuracy under the presence of magnetic disturbance. However, it is unlikely that sensor fusion algorithms would eliminate magnetic disturbances as long as magnetometers remain the source of information regarding orientation about the gravity vector.

3.5 Conclusion

The use of IMUs in field-based ergonomics research is expected to increase as hardware development accelerates and more commercial options are available. We did not observe an interaction between movement speed and magnetic disturbance on the accuracy of IMU spatial orientation in this study. We observed substantially greater accuracy in IMU pitch and roll angles when using sensor fusion compared to using an accelerometer alone. This finding is important, as it suggests the increase in technical complexity when using an IMU with sensor fusion (vs. an accelerometer only) is offset by meaningful

improvements in measurement accuracy for describing the postures and movements of certain body segments, especially in dynamic situations with fast motion speeds. Another key observation is that the non-proprietary Kalman filters used in this study performed similarly to the embedded, proprietary Kalman filter packaged with the IMU hardware (although somewhat poorer with magnetic disturbance). Making such open-source processing alternatives available to the ergonomics community can, over time, reduce the reliance on proprietary solutions and improve the comparability within IMU-based research. The algorithms and MATLAB code used in this study will be made available (see Appendix C). Finally, the full potential of IMU-based motion capture for field research is not likely to be realized without methods to identify and/or minimize the effects of local magnetic field disturbances.

CHAPTER 4

ACCURACY OF ANGULAR DISPLACEMENTS AND VELOCITIES FROM INERTIAL-BASED INCLINOMETERS

4.1 Introduction

Measuring human motion with accuracy and precision is critical for many applications in occupational ergonomics, such as estimating exposure to non-neutral working postures (Douphrate et al. 2012) and evaluating workplace designs (Fethke, Gant, and Gerr 2011). Human motion is most accurately quantified using laboratory-based electromagnetic or optical motion capture systems (OMC). However, high equipment costs and constrained recording areas prevent such systems from deployment in field-based occupational research (Cuesta-Vargas, Galán-Mercant, and Williams 2010; Sabatini 2006).

Electrogoniometers and inclinometers are frequently used in workplace settings to directly measure human motion, particularly the motions of the distal upper extremity (Fethke et al. 2012; Asundi, Johnson, and Dennerlein 2012; Balogh et al. 2009; Cook, Burgess-Limerick, and Papalia 2004). An electrogoniometer is a mechanical device that spans a human joint and measures its angular displacement (Buchholz and Wellman 1997). Single-axis, dual-axis, and tri-axial elecrogoniometers are available to accommodate measurement of angular displacement in multiple movement planes (e.g., dual-axis devices are used to measure flexion/extension and radial/ulnar deviation of the wrist). Electrogonimeters, however, may restrict the natural movement of a joint, causing measurement error and potential misinterpretation of the results (Buckle and Jason Devereux 2002; Buchholz and Wellman 1997; Jonsson and Johnson 2001). Piezoresistive accelerometers are used as inclinometers to measure the angular displacement of the trunk and upper arm with respect to gravity (Fethke, Gant, and Gerr 2011; Fethke et al. 2016). Dual-axis and tri-axial accelerometers are most commonly used for this purpose (Douphrate et al. 2012; Fethke, Gant, and Gerr 2011; Fethke et al. 2016; Hess et al. 2010). Accelerometer-based inclinometers, however, (i) are adversely affected by increased motion speeds and (ii) cannot accurately capture rotation about the gravity vector (heading), which is important for capturing joint angles of the wrist and elbow and to separate the motion planes for the trunk and shoulder (Bernmark and Wiktorin 2002; Amasay et al. 2009; Korshøj et al.

2014). Inertial measurement units (IMUs) overcome these limitations, in theory, through the addition of gyroscopes and magnetometers.

An IMU measures the orientation of an object in three-dimensional space using a sensor fusion algorithm (e.g. Kalman filter) to combine measurements from solid-state gyroscopes, accelerometers, and magnetometers (Yun, Bachmann, and McGhee 2008; Daniel Roetenberg et al. 2005; Sun et al. 2013). Joint angle measurements can be subsequently calculated based on the relative orientation of two IMUs attached to adjacent body segments (Martori et al. 2013). Modern IMU hardware often packages the sensors with long-life batteries and onboard flash memory to enable prolonged data logging functionality. Thus, with respect to field-based research, IMUs are attractive for posture measurements because of their unobtrusive size, low system cost, durability, and ability to collect data over full working shifts (Douphrate et al. 2012). While studies have shown that these systems can be highly accurate (<6° average error) (Bergamini et al. 2014; Faber et al. 2013; Kim and Nussbaum 2013; Plamondon et al. 2007; Robert-Lachaine et al. 2016), magnetic disturbance and increased motion speeds will negatively affect IMU accuracy (Lebel et al. 2013; Ricci, Taffoni, and Formica 2016; Bachmann, Yun, and Peterson 2004; de Vries et al. 2009). In particular, fluctuations within the local magnetic field expected in unconstrained environments can lead to deviations of 180° (Bachmann, Yun, and Peterson 2004).

Strategies such as magnetic field rejection (Sun et al. 2013; Sabatini 2006; Gabriele Ligorio and Sabatini 2016), zero velocity updating (Schiefer et al. 2014), and kinematic modeling (El-Gohary and McNames 2012; El-Gohary and McNames 2015; Miezal, Taetz, and Bleser 2016), have been implemented within sensor fusion algorithms to improve the accuracy of IMU-based motion capture. These approaches, however, can only compensate for magnetic disturbances over short measurement durations (minutes) (El-Gohary and McNames 2015; Lebel et al. 2015). Consequently, and despite considerable research concerning IMU-based motion capture and continued improvements to IMU hardware, systems capable of recording full three-dimensional motion for longer time periods (hours) in unconstrained environments have been largely elusive. Given the current capabilities of inertial-based motion capture systems and the advantages in cost and practicality associated with single-device solutions, several researchers have instead focused on using sensor fusion algorithms to attenuate motion-related artifacts in an effort to improve

50

inclinometer accuracy (Lee, Park, and Robinovitch 2012; Gabriele Ligorio and Sabatini 2015; Schall Jr. et al. 2015; Schall et al. 2015).

Several studies have reported accurate (<5°) IMU-derived angular displacement measurements (Gabriele Ligorio and Sabatini 2015; Bergamini et al. 2014; Lee, Park, and Robinovitch 2012; Gabriele Ligorio and Sabatini 2016). However, none of these studies have reported the accuracy of (i) accelerometer-derived angular displacement measurements, (ii) angular velocity measurements, or (iii) posture and movement summary measures used for health-based decision making in the context of occupational ergonomics. Thus, the ability of IMU-based inclinometers to improve measurement accuracy compared to established accelerometer-based approaches remains unknown. Previous work provided direct comparisons of accelerometer and IMU-based inclinometers to an electrogoniometer used to measure trunk motion (Schall Jr. et al. 2015) and to a biomechanical-based optical motion capture system (Schall et al. 2015). The results showed (i) higher errors in the IMU measurements relative to the reference device (5-9° depending on motion plane and body segment) compared to previous studies and (ii) marginal differences between accelerometer-based and IMU-based inclination measurements. However, error sources not reflective of sensor accuracy (e.g. measurement system misalignment (Mecheri et al. 2016), biomechanical modeling differences (Robert-Lachaine et al. 2016), soft-tissue artifacts (Cutti, Cappello, and Davalli 2006)) were not fully managed in Schall et al.'s work. Furthermore, the similarities in measurement accuracy between accelerometer and IMU-based inclinometers reported in previous studies may be due to a combination of relatively slow motion speeds and sub-optimal sensor fusion tuning parameters that relied on accelerometer measurements more than necessary.

The primary objective of this study was to evaluate the effects of motion speed and sensor fusion algorithm on the accuracy of accelerometer- and IMU-derived upper arm elevation measurements. In addition, the impact on sensor fusion algorithm on metrics of upper arm elevation and velocity used in ergonomics exposure assessment was also explored.

4.2 Methods

4.2.1 Participants

Thirteen participants were recruited from the University of Iowa community. All participants (11 male, mean age= 27.2 ± 6.6 years, right-handed dominant) were screened for any self-reported cases of: (i) physician-diagnosed musculoskeletal disorder in the past six months, (ii) pain for the previous two weeks prior to enrollment, and (iii) medical history of orthopedic surgery in the upper extremity (shoulder, elbow, wrist, hand). Each participant provided written informed consent prior to participation. The University of Iowa Institutional Review Board approved all study procedures.

4.2.2 Task

Each participant completed six trials of a simulated work task that involved transferring wooden dowels (2 cm diameter x 8 cm length) from a waist-high container in front of the participant to a shoulder-height container located 45° diagonally from the participant (Figure 4.1). Each transfer required the participant to (i) grasp the dowel, (ii) transfer the dowel to the unloading container, and (iii) return to the material feed container. Each participant completed two trials at the given material transfer rate: slow (15 cycles/min), medium (30 cycles/min), and fast (45 cycles/min). The transfer rate was controlled using a metronome and experimental conditions were randomized to control for potential order effects. Each participant was given time to acclimate to the assigned motion speed before each trial was captured. Each trial was one minute in duration and was followed by a rest period of five minutes.

Figure 4.1. Placement of the waist-height container holding the wooden dowels and the shoulder-height container.

4.2.3 Instrumentation

An IMU (series SXT, Nexgen Ergonomics, Inc., Pointe Claire, Quebec, CA) was secured to the lateral aspect of the dominant upper arm midway between the acromion and the lateral epicondyle (Figure 4.2). Accelerometer, gyroscope, and spatial orientation measurements (quaternions from an embedded Kalman filter) were captured from the IMU at 128 Hz. Spatial orientation was also simultaneously recorded using a six-camera OMC system (Optitrack Flex 13, NaturalPoint, Inc., Corvallis, OR, USA) that tracked a cluster of four reflective markers mounted to the surface of the IMU with double-sided tape (Figure 4.2). This was used in contrast to a biomechanical-based marker set to control for soft-tissue artifacts in order to isolate sensor error. The OMC measurements were recorded at 120 Hz. Calibration of the IMU and OMC instrumentation systems was performed using manufacturer-specified procedures.

53

Figure 4.2. IMU and its associated marker cluster attached to the upper arm of a participant

4.2.4 Data Processing

The spatial orientation derived from the OMC marker cluster was calculated using the quaternion output of the OMC system software. All post-processing was accomplished using MATLAB (2016a, Mathworks, Natick, MA). The raw IMU data were down-sampled to 120 Hz to match the OMC sampling rate.

The upper arm elevation displacement was calculated by adding an offset to the inclination angle with respect to the gravity axis (θ). Upper arm angular velocity ($\dot{\theta}$) was calculated using the derivative of the upper arm elevation displacements with respect to time.

$$\theta_{ele} = \theta + 90° \tag{4.1}$$

$$\dot{\theta} = (\theta_i - \theta_{i-1})/\Delta t \tag{4.2}$$

IMU inclination angles pitch (θ) and roll (ϕ) were calculated using five different approaches: (i) using accelerometer measurements without sensor fusion, (ii) using a relatively simple first-order complementary filter, (iii) using a widely-implemented second-order complementary filter, (iv) using modifications of a published, non-proprietary sensor fusion algorithm, and (v) using the quaternion output from the IMU's embedded and proprietary Kalman filter.

54

4.2.4.1 Accelerometer-derived Displacements

IMU pitch (θ) and roll (ϕ) angles were calculated from the accelerometer output (a_x, a_y, a_z) using (4.3) and (4.4).

$$\theta = \tan^{-1}\left(-a_x\Big/\sqrt{a_y^2 + a_z^2}\right) \tag{4.3}$$

$$\phi = \tan^{-1}\left(a_y/a_z\right) \tag{4.4}$$

The raw accelerometer data stream was low-pass filtered (2nd order Butterworth, 3 Hz corner frequency) prior to the angle calculations. Pitch and roll angles calculated without sensor fusion are described using the designation "Accel".

4.2.4.2 First-order Complementary Filter

The first-order complementary filter contains the following structure (Roan et al. 2012):

$$\vartheta_{comp,i} = (1-\alpha)\left(\vartheta_{comp,i-1} + \dot{\vartheta}_i \Delta t\right) + \alpha\vartheta_{accel,i} \tag{4.5}$$

where $\vartheta_{comp,i}$ is the angle derived from the complementary filter, $\vartheta_{accel,i}$ is the angle derived from the accelerometer measurements, $\dot{\vartheta}_i$ is the rotational velocity, Δt is the sensor sampling period, and α is the filter tuning parameter. The tuning parameter, α is assigned a value between 0 and 1 (0 would rely solely on gyroscope-derived inclination measurements, and 1 would rely solely on accelerometer-derived inclination measurements). Equation (4.5) is written in terms of pitch and roll measurements as follows:

$$\begin{bmatrix} \theta_i \\ \phi_i \end{bmatrix} = \begin{bmatrix} 1-\alpha_\theta & 0 \\ 0 & 1-\alpha_\phi \end{bmatrix}\begin{bmatrix} \theta_{i-1} + \dot{\theta}\Delta t \\ \phi_{i-1} + \dot{\phi}\Delta t \end{bmatrix} + \begin{bmatrix} \alpha_\theta & 0 \\ 0 & \alpha_\phi \end{bmatrix}\begin{bmatrix} \theta_{accel} \\ \phi_{accel} \end{bmatrix} \tag{4.6}$$

where $\dot{\theta}$ and $\dot{\phi}$ are calculated using gyroscope measurements (ω_x, ω_y, ω_z) and the complementary filtered inclination measurements, as shown in (4.7).

$$\begin{bmatrix} \dot{\theta} \\ \dot{\phi} \end{bmatrix} = \begin{bmatrix} \omega_y \cos\phi - \omega_z \sin\phi \\ \omega_x + \omega_y \sin\phi \tan\theta + \omega_z \cos\phi \tan\theta \end{bmatrix} \tag{4.7}$$

Our first-order complementary filter was obtained by substituting (4.3), (4.4), and (4.7) into (4.6).

$$\begin{bmatrix} \theta_i \\ \phi_i \end{bmatrix} = \begin{bmatrix} (1 - \alpha_\theta)\left(\theta_{i-1} + \left(\omega_y \cos\phi_{i-1} - \omega_z \sin\phi_{i-1}\right)\Delta t\right) + \alpha_\theta \tan^{-1}\left(-a_x / \sqrt{a_y^2 + a_z^2}\right) \\ (1 - \alpha_\phi)\left(\phi_{i-1} + \left(\omega_x + \omega_y \sin\phi_{i-1}\tan\theta_{i-1} + \omega_z \cos\phi_{i-1}\tan\theta_{i-1}\right)\Delta t\right) + \alpha_\phi \tan^{-1}\left(a_y/a_z\right) \end{bmatrix} \quad (4.8)$$

For this study, both α_θ and α_ϕ were each assigned a value of 0.01, based on visual inspection of the complementary filter results and the OMC data. Pitch and roll angles calculated using the first-order complementary filter are described using the designation "Comp-1".

4.2.4.3 Second-order Complementary Filter

The design of the second-order complementary filter was a direct implementation of the filter developed by Madgwick et al., (2011). A detailed explanation can be found elsewhere (Mourcou et al. 2015; Madgwick, Harrison, and Vaidyanathan 2011). Equation (4.9) was used to convert the quaternion rotation vector output from the second-order complementary filter heading, pitch, and roll angles. For this study, the filter parameter β was assigned a value of 0.13. The angles calculated in this manner are described with the designation "Comp-2."

$$\begin{bmatrix} \psi \\ \theta \\ \phi \end{bmatrix} = \begin{bmatrix} \tan^{-1}\left(2(q_0 q_3 + q_1 q_2)/(q_0^2 + q_1^2 - q_2^2 - q_3^2)\right) \\ \sin^{-1}\left(2(q_0 q_2 - q_1 q_3)\right) \\ \tan^{-1}\left(2(q_0 q_1 + q_2 q_3)/(q_0^2 - q_1^2 - q_2^2 + q_3^2)\right) \end{bmatrix} \quad (4.9)$$

4.2.4.4 Kalman Filter: non-proprietary

The Extended Kalman Filter used in this study contains the generic process model (4.10) and measurement model (4.11). The process model estimates x_k, a column vector containing the parameters of interest, from prior estimate x_{k-1} with a random variation of w_{k-1}. The matrices F and W relate x_{k-1} and w_{k-1} to x_k, respectively. The measurement model compares x_k to sensor measurements z_k, where G is a matrix that relates x_k to z_k, and v_k is the random variation within the measurement model. The random parameters w_{k-1} and v_k are assumed to follow normal distributions of $p(w) \sim N(0, Q)$ and $p(v) \sim N(0, R)$, respectively.

56

www.manaraa.com

$$x_k = Fx_{k-1} + W_{k-1}w_{k-1} \tag{4.10}$$

$$z_k = Gx_{k-1} + V_kv_k \tag{4.11}$$

The implementation of the Kalman filter consists of a series of five recursive equations:

$$x_k^- = Fx_{k-1} \tag{4.12}$$

$$P_k^- = AP_{k-1}A^T + W_kQW_k^T \tag{4.13}$$

$$K_k = P_k^-H^T(HP_k^-H^T + V_kQ_kV_k^T)^{-1} \tag{4.14}$$

$$x_k = x_k^- + K_k(z_k - Gx_k^-) \tag{4.15}$$

$$P_k = (I - K_kH)\,P_k^- \tag{4.16}$$

where I is the identity matrix, P_k is the estimation error covariance, and K_k is the Kalman gain calculated from Q and R. Matrices A, W, H, and V are all Jacobin matrices. Matrix A contains the partial derivatives of F with respect x, W contains the partial derivatives of F with respect to w, H contains the partial derivatives of G with respect to x, and V contains the partial derivatives of G with respect to v.

The Kalman Filter implemented was modified from a validated Linear Kalman Filter (Gabriele Ligorio and Sabatini 2015). The filter was designed to discriminate the direction of gravity (g^b) from the linear acceleration (a^b) in the local coordinate frame when gyroscope measurements $\vec{\omega}^b = (\omega_x, \omega_y, \omega_z)$ and accelerometer measurements (a_x, a_y, a_z) are provided. The generic process (4.10) and measurement (4.11) models were provided by Ligorio et al., (2015) as follows:

$$\begin{bmatrix} g_k^b \\ a_k^b \end{bmatrix} = \begin{bmatrix} expm(-[\omega_{i-1}^b\times]\Delta t) & 0_{3x3} \\ 0_{3x3} & c_aI_{3x3}a_{i-1}^b \end{bmatrix}\begin{bmatrix} g_{k-1}^b \\ a_{k-1}^b \end{bmatrix} + \begin{bmatrix} -\Delta t[g_{i-1}^b\times] & 0_{3x3} \\ 0_{3x3} & c_bI_{3x3} \end{bmatrix}\begin{bmatrix} w_{k-1}^\omega \\ w_{k-1}^{gm} \end{bmatrix} \tag{4.17}$$

$$\begin{bmatrix} a_{x,k} \\ a_{y,k} \\ a_{z,k} \end{bmatrix} = \begin{bmatrix} I_{3x3} & I_{3x3} \end{bmatrix}\begin{bmatrix} g_k^b \\ a_k^b \end{bmatrix} + I_{3x3}v_k^a \tag{4.18}$$

where 0_{3x3} is a 3x3 matrix with zeros, I_{3x3} is a 3x3 identity matrix, $[\vec{u}\times]$ is the skew symmetric matrix associated for a given vector ($\vec{u}$), and c_a, c_b are the parameters of the first-order Gauss-Markov process

57

used to account for external acceleration. The gyroscope noise w^ω and accelerometer noise v^a are assumed to follow a normal distribution of $N(0, \sigma_\omega^2)$ and $N(0, \sigma_a^2)$, respectively. The white Gaussian noise w^{gm} is assumed to be zero mean with an identity covariance matrix.

This process model was modified into a first-order approximation (4.19) to reduce computation time. The gyroscope bias was also added to the process model (4.20) to improve measurement estimates, which is consistent with other Kalman Filter designs (Brigante et al. 2011; Gośliński, Nowicki, and Skrzypczyński 2015; Chang et al. 2008). The gyroscope bias was modeled as a random walk, where $\dot{b}_\omega$ is assumed to follow a normal distribution of $N(0, \sigma_{\omega_b}^2)$.

$$expm(-[\omega_{i-1}^b\times]\Delta t) \approx (I_{3x3} - [\omega_{i-1}^b\times]\Delta t) \tag{4.19}$$

$$b_{\omega,i} = b_{\omega,i-1} + \dot{b}_\omega\Delta t \tag{4.20}$$

Based on these changes, (4.17) and (4.18) becomes (4.21) and (4.22), respectively.

$$\begin{bmatrix} g_i^b \\ a_i^b \\ b_{\omega,i} \end{bmatrix} = \begin{bmatrix} I_{3x3} - [(\omega_{i-1}^b - b_{\omega,i-1})\times]\Delta t & 0_{3x3} & 0_{3x3} \\ 0_{3x3} & c_a I_{3x3} a_{i-1}^b & 0_{3x3} \\ 0_{3x3} & 0_{3x3} & I_{3x3} \end{bmatrix} \begin{bmatrix} g_{i-1}^b \\ a_{i-1}^b \\ b_{\omega,i-1} \end{bmatrix} + \begin{bmatrix} [g_{i-1}^b\times]\Delta t & 0_{3x3} & 0_{3x3} \\ 0_{3x3} & c_b I_{3x3} & 0_{3x3} \\ 0_{3x3} & 0_{3x3} & \Delta t I_{3x3} \end{bmatrix} \begin{bmatrix} w_{i-1}^\omega \\ w_{i-1}^{gm} \\ \dot{b}_\omega \end{bmatrix} \tag{4.21}$$

$$\begin{bmatrix} a_{x,k} \\ a_{y,k} \\ a_{z,k} \end{bmatrix} = \begin{bmatrix} I_{3x3} & I_{3x3} \end{bmatrix} \begin{bmatrix} g_k^b \\ a_k^b \end{bmatrix} + \begin{bmatrix} I_{3x3} & I_{3x3} & 0_{3x3} \end{bmatrix} \begin{bmatrix} g_k^b \\ a_k^b \\ b_{\omega,k} \end{bmatrix} v_k^a \tag{4.22}$$

Given that F is non-linear, A is defined as follows:

$$A = \begin{bmatrix} I_{3x3} - [(\omega_{i-1}^b - b_{\omega,i-1})\times]\Delta t & 0_{3x3} & -[g_i^b\times]\Delta t \\ 0_{3x3} & c_a I_{3x3} a_{i-1}^b & 0_{3x3} \\ 0_{3x3} & 0_{3x3} & I_{3x3} \end{bmatrix} \tag{4.23}$$

The process covariance matrix (Q) and the measurement covariance matrix (R) is defined as follows:

$$Q = \begin{bmatrix} I_{3x3}\sigma_\omega^2 & 0_{3x3} & 0_{3x3} \\ 0_{3x3} & I_{3x3} & 0_{3x3} \\ 0_{3x3} & 0_{3x3} & I_{3x3}\sigma_{\omega_b}^2 \end{bmatrix} \tag{4.24}$$

$$R = I_{3x3}\sigma_a^2 \tag{4.25}$$

Inclination measurements are calculated by substituting g_k^b into (4.3) and (4.4). The assigned filter parameters are shown in (Table 4.1). The angles calculated in this manner are described with the designation "Accel-KF."

Table 4.1. Kalman filter parameters.

	Gyro White Noise	Gyro Bias	Accel White Noise	c_a	c_b
Accel-KF	0.005 rad/s	0.0005 (rad/s^2)	0.005 m/s^2	0.001	0.1

4.2.4.5 Kalman Filter: Embedded (Proprietary)

Equation (4.9) was used to convert the quaternion rotation vector output from the IMU's embedded Kalman filter to heading, pitch, and roll angles. The angles calculated in this manner are described with the designation "Em-KF." The quaternion rotation vector output from the OMC system software was converted to heading, pitch, and roll angles using (4.9) as well.

4.2.4.6 Inclinometer Accuracy

The offset between the local coordinate frames of the OMC and the IMU was calculated using angular rate measurements according to de Vries et al. (2010). After applying the local offset, the offset between the global coordinate frames of the OMC and the IMU was determined under static conditions using Accel-derived inclination measurements. OMC-derived upper arm elevation displacements and velocities were calculated after the offsets were added to OMC-derived orientation measurements.

Root-mean-square error (RMS) was calculated using (4.26) to quantify the average error of inclinometer measurements (θ_{INC}) relative to the OMC (θ_{OMC}). Peak error was calculated using the 99th percentile measurement of the rectified (absolute value) sample-to-sample difference between the OMC and inclinometer-derived measurements.

$$RMS = \sqrt{\frac{1}{n}\sum_n (\theta_{OMC} - \theta_{INC})^2} \qquad (4.26)$$

A two-factor repeated measures analysis of variance (ANOVA) was used test the main and interactive effects of material transfer rate and upper arm elevation calculation method (e.g., accelerometer, comp-1, comp-2) on (i) RMS displacement error, (ii) peak displacement error, (iii) RMS velocity error, and (iv) peak velocity error. Preplanned pairwise comparisons using Bonferroni corrections were used to test differences between displacements and velocities calculated using (i) accelerometer and comp-1, (ii) accelerometer and comp-2, (iii) accelerometer and MLKF, and (iv) accelerometer and EMKF on RMS and peak displacement errors as well as RMS and peak velocity errors.

4.3 Results

4.3.1 Angular Displacements

The cyclic motion pattern and the changes to movement frequency associated with increased transfer rates (15, 30, 45 cycles/min) can be observed through the OMC-derived angular displacements (Figure 4.3). The within-trial acceleration measurements (average and variation) across all testing conditions are shown in Table 4.2. Statistically-significant ($p<0.01$) main effects of material transfer rate, calculation method, and their interaction were observed for both RMS and peak displacement error. All pairwise comparisons across each transfer rate were statistically significant for RMS displacement error ($p<0.05$) and peak displacement error ($p<0.01$). As expected, the accelerometer-derived displacements were similar to the OMC-derived displacements for the slowest transfer rate, but deviated substantially for the fastest transfer rate (Figure 4.4).

Although statistically-significant pairwise comparisons were observed for the RMS and peak error associated with the slowest transfer rate (Table 4.3), the measurement errors were minimal (2.3° RMS, 6.8° peak). Under the fastest transfer rate, the errors associated with accelerometer-derived displacements were more apparent (11.3° RMS, 28.9° peak). A simple first-order complementary filter reduced RMS error to 3.2°, while a Kalman filter reduced the RMS error to <1.5°. Similarly, a first-order complementary filter reduced peak error to 6.5°, while a Kalman filter reduced peak error to <3.2°. In general, the accelerometer-

derived displacements underestimated upper arm elevation as transfer rates increased, as evidenced by the 90th percentile measurements. This was mitigated by implementing a sensor fusion algorithm. Time-dependent errors were not observed for displacements calculated using sensor fusion algorithms (Figure 4.5).

Figure 4.3. OMC-derived upper arm elevation displacements (°) for one participant across three different material transfer rates: slow (15 cycles/min), medium (30 cycles/min), and fast (45 cycles/min).

Table 4.2. Mean(SD) within-trial acceleration measurements across all 13 participants and material transfer rates.

	Slow (15 cycles/min)	Medium (30 cycles/min)	Fast (45 cycles/min)
Average (m/s²)	9.9(0.3)	10.1(0.3)	10.4(0.2)
Standard Deviation (m/s²)	0.4(0.1)	1.0(0.2)	1.5(0.2)
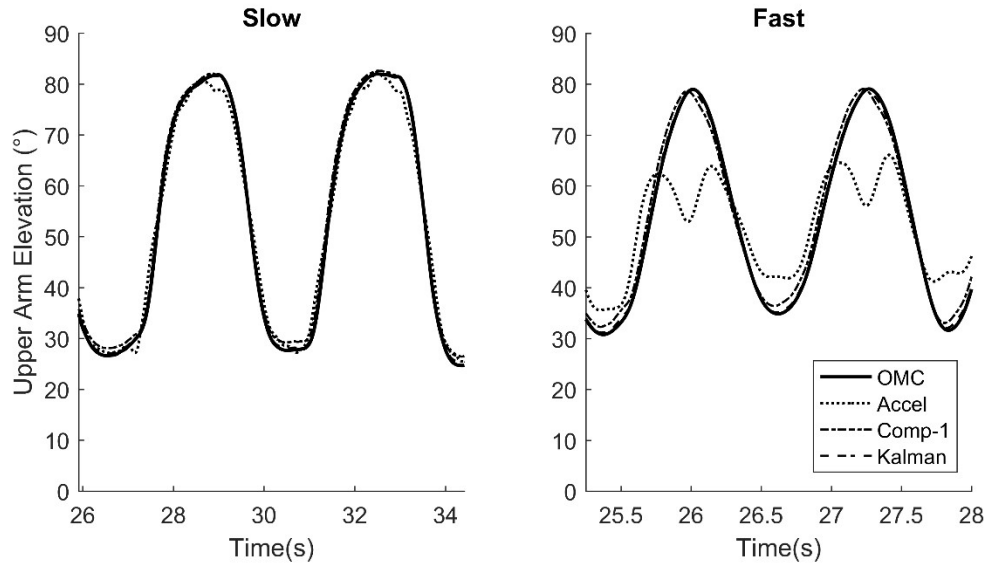
Figure 4.4. Upper arm elevation displacements across two cycles at two material transfer rates: slow (15 cycles/min), and fast (45 cycles/min). Displacements were measured by the optical motion capture system (OMC) and calculated using an accelerometer (Accel), first-order complementary filter (Comp-1), and a modified linear Kalman filter (Kalman).

Figure 4.5. Sample-to-sample displacement difference between OMC and IMU using a modified Linear Kalman Filter across two material transfer rates: slow (15 cycles/min) and fast (45 cycles/min).

Table 4.3. Mean (SD) Angular displacements of upper arm elevation across 13 participants and three material transfer rates: slow (15 cycles/min), medium (30 cycles/min), and fast (45 cycles/min) that was maintained for a period of one minute. Displacements were measured by the optical motion capture system (OMC) and calculated using an accelerometer (Accel), first-order complementary filter (Comp-1), a second-order complementary filter (Comp-2), a modified linear Kalman Filter (MLKF), and an embedded Kalman filter (EMKF).

Upper Arm Elevation Displacement	OMC	Accel	Comp-1	Comp-2	MLKF	EMKF
'Slow' Transfer Rate						
RMS (°)	-REF-	2.3(0.4)	1.6(0.9)*	1.8(0.5)**	1.1(0.6)**	1.2(0.9)**
Peak (°)	-REF-	6.8(1.7)	3.3(1.4)**	4.1(1.0)**	2.2(1.0)**	2.4(1.6)**
Mean (°)	47.4(7.7)	46.5(7.8)	46.9(8.2)	46.6(7.9)	46.7(7.8)	46.8(7.4)
10th Percentile (°)	20.5(6.4)	20.4(6.4)	21.0(6.9)	20.5(6.5)	20.4(6.6)	20.4(6.3)
50th Percentile (°)	46.1(8.9)	46.2(8.7)	45.5(9.2)	45.9(8.8)	45.4(8.8)	45.5(8.5)
90th Percentile (°)	75.4(8.7)	72.5(9.1)	74.2(9.2)	73.4(9.1)	74.2(8.8)	74.3(8.4)
Percentile Range (90th – 10th)(°)	54.9(4.4)	52.1(4.5)	53.2(4.1)	52.9(4.3)	53.7(4.0)	53.9(4.0)
Time in neutral posture (<20°) (%)	12.3(13.7)	12.0(12.9)	11.6(13.9)	12.2(13.4)	12.3(13.7)	12.1(13.2)
Time in extreme posture (≥45°)(%)	50.4(7.5)	50.6(8.3)	49.8(8.2)	50.2(8.1)	49.7(7.7)	49.9(7.2)
Time in extreme posture (≥60°)(%)	35.4(12.4)	33.4(13.7)	34.0(13.4)	33.8(13.4)	34.0(13.2)	34.7(11.8)
'Medium' Transfer Rate						
RMS (°)	-REF-	6.3(1.5)	2.4(1.0)**	2.4(0.6)**	1.3(0.6)**	1.4(1.0)**
Peak (°)	-REF-	17.5(4.6)	5.7(4.4)**	5.3(1.2)**	2.7(1.1)**	2.5(1.5)**
Mean (°)	44.4(7.3)	42.9(7.4)	43.8(7.6)	44.2(7.8)	43.7(7.4)	43.5(7.5)
10th Percentile (°)	19.0(6.8)	20.8(6.9)	19.8(7.0)	20.1(7.3)	19.1(6.9)	18.9(6.8)
50th Percentile (°)	41.8(8.1)	43.9(7.6)	41.1(8.1)	41.5(8.2)	41.1(8.0)	40.9(8.2)
90th Percentile (°)	73.1(9.1)	63.3(8.6)	71.4(9.1)	71.8(9.4)	71.7(9.0)	71.5(9.2)
Percentile Range (90th – 10th)(°)	54.1(5.4)	42.5(4.7)	51.6(5.2)	51.7(5.0)	52.7(5.3)	52.7(5.2)
Time in neutral posture (<20°) (%)	15.4(13.4)	11.7(11.9)	13.9(13.6)	13.6(13.9)	15.2(13.6)	15.5(13.7)
Time in extreme posture (≥45°)(%)	46.3(8.5)	46.9(12.3)	45.4(9.0)	45.8(9.1)	45.5(8.7)	45.2(8.8)
Time in extreme posture (≥60°)(%)	29.8(12.0)	21.0(15.8)	27.7(12.9)	28.0(13.0)	28.0(12.9)	27.6(13.2)
'Fast' Transfer Rate						
RMS (°)	-REF-	11.3(1.9)	3.2(0.8)**	2.9(1.1)**	1.5(0.5)**	1.2(0.8)**
Peak (°)	-REF-	28.9(5.2)	6.5(1.8)**	5.7(1.6)**	3.2(1.0)**	2.4(1.2)**
Mean (°)	43.6(7.2)	40.7(6.9)	43.3(7.4)	44.1(8.4)	42.9(7.3)	43.3(7.4)
10th Percentile (°)	18.1(5.8)	23.0(6.4)	19.5(6.3)	19.4(6.9)	18.2(6.0)	18.5(5.9)
50th Percentile (°)	42.3(7.9)	43.7(7.2)	42.0(7.9)	42.4(8.9)	41.6(7.9)	42.0(8.2)
90th Percentile (°)	71.1(9.1)	54.8(7.8)	69.2(9.2)	71.3(10.2)	69.8(9.2)	70.2(9.1)
Percentile Range (90th – 10th)(°)	53.0(6.2)	31.8(4.3)	49.7(6.1)	51.9(6.2)	51.6(6.1)	51.7(5.9)
Time in neutral posture (<20°) (%)	16.1(11.4)	8.0(9.6)	12.9(12.2)	14.2(13.3)	15.9(11.8)	15.5(12)
Time in extreme posture (≥45°)(%)	46.3(9.1)	41.1(20.9)	45.7(9.7)	46.5(10.3)	45.4(9.3)	45.9(9.5)
Time in extreme posture (≥60°)(%)	28.1(12.8)	8.3(10.2)	25.5(14.3)	27.7(14.6)	25.9(13.9)	26.7(13.9)

*Statistically-significant (p<0.05) pair-wise tests between the accel and the sensor fusion method
**Statistically-significant (p<0.01) pair-wise tests between the accel and the sensor fusion method

4.3.2 Angular Velocities

The increase in amplitude and frequency of OMC-derived angular velocities associated with increased material transfer rates can be observed in Figure 4.6. Statistically-significant ($p<0.01$) main effects of material transfer rate, calculation method, and their interaction were observed for both RMS and peak velocity error. All pairwise comparisons across each transfer rate was statistically significant for RMS velocity error ($p<0.01$) and peak velocity error ($p<0.01$). As expected, the accelerometer-derived velocities were similar to the OMC-derived velocities for the slow transfer rate, but deviated substantially for the fast transfer rate (Figure 4.7).

Unlike the accelerometer-derived displacements, the RMS and peak angular velocity error associated with accelerometer-derived angular velocities more noticeable (13.0°/s RMS and 42.7°/s peak). RMS and peak velocity error for accelerometer-derived measurements increased to 81.7°/s and 221.3°/s for the fastest motion condition. As expected, a first-order complementary filter reduced RMS error to 17°/s, while a Kalman filter decreased RMS error to <9.2°/s. Similarly, a first-order complementary filter reduced peak error to 46.2°/s, while a Kalman filter reduce peak error to <25.2°/s.
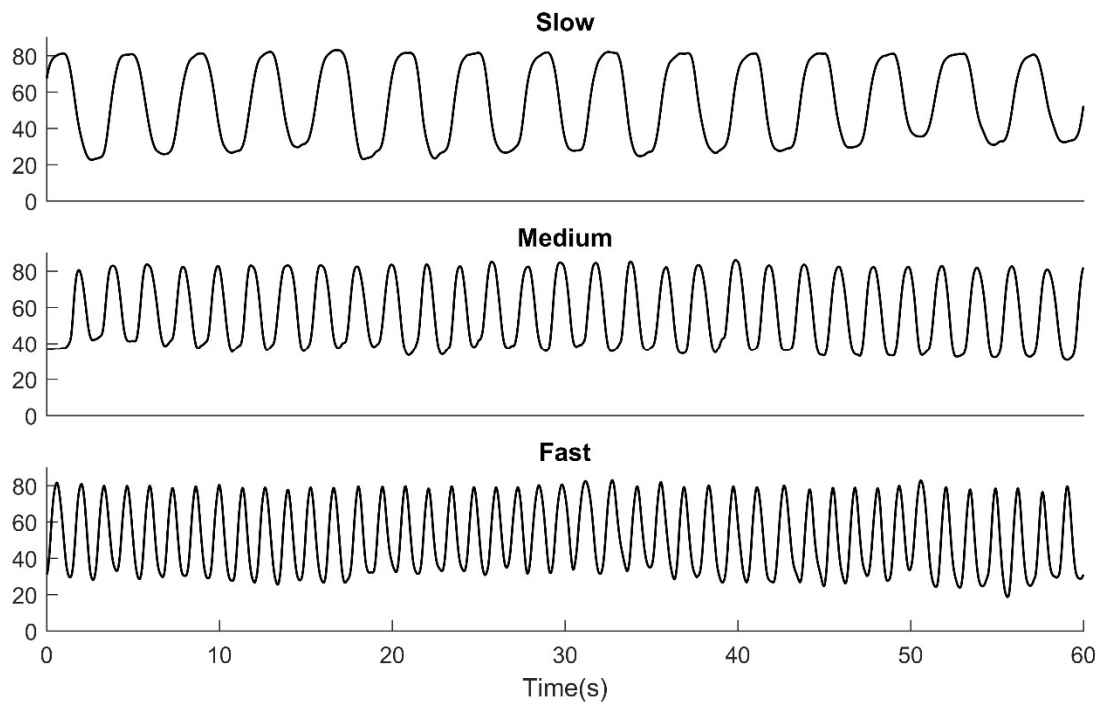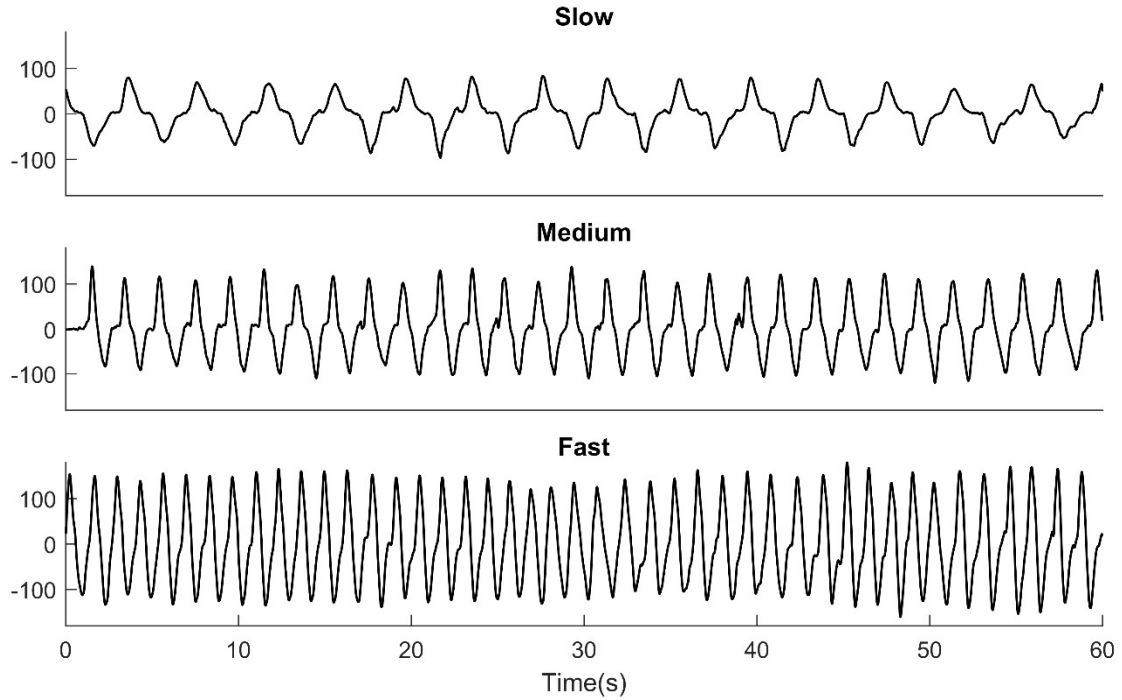
Figure 4.6. OMC-derived upper arm elevation velocities (one participant) across three material transfer rates: slow (15 cycles/min), medium (30 cycles/min), and fast (45 cycles/min).
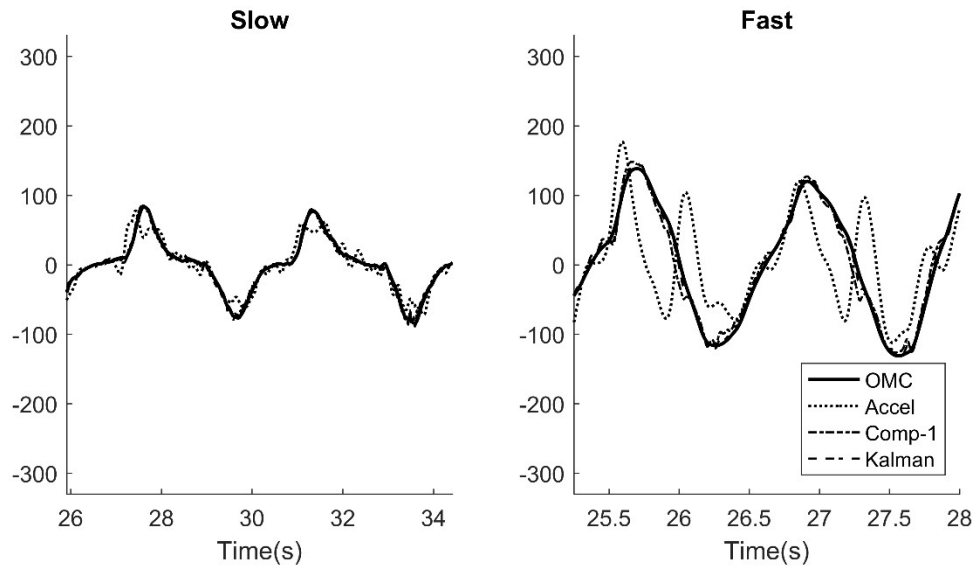
Figure 4.7. Upper arm elevation velocities (°/s) for one participant across two material transfer rates: slow (15 cycles /min), and fast (45 cycles /min). Angular velocities were derived using displacements measured from the optical motion capture (OMC) calculated using an accelerometer (Accel), first-order complementary filter (Comp-1), and a modified linear Kalman filter (Kalman).
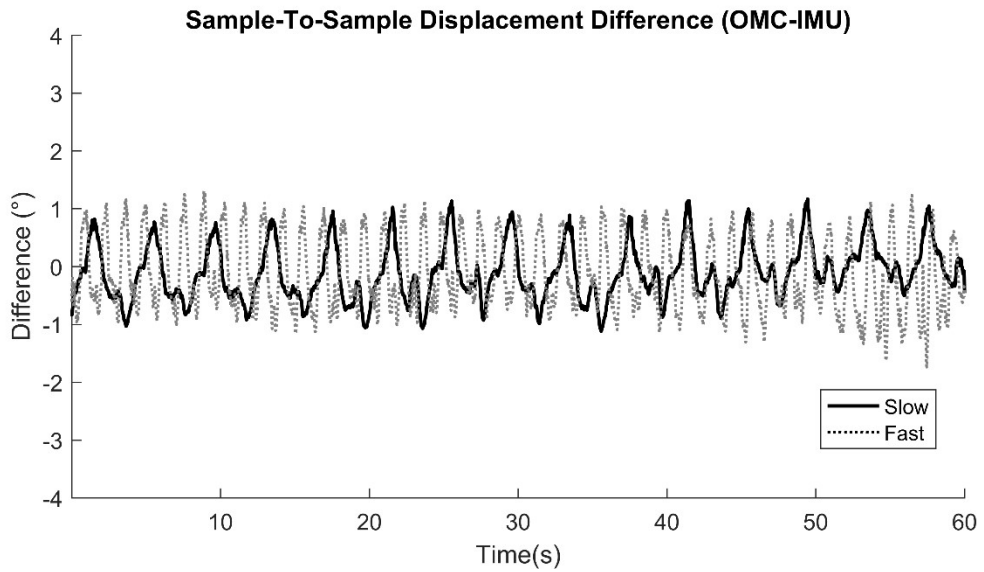
65

Table 4.4. Angular velocities of upper arm elevation across 13 participants and three material transfer rates: slow (15 cycles/min), medium (30 cycles/min), and fast (30 cycles/min) that was maintained for a period of one minute. Angular velocities were calculated using displacement measurements obtained from an optical motion capture system (OMC) an accelerometer (Accel), first-order complementary filter (Comp-1), a modified linear kalman filter (MLKF), and an embedded Kalman filter (EMKF).

Velocity	OMC	Accel	Comp-1	Comp-2	MLKF	EMKF
'Slow' Transfer Rate						
RMS (°/s)	-REF-	13.0(3.0)	4.4(1.1)**	9.9(0.8)**	3.1(0.9)**	2.8(1.0)**
Peak (°/s)	-REF-	42.7(11.4)	14.1(4.4)**	19.9(2.1)**	9.7(3.4)**	8.7(3.3)**
Mean (°/s)	28.2(2.1)	28.6(2.3)	27.5(2.1)	28.7(2.4)	27.6(2.0)	27.7(2.0)
10th Percentile (°/s)	2.6(1.1)	4.0(1.3)	2.9(1.3)	4.4(0.7)	2.7(1.2)	2.6(1.2)
50th Percentile (°/s)	22.8(3.8)	25.9(2.7)	22.4(3.3)	23.8(2.0)	22.4(3.4)	22.5(3.5)
90th Percentile (°/s)	61.3(8.7)	56.6(7.0)	59.4(8.4)	59.6(7.7)	59.9(8.4)	60.1(8.5)
Percentile Range (90th – 10th)(°/s)	58.7(9.5)	52.6(7.7)	56.5(9.3)	55.2(7.8)	57.2(9.3)	57.4(9.4)
Time at low velocities (<5°/s)(%)	19.5(6.4)	13.2(3.7)	18.1(6.2)	11.5(1.9)	19.0(6.3)	19.6(6.3)
Time at high velocities (≥90°/s)(%)	1.0(1.5)	0.4(0.6)	0.8(1.3)	0.8(1.2)	0.9(1.4)	0.8(1.4)
'Medium' Transfer Rate						
RMS (°/s)	-REF-	39.8(10.9)	10.3(2.4)**	11.1(1.4)**	5.9(1.4)**	5.1(2.0)**
Peak (°/s)	-REF-	112.5(29.1)	30.8(10.0)**	25.6(7.9)**	17.1(4.3)**	15.3(7.7)**
Mean (°/s)	56.0(5.3)	49.7(5.9)	54(5.4)	54.3(5.3)	54.8(5.3)	54.7(5.2)
10th Percentile (°/s)	7.5(2.8)	9.8(3.0)	7.8(2.9)	8.1(2.3)	7.8(2.8)	7.3(2.8)
50th Percentile (°/s)	52.6(6.1)	49.3(7.2)	50.0(5.5)	49.9(6.2)	51.3(5.8)	51.4(6.0)
90th Percentile (°/s)	109.7(17.3)	89.0(11.2)	106.4(16.4)	107.3(15.9)	107.4(16.8)	107.3(16.7)
Percentile Range (90th – 10th)(°/s)	102.2(19.0)	79.2(10.7)	98.6(17.7)	99.2(17.0)	99.6(18.4)	99.9(18.3)
Time at low velocities (<5°/s)(%)	7.9(3.8)	5.7(2.0)	7.5(3.6)	6.7(2.0)	7.6(3.7)	8.0(3.7)
Time at high velocities (≥90°/s)(%)	21.7(8.5)	9.8(6.0)	19(8.6)	19.5(8.1)	20.0(8.7)	20.2(8.7)
'Fast Transfer Rate						
RMS (°/s)	-REF-	79.0(14.1)	17.0(2.7)**	13.8(3.7)**	9.3(1.7)**	7.3(3.9)**
Peak (°/s)	-REF-	206.5(41.1)	46.2(8.4)**	36.2(18.6)**	25.2(5.8)**	21.4(13.8)**
Mean (°/s)	83.3(9.8)	62.5(7.2)	78.8(9.9)	81.9(10.2)	81.4(9.8)	81.6(9.4)
10th Percentile (°/s)	14.5(3.1)	11.4(2.5)	15.2(4.6)	13.5(4.0)	15.1(4.0)	15.0(3.6)
50th Percentile (°/s)	86.0(10.6)	57.6(7.6)	78.5(9.9)	82.6(10.8)	82.7(10.4)	83.5(9.9)
90th Percentile (°/s)	146.5(20.1)	118.5(16.6)	141.9(20.6)	148.5(19.7)	144.4(20.2)	144.0(19.7)
Percentile Range (90th – 10th)(°/s)	131.9(20.2)	107.1(16.2)	126.7(19.7)	135(18.9)	129.3(19.9)	128.9(19.8)
Time at low velocities (<5°/s)(%)	3.6(0.9)	4.6(1.3)	3.5(1.0)	4.0(1.3)	3.6(1.0)	3.5(1.0)
Time at high velocities (≥90°/s)(%)	46.7(6.1)	24.1(6.9)	41.3(7.6)	44.9(6.1)	44.6(6.5)	45.3(6.1)

*Statistically-significant ($p<0.05$) pair-wise tests between the accel and the sensor fusion method
**Statistically-significant ($p<0.01$) pair-wise tests between the accel and the sensor fusion method

The accelerometer-derived displacements were accurate (<2.5° RMS error, <7° peak error) for the slowest material transfer rates (15 cycles/min). This test condition corresponded to an acceleration average and standard deviation of 9.9 m/s^2 and 0.4 m/s^2 within each trial, respectively. The accelerometer-derived displacements were negatively affected by increased motion speeds. Under the fast motion condition, the RMS and peak displacement error increased to 11.3° and 28.9°, respectively. This observation was consistent with the expected increase in tangential and centripetal acceleration, which are both affected by increased angular velocities (Bernmark and Wiktorin 2002). The results of this study indicate a range of displacement errors (RMS <2.5° to >11°) that are comparable to (i) previous work that assessed accelerometer-based inclinometers under a variety of tasks and arm swing frequencies (RMS 2.0° to >13°) (Korshøj et al. 2014) and (ii) previous work that assessed accelerometer-derived displacements in static conditions (<2°) (Amasay et al. 2009). The accelerometer-based displacement RMS error for the medium material transfer rate (6.3°) was also consistent with previous work that reported an RMS error of 7.2° for upper arm elevation displacements during the prescribed work task (Schall et al. 2015).

As expected, the sensor fusion algorithms improved measurement accuracy for upper arm elevation displacement. For every transfer rate tested, a statistically-significant pairwise difference was observed between the accuracy of accelerometer-derived displacements and each of the sensor fusion algorithms. However, the improvements in measurement accuracy were more apparent with increased motion speeds. For the fast motion condition, a simple first-order complementary filter reduced the RMS displacement error from 11.3° to 3.2°. However, this filter design did not account for variability in gyroscope bias nor non-gravitational acceleration. The comp-2 filter, which reduced the RMS displacement error to <2.8°, accounted for gyroscope bias variability in the filter design. The modified linear Kalman filter also accounted for non-gravitational acceleration, which further reduced the error to <1.5°. In general, our errors were consistent with other studies (<4° RMS error) that provided inclination estimates using an identical comp-2 filter (Mourcou et al. 2015; Bergamini et al. 2014), an identical Embedded Kalman Filter (Lebel et al. 2013; Lebel et al. 2015), and a similar linear Kalman filter (Gabriele Ligorio and Sabatini 2016; Bergamini et al. 2014; Gabriele Ligorio and Sabatini 2015). The improvements in inclination accuracy with the Comp-1 filter was inconsistent with previous studies, which showed only marginal and inconsistent

improvements in measurement accuracy when used over accelerometer-derived measurements (Schall et al., 2015). We suspect this may be because the majority of the reported error may be attributed to methodological differences between the measurement systems (e.g. misalignment between measurement systems).

Similar error trends appeared in velocity measurements since velocity was calculated by taking the derivative of the angular displacements with respect to time. As expected, accelerometer-derived angular velocities were unusable for the fast motion conditions ($81.7°$/s RMS error). This was mitigated considerably using a sensor fusion algorithm, which resulted in RMS errors between $7.3°$/s and $17.0°$/s for the fastest transfer rate, depending on the sensor fusion algorithm. Few studies have published accuracy of angular velocity measurements. In general, our results are consistent with previous studies. For the accelerometer-derived angular velocities, Schall et al. (2015) reported angular velocity errors $<10°$/s through comparisons against a lumbar electrogoniometer, which was consistent with our study ($13°$/s RMS) with regards to the slow transfer rate. For IMU-based angular velocity measurements, Kim et al., (2013) reported errors $<10°$/s for the vast majority of joint angle velocities across all body segments through comparisons against an OMC (Kim and Nussbaum 2013), Plamondon et al. (2007) reported angular velocity errors $<13°$/s (Plamondon et al. 2007) and Schall et al. (2015) reported RMS angular velocity errors $<10.1°$/s, which is consistent with our observations ($<9.2°$/s using a Kalman filter).

In general, this study suggests that the dynamics associated with upper arm motion are (i) more than capable of adversely affecting accelerometer-derived angular displacement and velocity measurements that are commonly reported within the occupational ergonomics literature. We observed underestimation of the extreme postures and velocities (90th percentile) at increased motion speeds, which indicate that exposures to non-neutral postures may be underestimated in human health studies, in particularly when higher motion speeds are expected. These limitations, however, were mitigated by implementing a sensor fusion algorithm that combined accelerometer and gyroscope measurements.

68

4.4.1 Study Limitation

The main limitation in this study was the relatively short sampling period of one minute, given that the error of gyroscope-derived orientation measurements is time-dependent (Bergamini et al. 2014; Lebel et al. 2015). This sampling duration was chosen based on the material transfer rate. In preliminary tests, it was difficult for the participants to maintain the fastest transfer rate (45 cycles/min) for longer than one minute due to fatigue. While several studies have used similar sampling durations (Bergamini et al. 2014; M.a. Brodie, Walmsley, and Page 2008; El-Gohary and McNames 2012; Faber et al. 2013; Gabriele Ligorio and Sabatini 2016; Ricci, Taffoni, and Formica 2016), task-durations in the workplace setting may be considerably longer, which may result in larger error magnitudes. When designing this study, a compromise had to be made between maximizing IMU error due to increased motion speeds or increased sampling duration. However, the time-dependent error characteristics, if apparent, would be observable for the chosen task duration (Bergamini et al. 2014). This was not observed due, in part, to relatively 'conservative' tuning parameters that relied more on accelerometer-derived inclination measurements. Based on the chosen parameters for the sensor fusion algorithms, the accuracy of the IMU-derived inclination measurements will be more likely to be negatively affected by increased motion speeds.

A cyclic task was chosen to provide the maximum influence of motion to inclination error. However, the nature of the cyclic task precludes rest/recovery metrics that are also used to quantify motion-related exposures. Furthermore, this study focused on accuracy of inclinometers and completely disregarded the issue of magnetic disturbance. The use of relatively standard sensor fusion algorithms in this experiment facilitates comparisons across other studies. However, differences in sensor specifications and tuning parameters may provide different error magnitudes. Finally, this study considers strictly sensor error. A recent study, for example, demonstrated that accelerometer-based inclinometers may underestimate inclination measurements under static conditions, particularly at angles >60° (Jackson et al. 2015). Differences in error measurement due to measurement methodology, such as differences in the local coordinate frame defined using anatomical landmarks in comparison to the sensor local coordinate frame and errors due to soft tissue artifacts, were not considered.

4.5 Conclusion

The overall goal of this study was to evaluate the capability of IMU-based inclinometers to provide accurate measurements of upper arm elevation displacement and velocity. In general, the accelerometer-derived displacements were accurate (<2.5° RMS error, <7° peak error) for slow movement speeds. However, both accelerometer-derived displacements and velocities were negatively affected by increased motion speeds. Under the fast motion speeds, the RMS and peak displacement errors increased to 11.3° and 28.9°, respectively. More importantly, the RMS and peak errors associated with accelerometer-derived velocities were substantial (81.7°/s and 221.3°/s, respectively). A Kalman filter reduced peak displacement and velocity errors to <3.5° and <25.1°/s, respectively across all testing conditions. The results indicate that IMU-based inclinometers, in particular when using a Kalman filter, can substantially improve inclinometer accuracy compared to traditional accelerometer-based inclinometers for the assessment of upper arm elevation during increased motion speeds.

CHAPTER 5

THE RELATIONSHIP BETWEEN MAGNETIC FIELD STRENGTH AND LOCALIZED MAGNETIC FIELD DEVIATIONS: TOWARD THE INDIRECT ASSESSMENT OF MAGNETIC DISTURBANCE

5.1 Introduction

Inertial measurement units (IMUs) can measure human kinematics without the environmental constraints imposed by laboratory-based motion capture systems (Sabatini 2006). Because IMUs are small, wireless, and often provide on-board memory for data logging, they are attractive to ergonomists for use in field-based studies to quantify aspects of motion pertinent to workplace injuries. Continuous measurements of joint angles, for example, can be estimated using raw sensor data from IMUs attached to adjacent body segments (Cloete and Scheffer 2008; Martori et al. 2013) and then summarized using metrics to describe risk for work-related musculoskeletal health outcomes (Kazmierczak et al. 2005). Understanding the conditions that adversely impact the accuracy of IMU-based motion capture is critical to those interested in using such systems outside the laboratory.

Optical motion capture (OMC) systems are typically used as the reference device when assessing the accuracy of IMU-based motion measurements (Cuesta-Vargas, Galán-Mercant, and Williams 2010). Promising results (<6° average error) were reported in several studies (Bergamini et al. 2014; Faber et al. 2013; Kim and Nussbaum 2013; Plamondon et al. 2007; Robert-Lachaine et al. 2016). However, IMU accuracy has been observed to be negatively affected by magnetic field disturbances (de Vries et al. 2009; Bachmann, Yun, and Peterson 2004) and highly dynamic motion (Lebel et al. 2013; Ricci, Taffoni, and Formica 2016). Because disturbances of the local magnetic field can cause directional changes up to 180° (Bachmann, Yun, and Peterson 2004), IMU accuracy is typically evaluated using procedures to minimize this problem (Kim and Nussbaum 2013; Lebel et al. 2015; Lebel et al. 2013; Robert-Lachaine et al. 2016; Schiefer et al. 2014).

Fundamentally, IMU spatial orientation is derived with respect to magnetic north and gravity using magnetometer and accelerometer measurements (Yun, Bachmann, and McGhee 2008). These measurements generally assume a homogeneous local magnetic field and that the accelerometer is responding only to gravity (Bachmann, Yun, and Peterson 2004; Gabriele Ligorio and Sabatini 2016). Sensor fusion algorithms (e.g. Kalman filters) that combine magnetometer, accelerometer, and gyroscope measurements (Daniel Roetenberg et al. 2005; Sabatini 2011b; Sabatini 2006; Valenti, Dryanovski, and Xiao 2016; Valenti, Dryanovski, and Xiao 2015) are commonly used to attenuate the effects of local magnetic field disturbances and non-gravitational acceleration. However, IMU spatial orientation accuracy is ultimately bounded by the stability of the local magnetic field and accelerometer-derived gravity measurements.

Changes in magnetic field strength have been used to indicate periods of magnetic disturbance in recorded IMU data streams (Gabriele Ligorio et al. 2016; G. Ligorio and Sabatini 2015; Daniel Roetenberg et al. 2005). Sensor fusion algorithms may also disregard magnetometer measurements when the magnetic field strength is outside a pre-determined threshold (Gabriele Ligorio and Sabatini 2016; Daniel Roetenberg et al. 2005; Sabatini 2006; Sun et al. 2013; Y. Tian, Wei, and Tan 2013). Recently, magnetic strength measurements were used in a machine learning algorithm to automate identification of valid IMU data segments (Lebel et al. 2016). The relationship between magnetic field strength variation and directional changes in the magnetic field, however, has not been previously quantified.

Several studies have reported associations between motion speed and IMU accuracy using mechanical devices such as gimbals or robotic arms (Lebel et al. 2013; Ricci, Taffoni, and Formica 2016). In general, IMU accuracy appears to decrease as motion speed increases. However, while mechanical devices provide highly repeatable motion patterns, such patterns are not representative of human motion. Furthermore, no study has systematically evaluated the combined effects of magnetic disturbance and motion speed on IMU accuracy. The objectives of this study were, therefore, to (i) characterize the relationship between magnetic field strength variation and magnetic heading deviation and (ii) evaluate the effects of local magnetic disturbance and motion speed on the spatial orientation accuracy of IMUs in the context of repetitive distal upper extremity (upper arm, forearm, and hand) motion. We hypothesized that

72

variation in magnetic field strength could be used to indirectly assess the homogeneity of the magnetic field and consequently, the accuracy of IMU-derived orientation measurements captured in unconstrained environments. We also hypothesized that IMU error would increase as motion speed increased.

5.2 Methods

5.2.1 Experimental Setup

Thirteen participants (11 male and 2 female, mean age = 27.2 ± 6.6 years, all right hand dominant) were recruited from the University of Iowa community. All participants reported (i) no history of physician-diagnosed musculoskeletal disorders in the upper extremity during the previous six months, (ii) no history of orthopedic surgery of the upper extremity, and (iii) no pain in the upper extremity for two weeks prior to enrollment. The University of Iowa Institutional Review Board approved all study procedures and each participant provided written informed consent.

Participants completed a repetitive task that involved transferring wooden dowels (2 cm diameter x 8 cm length) from a material feed container (waist-high and directly in front of the participant) to an unloading container (shoulder-high and offset with respect to the mid-sagittal plane). Each transfer cycle consisted of (i) grasping a wooden dowel, (ii) transferring the dowel to the unloading container, and (iii) returning the hand to the material feed container to grasp the next dowel. Three levels of movement speed were assigned: 'slow' (15 transfers/min), 'medium' (30 transfers/min), and 'fast' (45 transfers/min). Pacing was controlled using a metronome. A metal plate (30.5 cm x 10 cm x 0.6 cm) placed within the unloading container was used to create a local magnetic field disturbance. Each participant performed one trial in each combination of movement speed (slow, medium, and fast) and magnetic disturbance (absent or present). Participants were given time to acclimate to the motion speeds before data collection. Each trial was performed for one minute followed by a rest period of five minutes, and the trial order was randomized.

73

An IMU (SXT, Nexgen Ergonomics, Inc., Pointe Claire, Quebec, CA) was secured to the dominant upper arm, forearm, and hand using elastic straps (Figure 5.1). Gyroscope, accelerometer, magnetometer, and spatial orientation measurements (quaternions, from an embedded Kalman filter) were sampled at 128 Hz. A six-camera OMC system (Optitrack Flex 13, NaturalPoint, Inc., Corvallis, OR, USA) was used as the reference device; a cluster of four reflective markers was mounted to the surface of each IMU. The spatial positions and orientations of each marker cluster were recorded at 120 Hz. Calibration of the IMU and OMC systems was performed using manufacturer-specified procedures. A minimum distance of 120 cm was maintained between the cameras and experimental area to minimize ambient magnetic disturbances (de Vries et al. 2009; Bachmann, Yun, and Peterson 2004).
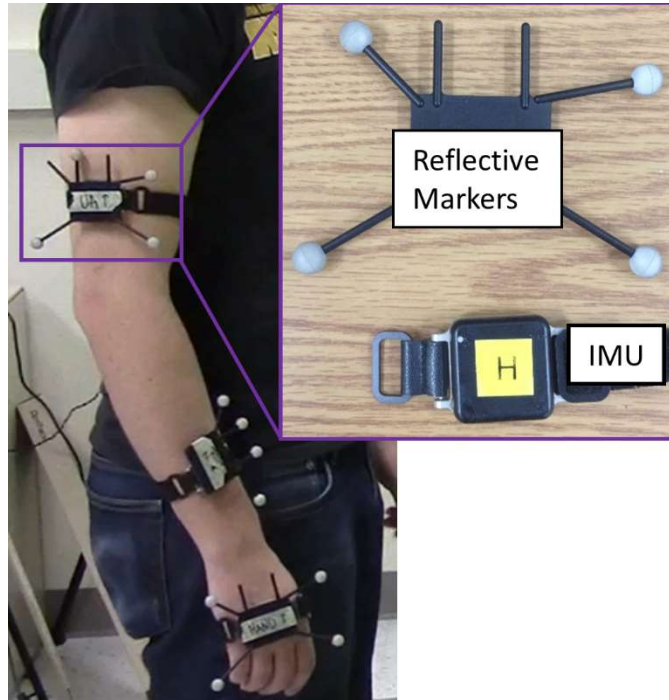
Figure 5.1. IMUs and associated clusters of reflective markers attached to a participant. Spatial orientation of each body segment was simultaneously measured using an IMU and an OMC that tracked the reflective markers attached to the top surface of each IMU.

5.2.3 Data Post-Processing

Post-processing was accomplished using Matlab (R2015a, The Mathworks, Inc., Natick, MA, USA). The raw IMU data were down-sampled from 128 Hz to 120 Hz to match the sampling rate of the OMC system. For each trial, the measurement systems were time-synced and aligned by orientation.

5.2.4 Orientation Estimation

The IMU and OMC orientation measurements were parameterized using quaternions. For each system, the quaternion rotation vector $\vec{q}_B^A$ defined in (5.1) consisted of scalar (q_0) and vector (q_1, q_2, q_3) components describing the angle and direction of rotation between frame A and frame B. Specifically, $\vec{q}_B^A$ defines the rotation from Frame B to Frame A, where u_x, u_y, u_z defined the x, y, and z-components of the unit vector describing the direction of rotation between the two coordinate frames, and α defined the angle of rotation about the unit vector.

$$\vec{q}_B^A = [\cos(\alpha/2) \quad u_x \sin(\alpha/2) \quad u_y \sin(\alpha/2) \quad u_z \sin(\alpha/2)]^T \tag{5.1}$$

A vector in Frame B ($\vec{v}_B$) can be expressed in Frame A ($\vec{v}_A$) as follows

$$[0 \quad \vec{v}_A]^T = \vec{q}_B^A \otimes [0 \quad \vec{v}_B]^T \otimes \vec{q}_B^{A^{-1}} \tag{5.2}$$

where $\otimes$ represents quaternion multiplication and $(q)^{-1}$ represents the quaternion inverse. The relationship between Frames A, B, and C is such that

$$\vec{q}_C^A = \vec{q}_B^A \otimes \vec{q}_C^B \tag{5.3}$$

$\vec{q}$ can be converted using (5.4) to the common Euler rotation sequence of heading (ψ), pitch (θ), and roll (ϕ). Similarly, spatial orientation given with an Euler rotation sequence can be converted to a quaternion vector using (5.5). More information on quaternion mathematics pertaining to spatial orientation can be found elsewhere (Yun, Bachmann, and McGhee 2008; Valenti, Dryanovski, and Xiao 2016).

$$\begin{bmatrix} \psi \\ \theta \\ \phi \end{bmatrix} = \begin{bmatrix} \text{atan2}(2(q_0q_3 + q_1q_2), 1 - 2(q_2^2 + q_3^2)) \\ \text{asin}(2(q_0q_2 - q_3q_1)) \\ \text{atan2}(2(q_0q_1 + q_2q_3), 1 - 2(q_1^2 + q_2^2)) \end{bmatrix} \tag{5.4}$$

$$\vec{q} = \begin{bmatrix} \cos(\psi/2) \\ 0 \\ 0 \\ \sin(\psi/2) \end{bmatrix} \otimes \begin{bmatrix} \cos(\theta/2) \\ 0 \\ \sin(\theta/2) \\ 0 \end{bmatrix} \otimes \begin{bmatrix} \cos(\phi/2) \\ \sin(\phi/2) \\ 0 \\ 0 \end{bmatrix} \tag{5.5}$$

5.2.5 Measurement System Alignment

Many methods have been used to align OMC and IMU measurement systems (Chardonnens, Favre, and Aminian 2012; de Vries et al. 2009; Dornaika and Horaud 1998; Faber et al. 2013; Mecheri et al. 2016; Sessa et al. 2012). In theory, if the offset between the IMU global frame (IGF) and OMC global frame (OGF) is known (q_{IGF}^{OGF}), and if the offset between the IMU local frame (ILF) and OMC local frame (OLF) is known (q_{OLF}^{ILF}), the OMC-derived orientation measurements ($q_{OLF}^{OGF}(t)$) will be equal to the IMU-derived orientation measurements ($q_{ILF}^{IGF}(t)$).

$$q_{OLF}^{OGF}(t) = q_{IGF}^{OGF} \otimes q_{ILF}^{IGF}(t) \otimes q_{OLF}^{ILF} \tag{5.6}$$

In this study, the Nelder-Mead simplex method was used to determine offsets that would minimize total RMS error (Lagarias et al. 1998). Offsets were converted from Euler angles to quaternions using (5.5) to formulate (5.6) into an unconstrained multivariable function.

5.2.6 Magnetometer and Accelerometer Measurements

The magnetic heading direction was measured using methods adopted from de Vries et al. (2009). Specifically, magnetometer measurements in the ILF (m_{Ix}, m_{Iy}, m_{Iz}) were first rotated to the OLF (m_{Ox}, m_{Oy}, m_{Oz}) using (5.7) and then to the OGF using (5.8). Magnetic heading (M_{head}) was then calculated using (5.9), where M_{Ox} and M_{Oy} are x and y-components of the magnetic field strength in the OGF. Local magnetic field variation within each trial was characterized using the standard deviation and the peak-to-peak amplitude ($90^{th} - 10^{th}$ percentiles) of the M_{head} values.

$$\begin{bmatrix} 0 \\ m_{Ox} \\ m_{Oy} \\ m_{Oz} \end{bmatrix} = q_{OLF}^{ILF \, -1} \otimes \begin{bmatrix} 0 \\ m_{Ix} \\ m_{Iy} \\ m_{Iz} \end{bmatrix} \otimes q_{OLF}^{ILF} \tag{5.7}$$

$$\begin{bmatrix} 0 \\ M_{Ox} \\ M_{Oy} \\ M_{Oz} \end{bmatrix} = q_{OLF}^{OGF} \otimes \begin{bmatrix} 0 \\ m_{Ox} \\ m_{Oy} \\ m_{Oz} \end{bmatrix} \otimes q_{OLF}^{OGF^{-1}}$$

(5.8)

$$M_{head} = \operatorname{atan}\left(\frac{M_{Ox}}{M_{Oy}}\right)$$

(5.9)

The total magnetic field strength (m_n), angular velocity (ω_n), and acceleration (a_n) at each sample were calculated using the magnetometer, gyroscope, and accelerometer vector magnitudes (5.10) to (5.12). Variations in magnetic field strength and acceleration within each trial were characterized using the standard deviation and the peak-to-peak amplitude (90th–10th percentiles) of the m_n and a_n values.

$$m_n = \sqrt{m_x^2 + m_y^2 + m_z^2}$$

(5.10)

$$\omega_n = \sqrt{\omega_x^2 + \omega_y^2 + \omega_z^2}$$

(5.11)

$$a_n = \sqrt{a_x^2 + a_y^2 + a_z^2}$$

(5.12)

5.2.7 IMU Accuracy

Sample-to-sample differences ($\Delta q(t)$) between the OMC and IMU orientations were defined as the relative orientation between the OGF and the IGF (Faber et al. 2013; Gabriele Ligorio et al. 2016).

$$\Delta q(t) = q_{IGF}^{OGF}(t) = q_{OLF}^{OGF}(t) \otimes (q_{ILF}^{IGF}(t))^{-1}$$

(5.13)

Total sample-to-sample error across all motion planes was calculated using the scalar component of the sample-to-difference ($\Delta q_0(t)$), which provides a non-redundant rotation between two coordinate frames independent of motion plane (de Vries et al. 2009; Lebel et al. 2013; Ricci, Taffoni, and Formica 2016).

$$err_{Tot}(t) = 2\operatorname{acos}(\Delta q_0(t))$$

(5.14)

$\Delta q(t)$ was decoupled into directional components to further describe its error characteristics. Error components in heading, pitch, and roll directions were calculated using (5.4). The attitude error component was calculated using (5.15) and (5.16), where $\Delta q_{0att}(t)$ is the scalar component of Δq_{att}. Attitude error is a combination of the pitch and roll error components, given each represents inclination with respect to gravity (Gabriele Ligorio et al. 2016; Bergamini et al. 2014; Gabriele Ligorio and Sabatini 2016).

$$\Delta q_{att}(t) = \begin{bmatrix} \cos(\Delta\theta(t)/2) \\ 0 \\ \sin(\Delta\theta(t)/2) \\ 0 \end{bmatrix} \otimes \begin{bmatrix} \cos(\Delta\phi(t)/2) \\ \sin(\Delta\phi(t)/2) \\ 0 \\ 0 \end{bmatrix} \tag{5.15}$$

$$err_{Att}(t) = 2\arccos(\Delta q_{0att}(t)) \tag{5.16}$$

RMS error was calculated to provide the "average" error for each trial using (17).

$$RMS_{err} = \sqrt{\frac{1}{n}\sum_{t=0}^{n} err(t)^2} \tag{5.17}$$

5.2.8 Statistical Analysis

Two-factor repeated measures analyses of variance (ANOVA) were used to estimate the fixed effects of motion speed (slow/medium/fast), magnetic disturbance (absent/present), and their interaction on (i) mean ω_n, mean a_n, mean m_n, and measures of variation in M_{head}, m_n, and a_n values and (ii) total and directional spatial IMU spatial orientation errors. Separate models were constructed for each IMU sensor location (i.e., upper arm, forearm, and hand) and summary measure, and the Greenhouse-Geisser correction was used to adjust for violations of sphericity. Post-hoc comparisons of summary measures between pairs of motion speed levels were made using the Tukey procedure. All statistical procedures were performed using SPSS Statistics 23 (IBM, SPSS, Chicago, Illinois, USA).

The repetitive task required roughly 35° of yaw, 50° of pitch, and 30° of roll ranges of motion (i.e., 90th–10th percentiles), on average, for the three sensor locations (Table 5.1). As expected, mean ω_n, mean a_n, and measures of a_n variation increased with motion speed (main effect of motion speed p<0.01 for all summary measures, and p<0.01 between all pairs of motion speed levels), with the greatest velocities in the hand sensor (Table 5.2). Neither the main effect of magnetic disturbance nor the interaction between motion speed and magnetic disturbance were statistically significant for these measures.

Table 5.1. Mean (SD) range of motion (90th–10th percentiles) across all participants and experimental trials.

IMU Location	Yaw (°)	Pitch (°)	Roll (°)
Upper Arm	36.2(20.6)	53.8(5.4)	35.3(21.2)
Forearm	35.9(8.1)	45.1(4.8)	29.8(6.4)
Hand	33.1(7.4)	55.1(6.3)	28.1(9.2)

Table 5.2. Main effect of motion speed on angular velocity, acceleration and measures of acceleration variation; all values reported as mean (SD). A statistically significant difference (p<0.01) between levels of motion speed was observed for all measures.

	Slow	Medium	Fast
Upper Arm			
Mean angular velocity vector magnitude [ω_n] (°/s)	36.5(2.8)	72.5(6.4)	108.8(14.3)
Acceleration vector magnitude [α_n] (m/s²)			
Mean	9.9(0.3)	10.1(0.3)	10.4(0.2)
Peak-to-peak	1.0(0.2)	2.4(0.6)	3.9(0.7)
Standard deviation	0.4(0.1)	1.0(0.2)	1.5(0.2)
Forearm			
Mean angular velocity vector magnitude [ω_n] (°/s)	40.7(4.9)	79.6(7.7)	117.0(10.9)
Acceleration vector magnitude [α_n] (m/s²)			
Mean	9.9(0.1)	10.0(0.1)	10.6(0.2)
Peak-to-peak	1.7(0.3)	4.7(0.6)	8.0(0.8)
Standard deviation	0.7(0.1)	1.8(0.2)	3.1(0.3)
Hand			
Mean angular velocity vector magnitude [ω_n] (°/s)	48.6(4.6)	99.9(10.7)	154.3(18.9)
Acceleration vector magnitude [α_n] (m/s²)			
Mean	9.9(0.03)	10.1(0.06)	10.9(0.2)
Peak-to-peak	2.2(0.4)	6.5(0.8)	12.1(1.2)
Standard deviation	0.9(0.2)	2.5(0.3)	4.7(0.5)

The main effect of magnetic disturbance on magnetic heading variation (i.e., standard deviation and peak-to-peak) was statistically significant for both the hand and forearm sensors (p < 0.01), but not for the upper arm sensor (Table 5.3). As expected, greater errors were observed when the metal plate was present. The nature of this effect was further observed through substantial changes in magnetic heading as

the hand approached the unloading container (Figure 5.2). Moreover, for the hand sensor, a clear relationship was observed between the total magnetic field strength and magnetic heading during trials with the metal plate (Figure 5.3). Similar effects were not observed for the IMUs on the forearm and upper arm. Neither the main effect of motion speed nor the interaction between motion speed and magnetic disturbance on measures of magnetic heading variation was statistically significant.

Table 5.3. Main effect of magnetic disturbance on measures of magnetic heading and magnetic field strength variation; all values reported as mean (SD).

	Metal Absent	Metal Present	p
Upper Arm			
Magnetic heading [M_{head}] (°)			
Peak-to-peak	4.6(1.3)	4.1(1.1)	
Standard deviation	1.8(0.5)	1.6(0.4)	
Magnetic field strength vector magnitude [m_n] (μT)			
Mean	52.1(0.6)	52.0(0.6)	
Peak-to-peak	2.5(0.5)	2.4(0.4)	
Standard deviation	0.4(0.1)	0.5(0.2)	
Forearm			
Magnetic heading [M_{head}] (°)			
Peak-to-Peak	5.8(1.6)	11.6(2.1)	< 0.01
Standard Deviation	2.4(0.8)	4.5(0.8)	< 0.01
Magnetic field strength vector magnitude [m_n] (μT)			
Mean	53.0(0.4)	53.0(0.7)	
Peak-to-Peak	2.0(0.3)	2.6(1.1)	
Standard deviation	0.8(0.1)	1.0(0.4)	
Hand			
Magnetic heading [M_{head}] (°)			
Peak-to-peak	5.6(1.3)	29.8(7.0)	< 0.01
Standard deviation	2.2(0.5)	11.6(2.8)	< 0.01
Magnetic field strength vector magnitude [m_n] (μT)			
Mean	53.3(0.5)	53.4(1.8)	
Peak-to-peak	2.5(0.2)	6.1(1.4)	< 0.01
Standard deviation	1.0(0.1)	2.4(0.5)	< 0.01
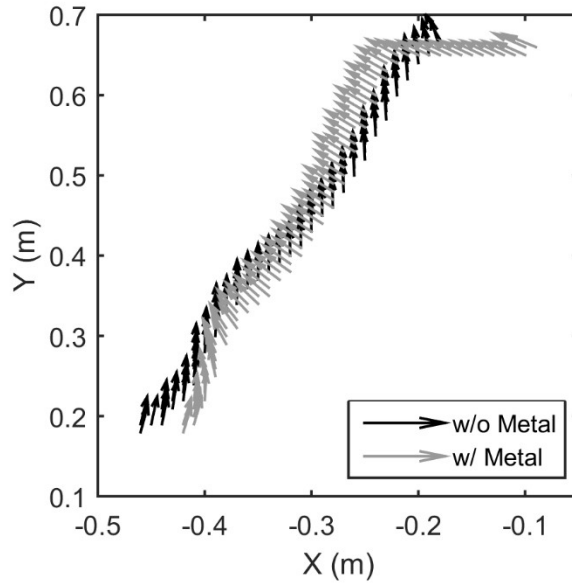
Figure 5.2. Effect of the metal plate on the direction of the local magnetic field for the hand sensor; data from one participant (medium motion speed).

The main effect of motion speed on IMU attitude and pitch RMS error was statistically significant for the IMU on the hand (Table 5.4), with error increasing as motion speed increased. However, the small differences in RMS errors between motion speed conditions suggest that the IMU gyroscope was able to attenuate motion-related artifacts for the range of motion speeds assigned. In general, neither the main effect of magnetic disturbance nor the interaction between magnetic disturbance and motion speed on IMU attitude, pitch, or roll RMS error was statistically significant. The effect of magnetic disturbance on IMU pitch error approached statistical significance, but the magnitude of the effect was small (< 0.1°).

Table 5.4. Mean (SD) root-mean-square IMU error components (in degrees) by local magnetic field disturbance (metal absent vs metal present) and motion speed (slow, medium, and fast).

	Metal Absent			Metal Present			Tests of Fixed Effects[1] (p)		
	Slow	Medium	Fast	Slow	Medium	Fast	Speed	Mag.	Int.
Upper Arm									
Pitch	0.7(0.4)	0.7(0.4)	0.7(0.4)	0.6(0.3)	0.7(0.4)	0.7(0.4)	0.16	0.15	0.24
Roll	0.6(0.5)	0.6(0.3)	0.6(0.3)	0.5(0.2)	0.6(0.2)	0.6(0.2)	0.72	0.28	0.82
Attitude[2]	0.9(0.6)	0.9(0.5)	1.0(0.4)	0.8(0.4)	0.9(0.4)	0.9(0.4)	0.28	0.17	0.50
Heading	1.5(2.1)	1.5(1.4)	1.4(0.8)	1.2(0.9)	1.2(1.0)	1.2(0.9)	0.97	0.25	0.91
Total[3]	1.8(2.2)	1.8(1.5)	1.7(0.8)	1.5(0.9)	1.6(0.9)	1.6(0.9)	0.97	0.25	0.94
Forearm									
Pitch	0.5(0.2)	0.6(0.3)	0.7(0.9)	0.5(0.2)	0.5(0.2)	0.6(0.4)	0.11	0.05	0.84
Roll	0.9(0.6)	1.0(0.6)	0.9(0.4)	1.0(0.6)	0.8(0.4)	0.9(0.4)	0.62	0.44	0.40
Attitude	1.1(0.6)	1.2(0.7)	1.2(0.7)	1.1(0.6)	1.0(0.4)	1.1(0.5)	0.67	0.17	0.56
Heading	1.0(0.8)	1.1(0.8)	1.4(2.1)	1.2(0.6)	1.3(0.6)	1.3(0.7)	0.56	0.58	0.61
Total	1.5(1.0)	1.6(0.9)	1.9(2.1)	1.7(0.7)	1.7(0.7)	1.8(0.7)	0.57	0.82	0.60
Hand									
Pitch	0.4(0.3)	0.5(0.2)	0.6(0.2)	0.3(0.1)	0.4(0.2)	0.7(0.2)	<0.01	0.93	0.29
Roll	0.6(0.4)	0.5(0.1)	0.5(0.1)	0.4(0.1)	0.5(0.1)	0.5(0.1)	0.51	0.52	0.14
Attitude	0.7(0.4)	0.7(0.2)	0.8(0.2)	0.6(0.1)	0.6(0.2)	0.9(0.3)	0.02	0.63	0.16
Heading	1.2(1.3)	0.8(0.3)	2.1(1.4)	1.8(1.0)	1.8(1.0)	2.1(1.4)	0.27	0.03	0.71
Total	1.4(1.3)	1.1(0.3)	1.6(0.8)	1.9(1.3)	1.9(1.0)	2.4(1.3)	0.19	0.03	0.66

[1] p-values from ANOVA tests of fixed effects (i.e., main effects of motion speed and magnetic disturbance, and their interaction)

[2] Attitude is the combination of pitch and roll

[3] Total is the combination of pitch, roll and heading

We expected to observe time-dependent sample-to-sample differences between the OMC and IMU measurements in the heading direction when the metal plate was present, but not when the metal plate was absent. While this behavior was observed for some trials (Figure 5.4), time-dependence was observed across all trials upon examination of ensemble averages of the heading error (i.e., across all participants both with and without the metal plate, Figure 5.5). Not considering the time-dependence, the main effect of magnetic disturbance on IMU heading error was statistically significant only for the IMU on the hand (Table 5.4), with larger errors observed during trials with the metal plate.
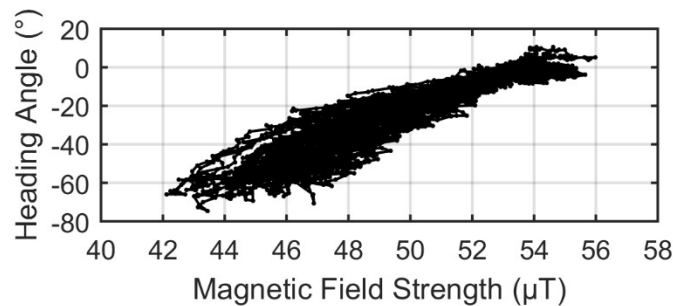
Figure 5.3. Relationship between magnetic field strength and magnetic heading angle for a single trial.
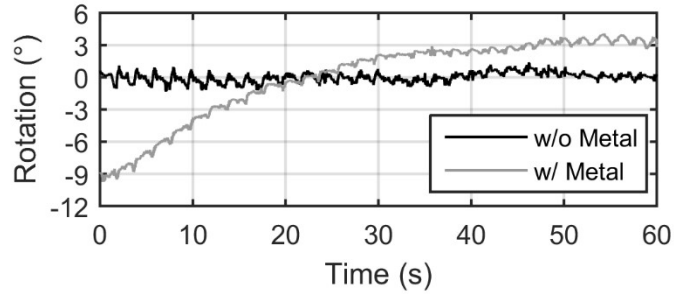
Figure 5.4. Sample-to-sample differences between the OMC and IMU heading measurements for the hand sensor across two trials (data from one participant at medium speed).
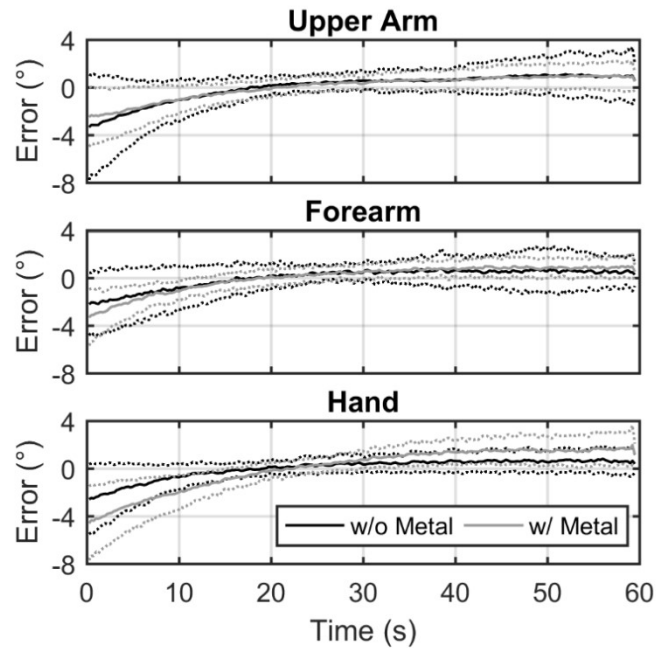
Figure 5.5. Ensemble averages of the sample-to-sample differences between the OMC and IMU heading measurements with and without the metal plate. Standard deviations at each sample time are denoted with dotted lines.

5.4 Discussion

We examined errors in IMU spatial orientation measurements at upper extremity motion speeds common to industrial environments and both with and without the presence of a local magnetic field disturbance. In general, the magnitude of IMU error associated with magnetic disturbance was greater than that associated with motion speed. Statistically significant interactions between motion speed and magnetic disturbances were not observed.

83

5.4.1 Relationship between Magnetic Field Strength and Magnetic Heading Direction

The ambient magnetic field within the experimental area was relatively homogenous. The magnetic heading standard deviation under ambient conditions was <3° across all IMUs, consistent with de Vries et al., (2009). For the hand sensor and during trials without the metal plate, the average peak-to-peak variation in magnetic heading was <6° while the average magnetic field strength standard deviation was 1.0uT. Conversely, during trials with the metal plate, the average peak-to-peak variation in magnetic heading increased to approximately 30° while the average magnetic field strength standard deviation increased to 2.4uT. While this relationship may differ across other sources of magnetic disturbance, the results reinforce the notion that local magnetic field disturbances should be minimized when using IMUs for human motion capture. From a practical perspective, these results suggest it may be possible to use computationally simple methods to indirectly infer magnetometer data quality.

5.4.2 Magnitude of IMU Error

For the IMU on the hand, motion speed affected IMU attitude and pitch RMS error, whereas magnetic disturbance affected IMU heading error. Consistent with our results, previous studies have reported RMS errors between 1° and 6° in heading, less than 3.5° in attitude, and total RMS error less than 2.1° (Bergamini et al. 2014; Faber et al. 2013; Lebel et al. 2013; Gabriele Ligorio et al. 2016; Ricci, Taffoni, and Formica 2016). Differences in sampling timeframe (Lebel et al. 2015), methods used to align the IMU and OMC systems (Robert-Lachaine et al. 2016), and error calculation (Faber et al. 2013) may explain the range of values. (Lebel et al. 2013)) also evaluated the effect of motion speed on IMU error (using the same sensor model and embedded Kalman filter in the current study). In their study, IMUs were exposed to 'slow' (90°/s) and 'fast' (180°/s) angular velocities using a mechanical gimbal. Average total RMS errors of 1.2° and 2.1° were observed (i.e., within 1° of the total RMS of the current study). Similarly, (Ricci, Taffoni, and Formica 2016)) observed small increases (<2°) of IMU error with increases in motion frequency and amplitude. Regardless, the IMU attitude and pitch RMS errors appeared stable and consistent, indicating that pitch and roll measurements can be used in lieu of error-prone, accelerometer-

only methods common to field-based measurement of human motion in ergonomics (David 2005; Li and Buckle 1999).

Time-dependent error characteristics were observed in the heading direction both with and without the presence of the metal plate. This behavior has been observed in studies describing methods of minimizing the effect of magnetic disturbance in the sensor fusion process (Gabriele Ligorio and Sabatini 2016; Madgwick, Harrison, and Vaidyanathan 2011; Daniel Roetenberg et al. 2005; Sabatini 2006). Consistent with (Lebel et al. 2015), the time-dependent error characteristics were apparent under our one-minute sampling timeframe.

5.4.3 Methodological Considerations

Although similar trends have been observed in published Kalman filter designs (Bergamini et al. 2014; Gabriele Ligorio and Sabatini 2016), the IMU error magnitudes and characteristics observed in this study are applicable to the specific hardware and Kalman filter specifications (which are proprietary). Other inertial-based motion capture systems may use proprietary filters based on other strategies to minimize the effects of magnetic disturbances, such as zero-velocity updates (Schiefer et al. 2014) or dynamics-based kinematic modeling (El-Gohary and McNames 2012). Also, the relationship between magnetic field strength standard deviation and magnetic heading deviation may be different with other sources of magnetic disturbance. More powerful disturbances may increase errors due to larger directional changes within the local magnetic field and increased time any single IMU remains within the disrupted area.

In preliminary tests, the fast transfer speed (45 transfers/min) was difficult for participants to maintain for longer than one minute due to fatigue. While task durations of one minute or less have been reported in studies describing IMU accuracy (Bergamini et al. 2014; M.a. Brodie, Walmsley, and Page 2008; El-Gohary and McNames 2012; Faber et al. 2013; Gabriele Ligorio and Sabatini 2016; Ricci, Taffoni, and Formica 2016), longer sampling durations are generally needed in field studies and, therefore, more likely to result in greater measurement error. Furthermore, the relatively short sampling duration and per-trial alignment of the IMU and OMC likely resulted in underestimation of the true IMU error. Finally, this study examined the errors in estimation of the spatial orientation of IMUs and not errors in the

estimation of kinematic constructs (such as joint angles). Differences in biomechanical models (Robert-Lachaine et al. 2016) and the potential compounding of errors between two IMUs (Lebel et al. 2013) may partially explain the larger joint angle errors observed in recent studies evaluating the IMU accuracy for field-based applications (Cuesta-Vargas, Galán-Mercant, and Williams 2010; Kim and Nussbaum 2013; Schall et al. 2015). Continued development of smaller, cheaper, and more accurate IMU hardware designs as well as strategies to identify and compensate for local magnetic field disturbances will allow for improved kinematic estimations as time progresses.

In conclusion, we evaluated (i) the relationship between magnetic field strength and magnetic heading angle and (ii) the effects of motion speed and magnetic disturbance on the spatial orientation accuracy of IMUs worn on the distal upper extremity. In general, we observed small magnetic heading angle variation ($< \sim 2.5°$ standard deviation) when the standard deviation of the magnetic field strength vector magnitude was $<1.0 \ \mu$T. While heading error was time-dependent both with and without the presence of magnetic disturbance, attitude and pitch errors were stable with respect to time. Motion speed affected IMU error to a lesser extent than magnetic disturbance, and no statistically significant interactions were observed. These results suggest that (i) motion speed has a negligible effect on IMU spatial orientation accuracy, and (ii) magnetic disturbances leading to a magnetic field strength standard deviation exceeding $1.0 \ \mu$T may hinder the use of IMUs to capture three-dimensional kinematics. Assessing repeatability of IMUs across trials and for longer timeframes, effects of larger magnetic disturbances on IMU error, accuracy of relative orientation measurements between two IMUs, as well as IMU alignment methods are to be investigated in the future.

CHAPTER 6

CONCLUSIONS, STUDY LIMITATIONS, AND FUTURE WORK

The use of IMUs in field-based ergonomics research is expected to increase as hardware development accelerates and more commercial options become available. Quantifying exposure to non-neutral postures is one of many applications for IMUs for ergonomists. Quantifying joint loadings and task-level information (e.g. task identification, task frequency, task duration) may be other applications of IMUs within occupational ergonomics.

Overall, the findings from this thesis contribute to the ergonomics community's understanding of the current capabilities and limitations of IMUs. These studies suggest that while the touted capability of the IMUs (i.e, full-body motion capture in workplace settings) is not likely achievable at this time, IMUs are still substantially more accurate than the accelerometer-based inclinometers commonly used by ergonomists to measure motions of the upper arms.

The primary strength of this research is the systematic isolation and control of error sources that may affect measurement differences between the optical motion capture systems (OMC) and IMUs. Errors due to soft tissue artifacts were controlled by attaching a rigid marker cluster to the IMU surface. Any deviations due to soft tissue artifacts, therefore, affect both measurement systems equally. The two measurement systems were aligned using established procedures to control for misalignment between the measurement systems. All trials were also kept to a consistent measurement timeframe to control for potential time dependent IMU errors. Finally, the fastest of the motion speeds tested was selected based on extensive pilot testing to represent the upper limits of sustainable human speeds expected within the workplace setting.

This study is not without limitations that should be accounted in the future. The failure to use a biomechanical-based marker set instead of a rigid marker cluster may limit the generalizability of the results, given that differences in protocol applied to the measurement systems is a source of error regardless of IMU accuracy. While the one-minute trials enabled higher motion speeds, the trial length have prevented the accumulation of the time-dependent errors observed, particularly in the heading direction. In this study, an available, non-proprietary Kalman filter design was implemented to enhance the ability of others to

reproduce our findings. We suspect that newer IMU hardware with more accurate gyroscopes may result in lower error magnitudes. Furthermore, the implemented Kalman filter was not optimally designed nor tuned to attenuate for magnetic disturbances. Finally, there are also inherent errors within the OMC reference device. The accuracy of our system, for example, is <1mm for linear positions. However, the accuracy of OMC-derived spatial orientation is also dependent on the spacing between the markers attached to the rigid body. While the OMC displays a known and consistent error characteristic, the limits of agreement are also bounded by the OMC system.

Both the application and development of IMUs should be investigated into the distant future. While magnetic disturbance is a major source of IMU error, stable and accurate inclination measurements may be relevant towards (i) assessing within-subject posture variability to better understand occupational exposure, and (ii) applying machine learning concepts to recognize other dimensions of exposure such as task frequency and task duration. The continual development of IMUs may focus on combining gyroscopes and accelerometers with body-worn vision sensors, indoor positioning sensors, and gyroscope arrays to improve measurement accuracy. Methodological considerations to improve comparability with OMC systems using a biomechanical marker set.

REFERENCES

Åkesson, I., G.-Å Hansson, I. Balogh, U. Moritz, and S. Skerfving. 1997. "Quantifying Work Load in Neck, Shoulders and Wrists in Female Dentists." *International Archives of Occupational and Environmental Health* 69 (6): 461–474. doi:10.1007/s004200050175.

Ali, Abdelrahman, and Naser El-Sheimy. 2013. "Low-Cost MEMS-Based Pedestrian Navigation Technique for GPS-Denied Areas." *Journal of Sensors* 2013 (August): e197090. doi:10.1155/2013/197090.

Amasay, Tal, Keely Zodrow, Laurel Kincl, Jennifer Hess, and Andrew Karduna. 2009. "Validation of Tri-Axial Accelerometer for the Calculation of Elevation Angles." *International Journal of Industrial Ergonomics* 39 (5): 783–789. doi:10.1016/j.ergon.2009.03.005.

American Academy of Orthopaedic Surgeons. 2008. "The Burden of Musculoskeletal Diseases in the United States: Prevalence, Societal and Economic Cost." *Rosemont, IL*.

Asundi, Krishna, Peter W. Johnson, and Jack T. Dennerlein. 2012. "Variance in Direct Exposure Measures of Typing Force and Wrist Kinematics across Hours and Days among Office Computer Workers." *Ergonomics* 55 (8): 874–884. doi:10.1080/00140139.2012.681807.

Bachmann, Eric R. 2000. "Inertial and Magnetic Tracking of Limb Segment Orientation for Inserting Humans into Synthetic Environments." Monterey, CA: Naval Postgraduate School.

Bachmann, Eric R., Robert B. McGhee, Xiaoping Yun, and Michael J. Zyda. 2001. "Inertial and Magnetic Posture Tracking for Inserting Humans into Networked Virtual Environments." In *Proceedings of the ACM Symposium on Virtual Reality Software and Technology*, 9–16. VRST '01. New York, NY, USA: ACM. doi:10.1145/505008.505011.

Bachmann, Eric R., Xiaoping Yun, and Christopher W. Peterson. 2004. "An Investigation of the Effects of Magnetic Variations on Inertial/Magnetic Orientation Sensors." In *2004 IEEE International Conference on Robotics and Automation, 2004. Proceedings. ICRA '04*, 2:1115–1122 Vol.2. doi:10.1109/ROBOT.2004.1307974.

Balogh, I., K. Ohlsson, C. Nordander, S. Skerfving, and G. -Å. Hansson. 2009. "Precision of Measurements of Physical Workload during Standardized Manual Handling Part III: Goniometry of the Wrists." *Journal of Electromyography and Kinesiology* 19 (5): 1005–1012. doi:10.1016/j.jelekin.2008.07.003.

Bergamini, Elena, Gabriele Ligorio, Aurora Summa, Giuseppe Vannozzi, Aurelio Cappozzo, and Angelo Maria Sabatini. 2014. "Estimating Orientation Using Magnetic and Inertial Sensors and Different Sensor Fusion Approaches: Accuracy Assessment in Manual and Locomotion Tasks." *Sensors* 14 (10): 18625–18649. doi:10.3390/s141018625.

Bernard, Bruce P. 1997. "Musculoskeletal Disorders and Workplace Factors: A Critical Review of Epidemiologic Evidence for Work-Related Musculoskeletal Disorders of the Neck, Upper Extremity, and Low Back." In *Musculoskeletal Disorders and Workplace Factors: A Critical Review of Epidemiologic Evidence for Work-Related Musculoskeletal Disorders of the Neck, Upper Extremity, and Low Back*. NIOSH.

Bernmark, Eva, and Christina Wiktorin. 2002. "A Triaxial Accelerometer for Measuring Arm Movements." *Applied Ergonomics* 33 (6): 541–547. doi:10.1016/S0003-6870(02)00072-8.

BLS. 2013. *Nonfatal Occupational Injuries and Illnesses Requiring Days Away from Work, 2014*. United States Bureau of Labor Statistics.

BLS. 2015. *Nonfatal Occupational Injuries and Illnesses Requiring Days Away from Work, 2012*. USDL 15-2205. United States Bureau of Labor Statistics. www.bls.gov/news.release/pdf/osh2.pdf.

Bó, A. P. L., M. Hayashibe, and P. Poignet. 2011. "Joint Angle Estimation in Rehabilitation with Inertial Sensors and Its Integration with Kinect." In *2011 Annual International Conference of the IEEE Engineering in Medicine and Biology Society*, 3479–3483. doi:10.1109/IEMBS.2011.6090940.

Bongers, P. M., S. Ijmker, S. van den Heuvel, and B. M. Blatter. 2006. "Epidemiology of Work Related Neck and Upper Limb Problems: Psychosocial and Personal Risk Factors (Part I) and Effective Interventions from a Bio Behavioural Perspective (Part II)." *Journal of Occupational Rehabilitation* 16 (3): 272–295. doi:10.1007/s10926-006-9044-1.

Bonnechère, B., B. Jansen, P. Salvia, H. Bouzahouene, V. Sholukha, J. Cornelis, M. Rooze, and S. Van Sint Jan. 2014. "Determination of the Precision and Accuracy of Morphological Measurements Using the Kinect™ Sensor: Comparison with Standard Stereophotogrammetry." *Ergonomics* 57 (4): 622–631. doi:10.1080/00140139.2014.884246.

Brigante, Carmen M.N., Nunzio Abbate, Adriano Basile, Alessandro Carmelo Faulisi, and Salvatore Sessa. 2011. "Towards Miniaturization of a MEMS-Based Wearable Motion Capture System." *IEEE Transactions on Industrial Electronics* 58 (8): 3234–3241. doi:10.1109/TIE.2011.2148671.

Brodie, M.a., A. Walmsley, and W. Page. 2008. "Dynamic Accuracy of Inertial Measurement Units during Simple Pendulum Motion." *Computer Methods in Biomechanics and Biomedical Engineering* 11 (3): 235–242. doi:10.1080/10255840802125526.

Brodie, Matthew, Alan Walmsley, and Wyatt Page. 2008. "Fusion Motion Capture: A Prototype System Using Inertial Measurement Units and GPS for the Biomechanical Analysis of Ski Racing." *Sports Technology* 1 (1): 17–28. doi:10.1002/jst.6.

Buchholz, Bryan, and Helen Wellman. 1997. "Practical Operation of a Biaxial Goniometer at the Wrist Joint." *Human Factors: The Journal of the Human Factors and Ergonomics Society* 39 (1): 119–129. doi:10.1518/001872097778940696.

Buckle, Peter W, and J Jason Devereux. 2002. "The Nature of Work-Related Neck and Upper Limb Musculoskeletal Disorders." *Applied Ergonomics*, Fundamental Reviews in Applied Ergonomics 2002, 33 (3): 207–217. doi:10.1016/S0003-6870(02)00014-5.

Carmi, Avishy, and Yaakov Oshman. 2009. "Adaptive Particle Filtering for Spacecraft Attitude Estimation from Vector Observations." *Journal of Guidance, Control, and Dynamics* 32 (1): 232–241. doi:10.2514/1.35878.

Chang, Honglong, Liang Xue, Wei Qin, Guangmin Yuan, and Weizheng Yuan. 2008. "An Integrated MEMS Gyroscope Array with Higher Accuracy Output." *Sensors* 8 (4): 2886–2899. doi:10.3390/s8042886.

Chardonnens, Julien, Julien Favre, and Kamiar Aminian. 2012. "An Effortless Procedure to Align the Local Frame of an Inertial Measurement Unit to the Local Frame of Another Motion Capture System." *Journal of Biomechanics* 45 (13): 2297–2300. doi:10.1016/j.jbiomech.2012.06.009.

Cloete, T., and C. Scheffer. 2008. "Benchmarking of a Full-Body Inertial Motion Capture System for Clinical Gait Analysis." In *2008 30th Annual International Conference of the IEEE Engineering in Medicine and Biology Society*, 4579–4582. doi:10.1109/IEMBS.2008.4650232.

Cook, Catherine, Robin Burgess-Limerick, and Shona Papalia. 2004. "The Effect of Wrist Rests and Forearm Support during Keyboard and Mouse Use." *International Journal of Industrial Ergonomics* 33 (5): 463–472. doi:10.1016/j.ergon.2003.12.002.

Corazza, S., L. Mündermann, A. M. Chaudhari, T. Demattio, C. Cobelli, and T. P. Andriacchi. 2006. "A Markerless Motion Capture System to Study Musculoskeletal Biomechanics: Visual Hull and Simulated Annealing Approach." *Annals of Biomedical Engineering* 34 (6): 1019–1029. doi:10.1007/s10439-006-9122-8.

Cuesta-Vargas, Antonio I., Alejandro Galán-Mercant, and Jonathan M. Williams. 2010. "The Use of Inertial Sensors System for Human Motion Analysis." *Physical Therapy Reviews* 15 (6): 462–473. doi:10.1179/1743288X11Y.0000000006.

Cutti, Andrea Giovanni, Angelo Cappello, and Angelo Davalli. 2006. "In Vivo Validation of a New Technique That Compensates for Soft Tissue Artefact in the Upper-Arm: Preliminary Results." *Clinical Biomechanics*, Proceedings of the 5th Meeting of the International Shoulder Group, 21, Supplement 1: S13–S19. doi:10.1016/j.clinbiomech.2005.09.018.

Cutti, Andrea Giovanni, Andrea Giovanardi, Laura Rocchi, Angelo Davalli, and Rinaldo Sacchetti. 2007. "Ambulatory Measurement of Shoulder and Elbow Kinematics through Inertial and Magnetic Sensors." *Medical & Biological Engineering & Computing* 46 (2): 169–178. doi:10.1007/s11517-007-0296-5.

Dartt, Angela, John Rosecrance, Fred Gerr, Peter Chen, Dan Anton, and Linda Merlino. 2009. "Reliability of Assessing Upper Limb Postures among Workers Performing Manufacturing Tasks." *Applied Ergonomics* 40 (3): 371–378. doi:10.1016/j.apergo.2008.11.008.

David, G. C. 2005. "Ergonomic Methods for Assessing Exposure to Risk Factors for Work-Related Musculoskeletal Disorders." *Occupational Medicine* 55 (3): 190–199. doi:10.1093/occmed/kqi082.

de Vries, W. H. K., H. E. J. Veeger, C. T. M. Baten, and F. C. T. van der Helm. 2009. "Magnetic Distortion in Motion Labs, Implications for Validating Inertial Magnetic Sensors." *Gait & Posture* 29 (4): 535–541. doi:10.1016/j.gaitpost.2008.12.004.

de Vries, W. H. K., H. E. J. Veeger, A. G. Cutti, C. Baten, and F. C. T. van der Helm. 2010. "Functionally Interpretable Local Coordinate Systems for the Upper Extremity Using Inertial & Magnetic Measurement Systems." *Journal of Biomechanics* 43 (10): 1983–1988. doi:10.1016/j.jbiomech.2010.03.007.

Dornaika, F., and R. Horaud. 1998. "Simultaneous Robot-World and Hand-Eye Calibration." *IEEE Transactions on Robotics and Automation* 14 (4): 617–622. doi:10.1109/70.704233.

Douphrate, David I., Nathan B. Fethke, Matthew W. Nonnenmann, John C. Rosecrance, and Stephen J. Reynolds. 2012. "Full Shift Arm Inclinometry Among Dairy Parlor Workers: A Feasibility Study in a Challenging Work Environment." *Applied Ergonomics* 43 (3): 604–613. doi:10.1016/j.apergo.2011.09.007.

Dutta, Tilak. 2012. "Evaluation of the Kinect^{TM} Sensor for 3-D Kinematic Measurement in the Workplace." *Applied Ergonomics* 43 (4): 645–649. doi:10.1016/j.apergo.2011.09.011.

El-Gohary, M., and J. McNames. 2012. "Shoulder and Elbow Joint Angle Tracking With Inertial Sensors." *IEEE Transactions on Biomedical Engineering* 59 (9): 2635–2641. doi:10.1109/TBME.2012.2208750.

El-Gohary, M., and J. McNames. 2015. "Human Joint Angle Estimation with Inertial Sensors and Validation with A Robot Arm." *IEEE Transactions on Biomedical Engineering* 62 (7): 1759–1767. doi:10.1109/TBME.2015.2403368.

Faber, Gert S., Chien-Chi Chang, Peter Rizun, and Jack T. Dennerlein. 2013. "A Novel Method for Assessing the 3-D Orientation Accuracy of Inertial/Magnetic Sensors." *Journal of Biomechanics* 46 (15): 2745–2751. doi:10.1016/j.jbiomech.2013.07.029.

Fahrenberg, Jochen, Friedrich Foerster, Manfred Smeja, and Wolfgang Müller. 1997. "Assessment of Posture and Motion by Multichannel Piezoresistive Accelerometer Recordings." *Psychophysiology* 34 (5): 607–612. doi:10.1111/j.1469-8986.1997.tb01747.x.

Faragher, R. 2012. "Understanding the Basis of the Kalman Filter Via a Simple and Intuitive Derivation [Lecture Notes]." *IEEE Signal Processing Magazine* 29 (5): 128–132. doi:10.1109/MSP.2012.2203621.

Fethke, Nathan B., Lauren C. Gant, and Fred Gerr. 2011. "Comparison of Biomechanical Loading during Use of Conventional Stud Welding Equipment and an Alternate System." *Applied Ergonomics* 42 (5): 725–734. doi:10.1016/j.apergo.2010.11.007.

Fethke, Nathan B., Fred Gerr, Dan Anton, Joseph E. Cavanaugh, and Mark T. Quickel. 2012. "Variability in Muscle Activity and Wrist Motion Measurements Among Workers Performing Non-Cyclic Work." *Journal of Occupational and Environmental Hygiene* 9 (1): 25–35. doi:10.1080/15459624.2012.634361.

Fethke, Nathan B., Linda A. Merlino, Fredric Gerr, Mark C. Schall, and Cassidy A. Branch. 2015. "Musculoskeletal Pain among Midwest Farmers and Associations with Agricultural Activities." *American Journal of Industrial Medicine* 58 (3): 319–330. doi:10.1002/ajim.22398.

Fethke, Nathan B., Thomas M. Peters, Stephanie Leonard, Mahmoud Metwali, and Imali A. Mudunkotuwa. 2016. "Reduction of Biomechanical and Welding Fume Exposures in Stud Welding." *Annals of Occupational Hygiene* 60 (3): 387–401. doi:10.1093/annhyg/mev080.

Foxlin, E. 1996. "Inertial Head-Tracker Sensor Fusion by a Complementary Separate-Bias Kalman Filter." In *Virtual Reality Annual International Symposium, 1996., Proceedings of the IEEE 1996*, 185–194, 267. doi:10.1109/VRAIS.1996.490527.

Gerr, Fred, Nathan Fethke, Linda Merlino, Dan Anton, John Rosecrance, Michael P. Jones, Michele Marcus, and Alysha Meyers. 2013. "A Prospective Study of Musculoskeletal Outcomes Among Manufacturing Workers I. Effects of Physical Risk Factors." *Human Factors: The Journal of the Human Factors and Ergonomics Society*, June, 0018720813491114. doi:10.1177/0018720813491114.

Godwin, Alison, Michael Agnew, and Joan Stevenson. 2009. "Accuracy of Inertial Motion Sensors in Static, Quasistatic, and Complex Dynamic Motion." *Journal of Biomechanical Engineering* 131 (11): 114501–114501. doi:10.1115/1.4000109.

Gośliński, J., M. Nowicki, and P. Skrzypczyński. 2015. "Performance Comparison of EKF-Based Algorithms for Orientation Estimation on Android Platform." *IEEE Sensors Journal* 15 (7): 3781–3792. doi:10.1109/JSEN.2015.2397397.

Hess, Jennifer A., Laurel Kincl, Tal Amasay, and Peter Wolfe. 2010. "Ergonomic Evaluation of Masons Laying Concrete Masonry Units and Autoclaved Aerated Concrete." *Applied Ergonomics*, Special Section: Recycling centres and waste handling – a workplace for employees and users., 41 (3): 477–483. doi:10.1016/j.apergo.2009.10.003.

Hsu, Yin-Hsin, Wen-Yin Chen, Hsiu-Chen Lin, Wendy T. J. Wang, and Yi-Fen Shih. 2009. "The Effects of Taping on Scapular Kinematics and Muscle Performance in Baseball Players with Shoulder Impingement Syndrome." *Journal of Electromyography and Kinesiology* 19 (6): 1092–1099. doi:10.1016/j.jelekin.2008.11.003.

Jackson, Jennie A., Svend Erik Mathiassen, Jens Wahlström, Per Liv, and Mikael Forsman. 2015. "Is What You See What You Get? Standard Inclinometry of Set Upper Arm Elevation Angles." *Applied Ergonomics* 47 (March): 242–252. doi:10.1016/j.apergo.2014.08.014.

Jonsson, Per, and Peter W. Johnson. 2001. "Comparison of Measurement Accuracy between Two Types of Wrist Goniometer Systems." *Applied Ergonomics* 32 (6): 599–607. doi:10.1016/S0003-6870(01)00036-9.

Karasek, Robert, Chantal Brisson, Norito Kawakami, Irene Houtman, Paulien Bongers, and Benjamin Amick. 1998. "The Job Content Questionnaire (JCQ): An Instrument for Internationally Comparative Assessments of Psychosocial Job Characteristics." *Journal of Occupational Health Psychology* 3 (4): 322–355. doi:10.1037/1076-8998.3.4.322.

Kazmierczak, Karolina, Svend Erik Mathiassen, Mikael Forsman, and Jørgen Winkel. 2005. "An Integrated Analysis of Ergonomics and Time Consumption in Swedish 'craft-Type' Car Disassembly." *Applied Ergonomics* 36 (3): 263–273. doi:10.1016/j.apergo.2005.01.010.

Kim, Sunwook, and Maury A. Nussbaum. 2013. "Performance Evaluation of a Wearable Inertial Motion Capture System for Capturing Physical Exposures During Manual Material Handling Tasks." *Ergonomics* 56 (2): 314–326. doi:10.1080/00140139.2012.742932.

Kok, M., J. D. Hol, and T. B. Schön. 2015. "Indoor Positioning Using Ultrawideband and Inertial Measurements." *IEEE Transactions on Vehicular Technology* 64 (4): 1293–1303. doi:10.1109/TVT.2015.2396640.

Kontaxis, A., A. G. Cutti, G. R. Johnson, and H. E. J. Veeger. 2009. "A Framework for the Definition of Standardized Protocols for Measuring Upper-Extremity Kinematics." *Clinical Biomechanics* 24 (3): 246–253. doi:10.1016/j.clinbiomech.2008.12.009.

Korshøj, Mette, Jørgen H. Skotte, Caroline S. Christiansen, Pelle Mortensen, Jesper Kristiansen, Christiana Hanisch, Jørgen Ingebrigtsen, and Andreas Holtermann. 2014. "Validity of the Acti4 Software Using Actigraph Gt3x+accelerometer for Recording of Arm and Upper Body Inclination in Simulated Work Tasks." *Ergonomics* 57 (2): 247–253. doi:10.1080/00140139.2013.869358.

Kraft, Edgar. "A Quaternion-Based Unscented Kalman Filter for Orientation Tracking." In , 1:47–54. Cairns, Queensland, Australia: IEEE.

Lagarias, Jeffrey C., James A. Reeds, Margaret H. Wright, and Paul E. Wright. 1998. "Convergence Properties of the Nelder--Mead Simplex Method in Low Dimensions." *SIAM Journal on Optimization* 9 (1): 36. doi:http://dx.doi.org.proxy.lib.uiowa.edu/10.1137/S1052623496303470.

Landsbergis, Paul A., Joseph G. Grzywacz, and Anthony D. LaMontagne. 2014. "Work Organization, Job Insecurity, and Occupational Health Disparities." *American Journal of Industrial Medicine* 57 (5): 495–515. doi:10.1002/ajim.22126.

Latko, Wendi A., Thomas J. Armstrong, James A. Foulke, Gary D. Herrin, Randall A. Rabourn, and Sheryl S. Ulin. 1997. "Development and Evaluation of an Observational Method for Assessing Repetition in Hand Tasks." *American Industrial Hygiene Association Journal* 58 (4): 278–285. doi:10.1080/15428119791012793.

LaViola, J. J. 2003. "A Comparison of Unscented and Extended Kalman Filtering for Estimating Quaternion Motion." In *American Control Conference, 2003. Proceedings of the 2003*, 3:2435–2440 vol.3. doi:10.1109/ACC.2003.1243440.

Lebel, Karina, Patrick Boissy, Mathieu Hamel, and Christian Duval. 2013. "Inertial Measures of Motion for Clinical Biomechanics: Comparative Assessment of Accuracy under Controlled Conditions - Effect of Velocity." *PLOS ONE* 8 (11): e79945. doi:10.1371/journal.pone.0079945.

Lebel, Karina, Patrick Boissy, Mathieu Hamel, and Christian Duval. 2015. "Inertial Measures of Motion for Clinical Biomechanics: Comparative Assessment of Accuracy under Controlled Conditions – Changes in Accuracy over Time." *PLOS ONE* 10 (3): e0118361. doi:10.1371/journal.pone.0118361.

Lebel, Karina, Patrick Boissy, Hung Nguyen, and Christian Duval. 2016. "Autonomous Quality Control of Joint Orientation Measured with Inertial Sensors." *Sensors* 16 (7): 1037. doi:10.3390/s16071037.

Lee, J. K., E. J. Park, and S. N. Robinovitch. 2012. "Estimation of Attitude and External Acceleration Using Inertial Sensor Measurement During Various Dynamic Conditions." *IEEE Transactions on Instrumentation and Measurement* 61 (8): 2262–2273. doi:10.1109/TIM.2012.2187245.

Li, Guangyan, and Peter Buckle. 1999. "Current Techniques for Assessing Physical Exposure to Work-Related Musculoskeletal Risks, with Emphasis on Posture-Based Methods." *Ergonomics* 42 (5): 674–695. doi:10.1080/001401399185388.

Ligorio, G., and A. M. Sabatini. 2015. "A Linear Kalman Filtering-Based Approach for 3D Orientation Estimation from Magnetic/Inertial Sensors." In *2015 IEEE International Conference on Multisensor Fusion and Integration for Intelligent Systems (MFI)*, 77–82. doi:10.1109/MFI.2015.7295749.

Ligorio, Gabriele, Elena Bergamini, Ilaria Pasciuto, Giuseppe Vannozzi, Aurelio Cappozzo, and Angelo Maria Sabatini. 2016. "Assessing the Performance of Sensor Fusion Methods: Application to Magnetic-Inertial-Based Human Body Tracking." *Sensors* 16 (2): 153. doi:10.3390/s16020153.

Ligorio, Gabriele, and Angelo Maria Sabatini. 2015. "A Novel Kalman Filter for Human Motion Tracking With an Inertial-Based Dynamic Inclinometer." *IEEE Transactions on Biomedical Engineering* 62 (8): 2033–2043. doi:10.1109/TBME.2015.2411431.

Ligorio, Gabriele, and Angelo Maria Sabatini. 2016. "Dealing with Magnetic Disturbances in Human Motion Capture: A Survey of Techniques." *Micromachines* 7 (3): 43. doi:10.3390/mi7030043.

Luinge, H. J., P. H. Veltink, and C. T. M. Baten. 2007. "Ambulatory Measurement of Arm Orientation." *Journal of Biomechanics* 40 (1): 78–85. doi:10.1016/j.jbiomech.2005.11.011.

Luinge, H. J., and Professor P. H. Veltink. 2005. "Measuring Orientation of Human Body Segments Using Miniature Gyroscopes and Accelerometers." *Medical and Biological Engineering and Computing* 43 (2): 273–282. doi:10.1007/BF02345966.

Madgwick, Sebastian O.H., Andrew J.L. Harrison, and Ravi Vaidyanathan. 2011. "Estimation of IMU and MARG Orientation Using a Gradient Descent Algorithm." In *2011 IEEE International Conference on Rehabilitation Robotics*, 1–7. doi:10.1109/ICORR.2011.5975346.

Makni, A., H. Fourati, and A. Y. Kibangou. 2014. "Adaptive Kalman Filter for MEMS-IMU Based Attitude Estimation under External Acceleration and Parsimonious Use of Gyroscopes." In *Control Conference (ECC), 2014 European*, 1379–1384. doi:10.1109/ECC.2014.6862535.

Malchaire, J., N. Cock, and S. Vergracht. 2001. "Review of the Factors Associated with Musculoskeletal Problems in Epidemiological Studies." *International Archives of Occupational and Environmental Health* 74 (2): 79–90. doi:10.1007/s004200000212.

Malchaire, J., N. Cock, and S. Vergracht. "Review of the Factors Associated with Musculoskeletal Problems in Epidemiological Studies." *International Archives of Occupational and Environmental Health* 74 (2): 79–90. doi:10.1007/s004200000212.

Markley, F. Landis. 1988. "Attitude Determination Using Vector Observations and the Singular Value Decomposition." *The Journal of the Astronautical Sciences* 36 (3): 245–258.

Martori, Amanda L., Stephanie L. Carey, Redwan Alqasemi, Daniel Ashley, and Rajiv V. Dubey. 2013. "Characterizing Suitability of Wearable Sensors for Movement Analysis Using a Programmed Robotic Motion." In *Proceedings of the ASME 2013 International Mechanical Engineering Congress and Exposition IMECE2013*, V01AT20A032-V01AT20A032. San Diego, California, USA: American Society of Mechanical Engineers. doi:10.1115/IMECE2013-65064.

Mecheri, Hakim, Xavier Robert-Lachaine, Christian Larue, and André Plamondon. 2016. "Evaluation of Eight Methods for Aligning Orientation of Two Coordinate Systems." *Journal of Biomechanical Engineering* 138 (8): 084501–084501. doi:10.1115/1.4033719.

Meina, M., K. Rykaczewski, and A. Rutkowski. 2016. "Position Tracking Using Inertial and Magnetic Sensing Aided by Permanent Magnet." In *2016 Federated Conference on Computer Science and Information Systems (FedCSIS)*, 105–111.

Miezal, Markus, Bertram Taetz, and Gabriele Bleser. 2016. "On Inertial Body Tracking in the Presence of Model Calibration Errors." *Sensors* 16 (7): 1132. doi:10.3390/s16071132.

Miranda, H., L. Punnett, E. Viikari-Juntura, M. Heliövaara, and P. Knekt. 2008. "Physical Work and Chronic Shoulder Disorder. Results of a Prospective Population-Based Study." *Annals of the Rheumatic Diseases* 67 (2): 218–223. doi:10.1136/ard.2007.069419.

Moore, J. Steven, and Arun Garg. 1995. "The Strain Index: A Proposed Method to Analyze Jobs For Risk of Distal Upper Extremity Disorders." *American Industrial Hygiene Association Journal* 56 (5): 443–458. doi:10.1080/15428119591016863.

Mortari, Daniele. 1997. "ESOQ: A Closed-Form Solution to the Wahba Problem." *Journal of the Astronautical Sciences* 45 (2): 195–204.

Mourcou, Quentin, Anthony Fleury, Céline Franco, Frédéric Klopcic, and Nicolas Vuillerme. 2015. "Performance Evaluation of Smartphone Inertial Sensors Measurement for Range of Motion." *Sensors* 15 (9): 23168–23187. doi:10.3390/s150923168.

National Research Council. 2001. *Musculoskeletal Disorders and the Workplace: Low Back and Upper Extremities*. Washington DC. http://nationalacademies.org/hmd/Reports/2001/Musculoskeletal-Disorders-and-the-Workplace-Low-Back-and-Upper-Extremities.aspx.

Nordander, Catarina, Gert-Åke Hansson, Kerstina Ohlsson, Inger Arvidsson, Istvan Balogh, Ulf Strömberg, Ralf Rittner, and Staffan Skerfving. 2016. "Exposure–response Relationships for Work-Related Neck and Shoulder Musculoskeletal Disorders – Analyses of Pooled Uniform Data Sets." *Applied Ergonomics* 55 (July): 70–84. doi:10.1016/j.apergo.2016.01.010.

Nowicki, M., J. Wietrzykowski, and P. Skrzypczyński. 2015. "Simplicity or Flexibility? Complementary Filter vs. EKF for Orientation Estimation on Mobile Devices." In *2015 IEEE 2nd International Conference on Cybernetics (CYBCONF)*, 166–171. doi:10.1109/CYBConf.2015.7175926.

Ohlsson, K., R. G. Attewell, B. Pålsson, B. Karlsson, I. Balogh, B. Johnsson, A. Ahlm, and S. Skerfving. 1995. "Repetitive Industrial Work and Neck and Upper Limb Disorders in Females." *American Journal of Industrial Medicine* 27 (5): 731–747. doi:10.1002/ajim.4700270508.

Oskiper, T., Z. Zhu, S. Samarasekera, and R. Kumar. 2007. "Visual Odometry System Using Multiple Stereo Cameras and Inertial Measurement Unit." In *2007 IEEE Conference on Computer Vision and Pattern Recognition*, 1–8. doi:10.1109/CVPR.2007.383087.

Pasciuto, Ilaria, Gabriele Ligorio, Elena Bergamini, Giuseppe Vannozzi, Angelo Maria Sabatini, and Aurelio Cappozzo. 2015. "How Angular Velocity Features and Different Gyroscope Noise Types Interact and Determine Orientation Estimation Accuracy." *Sensors* 15 (9): 23983–24001. doi:10.3390/s150923983.

Plamondon, A., A. Delisle, C. Larue, D. Brouillette, D. McFadden, P. Desjardins, and C. Larivière. 2007. "Evaluation of a Hybrid System for Three-Dimensional Measurement of Trunk Posture in Motion." *Applied Ergonomics* 38 (6): 697–712. doi:10.1016/j.apergo.2006.12.006.

Punnett, Laura, Lawrence J Fine, W Monroe Keyserling, Gary D Herrin, and Don B Chaffin. 2000. "Shoulder Disorders and Postural Stress in Automobile Assembly Work." *Scandinavian Journal of Work, Environment & Health* 26 (4): 283–291.

Punnett, Laura, and David H. Wegman. 2004. "Work-Related Musculoskeletal Disorders: The Epidemiologic Evidence and the Debate." *Journal of Electromyography and Kinesiology*, State of the art research perspectives on muscoskeletal disorder causation and control, 14 (1): 13–23. doi:10.1016/j.jelekin.2003.09.015.

Ricci, Luca, Domenico Formica, Laura Sparaci, Francesca Romana Lasorsa, Fabrizio Taffoni, Eleonora Tamilia, and Eugenio Guglielmelli. 2014. "A New Calibration Methodology for Thorax and Upper Limbs Motion Capture in Children Using Magneto and Inertial Sensors." *Sensors* 14 (1): 1057–1072. doi:10.3390/s140101057.

Ricci, Luca, Fabrizio Taffoni, and Domenico Formica. 2016. "On the Orientation Error of IMU: Investigating Static and Dynamic Accuracy Targeting Human Motion." *PLOS ONE* 11 (9): e0161940. doi:10.1371/journal.pone.0161940.

Roan, P., N. Deshpande, Y. Wang, and B. Pitzer. 2012. "Manipulator State Estimation with Low Cost Accelerometers and Gyroscopes." In *2012 IEEE/RSJ International Conference on Intelligent Robots and Systems*, 4822–4827. doi:10.1109/IROS.2012.6385893.

Robert-Lachaine, Xavier, Hakim Mecheri, Christian Larue, and André Plamondon. 2016. "Validation of Inertial Measurement Units with an Optoelectronic System for Whole-Body Motion Analysis." *Medical & Biological Engineering & Computing*, July, 1–11. doi:10.1007/s11517-016-1537-2.

94

Roetenberg, D., P. J. Slycke, and P. H. Veltink. 2007. "Ambulatory Position and Orientation Tracking Fusing Magnetic and Inertial Sensing." *IEEE Transactions on Biomedical Engineering* 54 (5): 883–890. doi:10.1109/TBME.2006.889184.

Roetenberg, Daniel, Henk. J. Luinge, Chris T. M. Baten, and Peter H. Veltink. 2005. "Compensation of Magnetic Disturbances Improves Inertial and Magnetic Sensing of Human Body Segment Orientation." *IEEE Transactions on Neural Systems and Rehabilitation Engineering* 13 (3): 395–405. doi:10.1109/TNSRE.2005.847353.

Sabatini, Angelo Maria. 2006. "Quaternion-Based Extended Kalman Filter for Determining Orientation by Inertial and Magnetic Sensing." *IEEE Transactions on Biomedical Engineering* 53 (7): 1346–1356. doi:10.1109/TBME.2006.875664.

Sabatini, Angelo Maria. 2011a. "Estimating Three-Dimensional Orientation of Human Body Parts by Inertial/Magnetic Sensing." *Sensors* 11 (2): 1489–1525. doi:10.3390/s110201489.

Sabatini, Angelo Maria. 2011b. "Kalman-Filter-Based Orientation Determination Using Inertial/Magnetic Sensors: Observability Analysis and Performance Evaluation." *Sensors* 11 (10): 9182–9206. doi:10.3390/s111009182.

Schall Jr., Mark C., Nathan B. Fethke, Howard Chen, and Fred Gerr. 2015. "A Comparison of Instrumentation Methods to Estimate Thoracolumbar Motion in Field-Based Occupational Studies." *Applied Ergonomics* 48 (May): 224–231. doi:10.1016/j.apergo.2014.12.005.

Schall, Mark C., Nathan B. Fethke, Howard Chen, Sakiko Oyama, and David I. Douphrate. 2015. "Accuracy and Repeatability of an Inertial Measurement Unit System for Field-Based Occupational Studies." *Ergonomics*, August, 1–12. doi:10.1080/00140139.2015.1079335.

Schiefer, Christoph, Rolf P. Ellegast, Ingo Hermanns, Thomas Kraus, Elke Ochsmann, Christian Larue, and André Plamondon. 2014. "Optimization of Inertial Sensor-Based Motion Capturing for Magnetically Distorted Field Applications." *Journal of Biomechanical Engineering* 136 (12): 121008–121008. doi:10.1115/1.4028822.

Sessa, Salvatore, Massimiliano Zecca, Zhuohua Lin, Luca Bartolomeo, Hiroyuki Ishii, and Atsuo Takanishi. 2012. "A Methodology for the Performance Evaluation of Inertial Measurement Units." *Journal of Intelligent & Robotic Systems* 71 (2): 143–157. doi:10.1007/s10846-012-9772-8.

Shiratori, Takaaki, Hyun Soo Park, Leonid Sigal, Yaser Sheikh, and Jessica K. Hodgins. 2011. "Motion Capture from Body-Mounted Cameras." In *ACM SIGGRAPH 2011 Papers*, 31:1–31:10. SIGGRAPH '11. New York, NY, USA: ACM. doi:10.1145/1964921.1964926.

Shuster, Malcolm David, and S. D. Oh. 2012. "Three-Axis Attitude Determination from Vector Observations." *Journal of Guidance, Control, and Dynamics*.

Silverstein, Barbara A., Stephen S. Bao, Z Joyce Fan, Ninica Howard, Caroline Smith, Peregrin Spielholz, David Bonauto, and Eira Viikari-Juntura. 2008. "Rotator Cuff Syndrome: Personal, Work-Related Psychosocial and Physical Load Factors:" *Journal of Occupational and Environmental Medicine* 50 (9): 1062–1076. doi:10.1097/JOM.0b013e31817e7bdd.

Spielholz, Peregrin, Barbara Silverstein, Michael Morgan, Harvey Checkoway, and Joel Kaufman. 2001. "Comparison of Self-Report, Video Observation and Direct Measurement Methods for Upper Extremity Musculoskeletal Disorder Physical Risk Factors." *Ergonomics* 44 (6): 588–613. doi:10.1080/00140130118050.

Sun, Gang, Yong Yang, Jiawei Xie, Matthew Garrett, and Changming Wang. 2013. "Implementing Quaternion Based AHRS on a MEMS Multisensor Hardware Platform." In *International Global Navigation Satellite Systems Society*. Outrigger Gold Coast, Qld Australia.

Svendsen, S. W., J. P. Bonde, S. E. Mathiassen, K. Stengaard-Pedersen, and L. H. Frich. 2004. "Work Related Shoulder Disorders: Quantitative Exposure-Response Relations with Reference to Arm Posture." *Occupational and Environmental Medicine* 61 (10): 844–853.

Tadayon, P., T. Felderhoff, A. Knopp, and G. Staude. 2016. "Fusion of Inertial and Magnetic Sensors for 3D Position and Orientation Estimation." In *2016 38th Annual International Conference of the IEEE Engineering in Medicine and Biology Society (EMBC)*, 3362–3365. doi:10.1109/EMBC.2016.7591448.

Taunyazov, T., B. Omarali, and A. Shintemirov. 2016. "A Novel Low-Cost 4-DOF Wireless Human Arm Motion Tracker." In *2016 6th IEEE International Conference on Biomedical Robotics and Biomechatronics (BioRob)*, 157–162. doi:10.1109/BIOROB.2016.7523615.

Tian, Y., H. Wei, and J. Tan. 2013. "An Adaptive-Gain Complementary Filter for Real-Time Human Motion Tracking With MARG Sensors in Free-Living Environments." *IEEE Transactions on Neural Systems and Rehabilitation Engineering* 21 (2): 254–264. doi:10.1109/TNSRE.2012.2205706.

Tian, Yushuang, Xiaoli Meng, Dapeng Tao, Dongquan Liu, and Chen Feng. 2015. "Upper Limb Motion Tracking with the Integration of IMU and Kinect." *Neurocomputing* 159 (July): 207–218. doi:10.1016/j.neucom.2015.01.071.

Tognetti, Alessandro, Federico Lorussi, Nicola Carbonaro, and Danilo de Rossi. 2015. "Wearable Goniometer and Accelerometer Sensory Fusion for Knee Joint Angle Measurement in Daily Life." *Sensors* 15 (11): 28435–28455. doi:10.3390/s151128435.

Trawny, Nikolas, and Stergios I. Roumeliotis. 2005. *Indirect Kalman Filter for 3D Attitude Estimation*. 2005-002. Department of Computer Science and Engineering, MARS Lab: University of Minnesota. http://www-users.cs.umn.edu/~trawny/Publications/Quaternions_3D.pdf.

Valenti, Roberto G., Ivan Dryanovski, and Jizhong Xiao. 2015. "Keeping a Good Attitude: A Quaternion-Based Orientation Filter for IMUs and MARGs." *Sensors* 15 (8): 19302–19330. doi:10.3390/s150819302.

Valenti, Roberto G., Ivan Dryanovski, and Jizhong Xiao. 2016. "A Linear Kalman Filter for MARG Orientation Estimation Using the Algebraic Quaternion Algorithm." *IEEE Transactions on Instrumentation and Measurement* 65 (2): 467–481. doi:10.1109/TIM.2015.2498998.

Vignais, Nicolas, Markus Miezal, Gabriele Bleser, Katharina Mura, Dominic Gorecky, and Frédéric Marin. 2013. "Innovative System for Real-Time Ergonomic Feedback in Industrial Manufacturing." *Applied Ergonomics* 44 (4): 566–574. doi:10.1016/j.apergo.2012.11.008.

Wahba, Grace. 1965. "A Least Squares Estimate of Satellite Attitude." *SIAM Review* 7 (3): 409–409.

Welch, Greg, and Gary Bishop. 2006. *An Introduction to the Kalman Filter. Department of Computer Science, University of North Carolina*. Chapel Hill, NC, unpublished manuscript.

Welch, Greg, and Eric Foxlin. 2002. "Motion Tracking: No Silver Bullet, but a Respectable Arsenal." *IEEE Computer Graphics and Applications* 22 (6): 24–38. doi:10.1109/MCG.2002.1046626.

Won, S. h P., W. W. Melek, and F. Golnaraghi. 2010. "A Kalman/Particle Filter-Based Position and Orientation Estimation Method Using a Position Sensor/Inertial Measurement Unit Hybrid System." *IEEE Transactions on Industrial Electronics* 57 (5): 1787–1798. doi:10.1109/TIE.2009.2032431.

Woodman, Oliver J. 2007. *An Introduction to Inertial Navigation*. Technical 696. Cambridge, UK: University of Cambridge. https://www.cl.cam.ac.uk/techreports/UCAM-CL-TR-696.pdf.

Wu, Ge, Frans C. T. van der Helm, H. E. J. (DirkJan) Veeger, Mohsen Makhsous, Peter Van Roy, Carolyn Anglin, Jochem Nagels, et al. 2005. "ISB Recommendation on Definitions of Joint Coordinate Systems of Various Joints for the Reporting of Human Joint motion—Part II: Shoulder, Elbow, Wrist and Hand." *Journal of Biomechanics* 38 (5): 981–992. doi:10.1016/j.jbiomech.2004.05.042.

Xia, Dunzhu, Cheng Yu, and Lun Kong. 2014. "The Development of Micromachined Gyroscope Structure and Circuitry Technology." *Sensors* 14 (1): 1394–1473. doi:10.3390/s140101394.

Xu, Xu, and Raymond W. McGorry. 2015. "The Validity of the First and Second Generation Microsoft Kinect™ for Identifying Joint Center Locations during Static Postures." *Applied Ergonomics* 49 (July): 47–54. doi:10.1016/j.apergo.2015.01.005.

Xue, Liang, Cheng-Yu Jiang, Hong-Long Chang, Yong Yang, Wei Qin, and Wei-Zheng Yuan. 2012. "A Novel Kalman Filter for Combining Outputs of MEMS Gyroscope Array." *Measurement* 45 (4): 745–754. doi:10.1016/j.measurement.2011.12.016.

Yadav, Nagesh, and Chris Bleakley. 2014. "Accurate Orientation Estimation Using Ahrs Under Conditions of Magnetic Distortion." *Sensors* 14 (11): 20008–20024. doi:10.3390/s141120008.

Yoon, P. K., S. Zihajehzadeh, B. S. Kang, and E. J. Park. 2017. "Robust Biomechanical Model-Based 3-D Indoor Localization and Tracking Method Using UWB and IMU." *IEEE Sensors Journal* 17 (4): 1084–1096. doi:10.1109/JSEN.2016.2639530.

Yun, Xiaoping, and Eric. R. Bachmann. 2006. "Design, Implementation, and Experimental Results of a Quaternion-Based Kalman Filter for Human Body Motion Tracking." *IEEE Transactions on Robotics* 22 (6): 1216–1227. doi:10.1109/TRO.2006.886270.

Yun, Xiaoping, Eric. R. Bachmann, and Robert. B. McGhee. 2008. "A Simplified Quaternion-Based Algorithm for Orientation Estimation From Earth Gravity and Magnetic Field Measurements." *IEEE Transactions on Instrumentation and Measurement* 57 (3): 638–650. doi:10.1109/TIM.2007.911646.

Zhang, Zhiqiang, Wai Choong Wong, and Jiankang Wu. 2011. "Wearable Sensors for 3D Upper Limb Motion Modeling and Ubiquitous Estimation." *Journal of Control Theory and Applications* 9 (1): 10–17. doi:10.1007/s11768-011-0234-9.

Zhi, Ruoyu. 2016. "A Drift Eliminated Attitude & Position Estimation Algorithm In 3D." University of Vermont. http://scholarworks.uvm.edu/graddis/450.

Zhou, H., and H. Hu. 2010. "Reducing Drifts in the Inertial Measurements of Wrist and Elbow Positions." *IEEE Transactions on Instrumentation and Measurement* 59 (3): 575–585. doi:10.1109/TIM.2009.2025065.

Zhou, Huiyu, and Huosheng Hu. 2008. "Human Motion Tracking for rehabilitation—A Survey." *Biomedical Signal Processing and Control* 3 (1): 1–18. doi:10.1016/j.bspc.2007.09.001.

Zihajehzadeh, S., P. K. Yoon, B. S. Kang, and E. J. Park. 2015. "UWB-Aided Inertial Motion Capture for Lower Body 3-D Dynamic Activity and Trajectory Tracking." *IEEE Transactions on Instrumentation and Measurement* 64 (12): 3577–3587. doi:10.1109/TIM.2015.2459532.

APPENDIX A

IRB INFORMED CONSENT FORM

INFORMED CONSENT DOCUMENT

Project Title: **Characterizing Operable Conditions for Inertial Measurement Units**

Principal Investigator: Howard Chen, MSE

Research Team Contact: Howard Chen, MSE
164 IREH, UI Research Park
Phone: (319) 335-4996
E-mail: howard-chen@uiowa.edu

This consent form describes the research study to help you decide if you want to participate. This form provides important information about what you will be asked to do during the study, about the risks and benefits of the study, and about your rights as a research subject.
* If you have any questions about or do not understand something in this form, you should ask the research team for more information.
* You should discuss your participation with anyone you choose such as family or friends.
* Do not agree to participate in this study unless the research team has answered your questions and you decide that you want to be part of this study.

WHAT IS THE PURPOSE OF THIS STUDY?

This is a research study. We are inviting you to participate in this research study because you are a healthy adult between the ages of 18-65 years who does not have a history of musculoskeletal disease or injury of the upper extremity (shoulder, forearm, and wrist).

The purpose of this research study is to evaluate a new generation of sensors that is capable of capturing human motion in the workplace. Specifically, we are interested in investigating the conditions necessary to obtain accurate data from these sensors. Fast motions and presence of metals are known to degrade its accuracy. Ultimately, the use of this device will be used in the workplace to capture human motion in order to better our understanding of the relationship between posture and work-related musculoskeletal disorders.

HOW MANY PEOPLE WILL PARTICIPATE?

Approximately 13 people will take part in this study conducted by investigators at the University of Iowa.

HOW LONG WILL I BE IN THIS STUDY?

If you agree to take part in this study, your involvement will consist of one visit that will require approximately 1 hour (no longer than 2 hours) with no additional follow up.

WHAT WILL HAPPEN DURING THIS STUDY?

If you agree to participate, you will perform a simple work task six different times, during which your movement is tracked by two different sets of sensors. The task will involve transferring wooden dowel rods (1" diameter x 8" length) from a container placed at waist height to a container above and to the side of your shoulder at a constant speed for a period of one minute. This task will be performed six times, consisting of three different movement speed (slow, moderate, and fast) and with or without a piece of metal plate in the proximity of the unloading area. Auditory tones will help keep your motion constant at the specified speed. You will have the opportunity to rest for at least 5 minutes and then practice the task at the subsequent condition upon completion of your previous work task.

During your visit, you will be wearing three inertial measurement units (IMUs) to track your movement. A sensor will be placed on your dominant upper arm, forearm, and hand using Velcro® straps. Your movement will be simultaneously measured using a camera system that will track reflective markers attached to the top of each IMU.

Video Recording/Photographs

One aspect of this study involves making video recordings of you. These recordings will be used for documenting the movements that you maintained during the study, and to reconcile any unexpected data in the measurement data. The tapes will not be erased or destroyed. In addition, still photographs and/or video recordings may be obtained during your time in the lab for use in documents such as reports and/or publications. In the event that these materials are used in reports or publications, the images will be altered so no personally-identifiable information will appear.

Your name will not appear in the videotape. An identification number will appear in the videotape so we can associate the video with the other data collected.

[ ] Yes   [ ] No   I give you permission to make recordings/photographs of me during this study.

Data Storage for Future Use
As part of this study, we are obtaining data from you. We would like to study your data in the future, after this study is over.

The tests we might want to use to study your data may not even exist at this time. Therefore, we are asking for your permission to store your data so that we can study them in the future. These future studies may provide additional information that will be helpful in understanding work-related musculoskeletal disorders, but it is unlikely that what we learn from these studies will have a direct benefit to you. It is possible that your data might be used to develop products or tests that could be patented and licensed. There are no plans to provide financial compensation to you should this occur.

If you agree now to future use of your data, but decide in the future that you would like to have it removed from future research, you should contact Howard Chen (319) 335-4996. However, if some research with your data has already been completed, the information from that research may still be used.

www.manaraa.com

WHAT ARE THE RISKS OF THIS STUDY?

You may experience one or more of the risks indicated below from being in this study. In addition to these, there may be other unknown risks, or risks that we did not anticipate, associated with being in this study.

You may feel some muscle fatigue or soreness from the material handling task. Rest will be allowed before and following completion of the task to prevent muscle fatigue and soreness.

WHAT ARE THE BENEFITS OF THIS STUDY?

You will not benefit from being in this study. However, we hope that, in the future, other people might benefit from this study because of further understanding of the relationship between motion and its effect on musculoskeletal disorders.

WILL IT COST ME ANYTHING TO BE IN THIS STUDY?

You will not have any costs for being in this research study.

WILL I BE PAID FOR PARTICIPATING?

You will be paid for being in this research study. You may need to provide your address if a check will be mailed to you. You will be compensated a total of $25 for your time during your one-time visit.

WHO IS FUNDING THIS STUDY?

This research is being funded by the Centers for Disease Control and Prevention/National Institute for Occupational Safety and Health (CDC/NIOSH) through the Heartland Center for Occupational Health and Safety at the University of Iowa. This means that the University of Iowa is receiving payments from CDC/NIOSH to support the activities that are required to conduct the study. No one on the research team will receive a direct payment or increase in salary from CDC/NIOSH for conducting this study.

WHAT IF I AM INJURED AS A RESULT OF THIS STUDY?

- If you are injured or become ill from taking part in this study, medical treatment is available at the University of Iowa Hospitals and Clinics.
- The University of Iowa does not plan to provide free medical care or payment for treatment of any illness or injury resulting from this study unless it is the direct result of proven negligence by a University employee.
- If you experience a research-related illness or injury, you and/or your medical or hospital insurance carrier will be responsible for the cost of treatment.

WHAT ABOUT CONFIDENTIALITY?

We will keep your participation in this research study confidential to the extent permitted by law. However, it is possible that other people such as those indicated below may become aware of your

Page 3 of 5

participation in this study and may inspect and copy records pertaining to this research. Some of these records could contain information that personally identifies you.

- federal government regulatory agencies,
- auditing departments of the University of Iowa, and
- the University of Iowa Institutional Review Board (a committee that reviews and approves research studies)

To help protect your confidentiality, your information will be identified by number, cross-referenced to your name on a piece of paper kept separate from your file of data and visual materials. Video will be identified only with your subject number and the time of the test. All data will be kept in a locked lab or office, with appropriate backup. A list associating subject names with subject numbers will be kept in a location separate from the data and will only be accessible by the PI. The computer server is password-protected to ensure confidentiality of the electronic records. The data will be retained indefinitely. If we write a report or article about this study or share the study data set with others, we will do so in such a way that you cannot be directly identified.

IS BEING IN THIS STUDY VOLUNTARY?

Taking part in this research study is completely voluntary. You may choose not to take part at all. If you decide to be in this study, you may stop participating at any time. If you decide not to be in this study, or if you stop participating at any time, you won't be penalized or lose any benefits for which you otherwise qualify.

WHAT IF I HAVE QUESTIONS?

We encourage you to ask questions. If you have any questions about the research study itself, please contact: Howard Chen at howard-chen@uiowa.edu or (319) 335-4996. If you experience a research-related injury, please contact: Howard Chen at howard-chen@uiowa.edu or (319) 335-4996. or Nathan Fethke at 319-467-4563.

If you have questions, concerns, or complaints about your rights as a research subject or about research related injury, please contact the Human Subjects Office, 105 Hardin Library for the Health Sciences, 600 Newton Rd, The University of Iowa, Iowa City, IA 52242-1098, (319) 335-6564, or e-mail irb@uiowa.edu. General information about being a research subject can be found by clicking "Info for Public" on the Human Subjects Office web site, http://hso.research.uiowa.edu/. To offer input about your experiences as a research subject or to speak to someone other than the research staff, call the Human Subjects Office at the number above.

This Informed Consent Document is not a contract. It is a written explanation of what will happen during the study if you decide to participate. You are not waiving any legal rights by signing this Informed Consent Document. Your signature indicates that this research study has been explained to you, that your questions have been answered, and that you agree to take part in this study. You will receive a copy of this form.

Subject's Name (printed): _____

Do not sign this form if today's date is on or after $STAMP_EXP_DT.   _____   _____ (Signature of Subject)   (Date)

Statement of Person Who Obtained Consent

I have discussed the above points with the subject or, where appropriate, with the subject's legally authorized representative. It is my opinion that the subject understands the risks, benefits, and procedures involved with participation in this research study.

_____   _____
(Signature of Person who Obtained Consent)   (Date)

IRB LETTER OF APPROVAL

THE UNIVERSITY OF IOWA

**Human Subjects Office/
Institutional Review Board (IRB)**

105 Hardin Library for the Health Sciences
600 Newton Road
Iowa City, Iowa 52242-1098
319-335-6564   Fax 319-335-7310
irb@uiowa.edu
http://research.uiowa.edu/hso

IRB ID #:   201505706

To: Howard Chen

From: IRB-01   DHHS Registration # IRB00000099,
Univ of Iowa,   DHHS Federalwide Assurance # FWA00003007

Re: Characterizing Operable Conditions for Inertial Measurement Units

Protocol Number:
Protocol Version:
Protocol Date:
Amendment Number/Date(s):

Approval Date: 05/11/15

**Next IRB Approval
Due Before:**   05/10/16

Type of Application:	**Type of Application Review:**	**Approved for Populations:**
☒ New Project	☐ Full Board:	☐ Children
☐ Continuing Review	Meeting Date:	☐ Prisoners
☐ Modification	☒ Expedited	☐ Pregnant Women, Fetuses, Neonates
	☐ Exempt	

Source of Support: US Department of Health & Human Services, Centers for Disease Control &
Prevention

Investigational New Drug/Biologic Name:
Investigational New Drug/Biologic Number:
Name of Sponsor who holds IND:

Investigational Device Name:
Investigational Device Number:
Sponsor who holds IDE:

This approval has been electronically signed by IRB Chair:
Catherine Woodman, MD
05/11/15 1039

OFFICE OF THE VICE PRESIDENT
FOR RESEARCH

103

IRB Approval: IRB approval indicates that this project meets the regulatory requirements for the protection of human subjects. IRB approval does not absolve the principal investigator from complying with other institutional, collegiate, or departmental policies or procedures.

Agency Notification: If this is a New Project or Continuing Review application and the project is funded by an external government or non-profit agency, the original HHS 310 form, "Protection of Human Subjects Assurance Identification/IRB Certification/Declaration of Exemption," has been forwarded to the UI Division of Sponsored Programs, 100 Gilmore Hall, for appropriate action. You will receive a signed copy from Sponsored Programs.

Recruitment/Consent: Your IRB application has been approved for recruitment of subjects not to exceed the number indicated on your application form. If you are using written informed consent, the IRB-approved and stamped Informed Consent Document(s) are attached. Please make copies from the attached "masters" for subjects to sign when agreeing to participate. The original signed Informed Consent Document should be placed in your research files. A copy of the Informed Consent Document should be given to the subject. (A copy of the *signed* Informed Consent Document should be given to the subject if your Consent contains a HIPAA authorization section.) If hospital/clinic patients are being enrolled, a copy of the IRB approved Record of Consent form should be placed in the subject's electronic medical record.

Continuing Review: Federal regulations require that the IRB re-approve research projects at intervals appropriate to the degree of risk, but no less than once per year. This process is called "continuing review." Continuing review for non-exempt research is required to occur as long as the research remains active for long-term follow-up of research subjects, even when the research is permanently closed to enrollment of new subjects and all subjects have completed all research-related interventions and to occur when the remaining research activities are limited to collection of private identifiable information. Your project "expires" at 12:01 AM on the date indicated on the preceding page ("Next IRB Approval Due on or Before"). You must obtain your next IRB approval of this project on or before that expiration date. You are responsible for submitting a Continuing Review application in sufficient time for approval before the expiration date, however the HSO will send a reminder notice approximately 60 and 30 days prior to the expiration date.

Modifications: Any change in this research project or materials must be submitted on a Modification application to the IRB for prior review and approval, except when a change is necessary to eliminate apparent immediate hazards to subjects. The investigator is required to promptly notify the IRB of any changes made without IRB approval to eliminate apparent immediate hazards to subjects using the Modification/Update Form. Modifications requiring the prior review and approval of the IRB include but are not limited to: changing the protocol or study procedures, changing investigators or funding sources, changing the Informed Consent Document, increasing the anticipated total number of subjects from what was originally approved, or adding any new materials (e.g., letters to subjects, ads, questionnaires).

Unanticipated Problems Involving Risks: You must promptly report to the IRB any serious and/or unexpected adverse experience, as defined in the UI Investigator's Guide, and any other unanticipated problems involving risks to subjects or others. The Reportable Events Form (REF) should be used for reporting to the IRB.

Audits/Record-Keeping: Your research records may be audited at any time during or after the implementation of your project. Federal and University policies require that all research records be maintained for a period of three (3) years following the close of the research project. For research that involves drugs or devices seeking FDA approval, the research records must be kept for a period of three years after the FDA has taken final action on the marketing application.

Additional Information: Complete information regarding research involving human subjects at The University of Iowa is available in the "Investigator's Guide to Human Subjects Research." Research investigators are expected to comply with these policies and procedures, and to be familiar with the University's Federalwide Assurance, the Belmont Report, 45CFR46, and other applicable regulations prior to conducting the research. These documents and IRB application and related forms are available on the Human Subjects Office website or are available by calling 335-6564.

APPENDIX C

MATLAB CODE

```matlab
function [ out ] = LKF(processData,measureData, freq, processNoise, measureNoise,ca,cb)
%LKF Linear kalman filter
%   Implementation of the code in the following paper:
%   Ligorio, G., & Sabatini, A. M. (2015). A novel Kalman filter for human motion
%   tracking with an inertial-based dynamic inclinometer.
%   IEEE Transactions on Biomedical Engineering, 62(8), 2033-2043.
%
%   measureData: n x 3 array contating vector measurements (accelerometer or
magnetometer)
%   processData: n x 3 array containing angular rate measurements (gyroscope)
%   measureNoise: measurement noise
%   processNoise: process noise
%   dT: Sampling period (seconds)
%   ca, cb: Gauss Markov Parameters
%   output: n x 6 vector
%           col 1 to 3: gravity (local frame)
%           col 4 to 6: acceleration (local frame)
%
%   Author: Howard Chen

% Sampling period
dT = 1/freq;

% Process Covariance Matrix
Q = eye(6);
Q(1:3,1:3) = processNoise^2.*eye(3);

% Measurement Covariance Matrix
R = measureNoise^2.*eye(3);

A = zeros(6,6);
P = zeros(6,6);
W = zeros(6,6);
H = [eye(3),eye(3)];
x = zeros(6,1);
x(1:3) = measureData(1,:)';
out = zeros(length(measureData),6);

    for i=1:length(measureData);
        A(1:3,1:3) = expm(- skew(processData(i,:)).*dT);
        A(4:6,4:6) = ca.*eye(3);
        x = A*x;

        W(1:3,1:3) = skew(x(1:3).*dT);
        W(4:6,4:6) = cb.*eye(3);
        P = A*P*A'+W*Q*W';

        K = P*H'*(H*P*H'+R)^-1;
        x = x+K*(measureData(i,:)'-H*x);
        P = (eye(6)-K*H)*P;
        out(i,:) = x';
    end
end

function [ wx ] = skew( a )
    % Skew symmetric matrix
    wx = [0 -a(3) a(2); a(3) 0 -a(1); -a(2) a(1) 0];
end
```

105

```matlab
function [ quat ] = incComp(gyro, accel, freq, alpha)
%INCCOMP calculates inclination from accel and gyro measurements
%    calculations is done in yaw-pitch-roll and converted to quaternions
%    input: accel- accelerometer measurements
%           gyro- gyroscope mearements
%           freq- sampling frequency
%           alpha- filter coefficient (1 = all accel)
%                  alpha(1): pitch
%                  alpha(2): roll
%    output: q- quaternion measurements (can be converted back to Euler)
%
%    Author: Howard Chen

ln = length(accel);
quat = zeros(ln,4);

dT = 1/freq;

%calculate pitch and roll from accelerometer
aPitch = atan(-accel(:,1)./sqrt(accel(:,2).^2+accel(:,3).^2));
aRoll = atan(accel(:,2)./accel(:,3));

cPitch = aPitch(1);
cRoll = aRoll(1);
for i=1:ln
    cPitch = (1-alpha(1))*(cPitch+(gyro(i,2)*cos(cRoll)-
gyro(i,3)*sin(cRoll))*dT)+alpha(1)*aPitch(i);
    cRoll = (1-
alpha(2))*(cRoll+(gyro(i,1)+gyro(i,2)*sin(cRoll)*tan(cPitch)+gyro(i,3)*cos(cRoll)*tan(cPi
tch))*dT)+alpha(2)*aRoll(i);

    %Convert to quaternion
    quat(i,1)=cos(cPitch./2).*cos(cRoll./2);
    quat(i,2)=cos(cPitch./2).*sin(cRoll./2);
    quat(i,3)=sin(cPitch./2).*cos(cRoll./2);
    quat(i,4)=-sin(cPitch./2).*sin(cRoll./2);
end
```

```matlab
function [ out ] = modLKF(gyro, accel, freq, gyroNoise, gyroBias, accelNoise,ca,cb)
%LKF Linear kalman filter
%   Adopted from the code in the following paper:
%   Ligorio, G., & Sabatini, A. M. (2015). A novel Kalman filter for
%   human motion tracking with an inertial-based dynamic inclinometer.
%   IEEE Transactions on Biomedical Engineering, 62(8), 2033-2043.
%
%   -The following adaptions were made:
%   -added a gyroscope bias random walk model
%   -used first order approximation for matrix exponential
%   -Used EKF filter structure
%   Author: Howard Chen

% Sampling period
dT = 1/freq;

ln = length(accel);
% Process Covariance Matrix
Q = eye(9);
Q(1:3,1:3) = gyroNoise^2.*eye(3);
Q(7:9,7:9) = gyroBias^2.*eye(3);

% Measurement Covariance Matrix
R = accelNoise^2.*eye(3);

A = zeros(9,9);
P = zeros(9,9);
W = zeros(9,9);
H = [eye(3),eye(3),zeros(3,3)];
x = zeros(9,1);
x(1:3) = accel(1,:)';
out = zeros(ln,9);

for i=1:ln;
    A(1:3,:) = [eye(3)-skew((gyro(i,:)-x(7:9)').*dT), zeros(3,3),-skew(x(1:3).*dT)];
    A(4:6,:) = [zeros(3,3), ca.*eye(3), zeros(3,3)];
    A(7:9,:) = [zeros(3,3), zeros(3,3), eye(3)];

    x = [A(1:6,1:6)*x(1:6);x(7:9)];
    W(1:3,:) = [skew(x(1:3).*dT), zeros(3,3), zeros(3,3)];
    W(4:6,:) = [zeros(3,3), cb.*eye(3),zeros(3,3)];
    W(7:9,:) = [zeros(3,3),zeros(3,3),dT.*eye(3)];

    P = A*P*A' + W*Q*W';
    K = P*H'*(H*P*H'+R)^-1;
    x = x+K*(accel(i,:)'-H*x);
    P = (eye(9)-K*H)*P;
    out(i,:) = x';
end
end

function [ wx ] = skew( a )
    % Skew symmetric matrix
    wx = [0 -a(3) a(2); a(3) 0 -a(1); -a(2) a(1) 0];
end
```

```matlab
function [ q ] = accelMag( accel,mag)
%ACCELMAG calculates orientation using accelerometer & magnetometers
%    calculations is done in yaw-pitch-roll and converted to quaternions
%    accel: nx3 vector with accelerometer measurements (gravity vector)
%    mag: nx3 vector with magnetometer measurements (magetic north vector)
%    q: nx4 quaternion rotation vector (q1 is real)
%
%    Author: Howard Chen

% calculate pitch and roll from accel

%pitch
pitch = atan2(-accel(:,1),sqrt(accel(:,2).^2+accel(:,3).^2));

%roll
roll = atan2(accel(:,2),accel(:,3));

% calculate yaw from mag and accel
yaw=atan2(mag(:,3).*sin(roll)-
mag(:,2).*cos(roll),mag(:,1).*cos(pitch)+mag(:,2).*sin(pitch).*sin(roll)+mag(:,3).*sin(pi
tch).*cos(roll));

% convert ypr to quaternion
q(:,1) =
cos(yaw./2).*cos(pitch./2).*cos(roll./2)+sin(yaw./2).*sin(pitch./2).*sin(roll./2);
q(:,2) = cos(yaw./2).*cos(pitch./2).*sin(roll./2)-
sin(yaw./2).*sin(pitch./2).*cos(roll./2);
q(:,3) =
cos(yaw./2).*sin(pitch./2).*cos(roll./2)+sin(yaw./2).*cos(pitch./2).*sin(roll./2);
q(:,4) = sin(yaw./2).*cos(pitch./2).*cos(roll./2)-
cos(yaw./2).*sin(pitch./2).*sin(roll./2);
end
```

```matlab
function [q2] = gyroAlign( omcQuat,imuGyro,freq )
%GYROALIGN aligns the OMC Local Frame to the IMU Local Frame
%
% LF alignment is conducted following:
% De Vries, W. H. K., Veeger, H. E. J., Baten, C. T. M., &
% Van Der Helm, F. C. T. (2009). Magnetic distortion in motion
% labs, implications for validating inertial magnetic sensors.
% Gait & posture, 29(4), 535-541.
%
% Angular rate measurements from OMC is calculated following:
% Brodie, M. A., Walmsley, A., & Page, W. (2008).
% Dynamic accuracy of inertial measurement units during simple
% pendulum motion: Technical Note. Computer methods in biomechanics
% and biomedical engineering, 11(3), 235-242.
%
% Input: omcQuat- quaternion from OMC
%        imuGyro- angular rate measurements (rad/s) from IMU gyroscope
%        freq- common sampling frequency

% Author: Howard Chen
% Date: 3/6/2017


% Low-pass filter to remove noise
filtCutoff=5;
[lowpass_b,lowpass_a]=butter(2,filtCutoff/(freq/2),'low');

imuGyro=filtfilt(lowpass_b,lowpass_a,imuGyro(2:end,:));
omcQuat=filtfilt(lowpass_b,lowpass_a,omcQuat);

% Get angular rate measurements from OMC quaternion
sz=size(omcQuat);
omcOmega=zeros(sz(1)-1,3);

for i=1:1:length(omcQuat)-1
    %calculate dQ
    dQ=quatMultiply(quatConj(omcQuat(i,:)),omcQuat(i+1,:));
    dQ=quatNormalize(dQ);

    %calculte theta and angle
    dTheta=2*acos(dQ(1));
    Ux=dQ(2)/sin(dTheta/2);
    Uy=dQ(3)/sin(dTheta/2);
    Uz=dQ(4)/sin(dTheta/2);

    %calculte Omega
    omegaNorm=freq*dTheta;
    omcOmega(i,1)=omegaNorm*Ux;
    omcOmega(i,2)=omegaNorm*Uy;
    omcOmega(i,3)=omegaNorm*Uz;
end

% calculate LF rotation matrix
R=imuGyro'*pinv(omcOmega');

%orthogonize matrix
[U,W,V]=svd(R');
R = U*V';

%Convert to Quaternion
q2 = zeros(1,4);
q2(1)=0.5.*sqrt(1+R(1,1)+R(2,2)+R(3,3));
q2(2)=(R(3,2) - R(2,3))./(4.*q2(1));
q2(3)=(R(1,3) - R(3,1))./(4.*q2(1));
q2(4)=(R(2,1) - R(1,2))./(4.*q2(1));

end
```